Balancing Cost, Water, Emissions, and Reliability in Power Systems Operations

by

Jacob Kravits

B.S., University of Massachusetts Amherst, 2019

A thesis submitted to the

Faculty of the Graduate School of the

University of Colorado in partial fulfillment

of the requirements for the degree of

Doctor of Philosophy

Department of Civil, Environmental and Architectural Engineering

2023

Committee Members:

Joseph Kasprzyk, Chair

Kyri Baker

Ashlynn S. Stillwell

Balaji Rajagopalan

Andrey Bernstein

Kravits, Jacob (Ph.D., Civil Engineering)

Balancing Cost, Water, Emissions, and Reliability in Power Systems Operations

Thesis directed by Prof. Joseph Kasprzyk and Prof. Kyri Baker

Traditionally, large-scale power generation has been operated to reduce system operational costs. To expedite the mitigation of the harmful effects of climate change, many have proposed additional incentives for system operation (i.e., policies) that consider greenhouse gas emissions. However, such policies rarely consider unforeseen impacts on the volumes of water required for cooling thermoelectric plants as well as the potential effects on electricity production from water/climate-related stressors. Each chapter in this dissertation incrementally develops a multi-objective framework to create holistic power system policies that balance cost, water, emissions, and reliability. Each incremental development is applied to a realistic case study to systematically demonstrate what types of insights are possible through the proposed framework.

One fundamental hurdle in water/energy/emissions policy is understanding how such quantities tradeoff with one another. The third chapter of this thesis uses visual and statistical methods to qualitatively and quantitatively understand the interplay of these quantities. Once the general interplay of these quantities is understood, the fourth chapter proposes a policy framework to incorporate the water used by power systems as an additional operational system incentive. A policy is defined by an operational penalty that gives the water used by power systems monetary value. However, actually selecting a monetary value for this water use is nontrivial as it is fundamentally rooted in human morals and the inherent uncertainty of water systems. Therefore, the fourth chapter's framework seeks to understand the relationship between policy decisions, external climatological stressors (e.g., heatwaves, droughts, etc.), and system performance (e.g., total cost, water use, etc.). The framework proposed in the fifth chapter uses the relationships established in the previous chapter to find *optimal* operational policies. These operational policies must effectively balance cost, water use, emissions, and reliability under many operational stressors (e.g., line

outage) in addition to the previously studied climatological stressors. This dissertation ultimately concludes that consideration of many criteria (cost, water, emissions, and reliability) is necessary for creating an effective water-energy-emissions policy.

Dedication

To my family

Acknowledgements

First and foremost, I thank Dr. Joseph Kasprzyk and Dr. Kyri Baker for their mentorship, care, and investment in me as both an individual and scholar. I have heard that Ph.D. programs equip people with a "toolbelt" of skills - under your tutelage, I gained *mechanic's chest* of technical, academic, and interpersonal skills that I will use throughout my career. I thank all my collaborators for their input and thoughts on our various publications. Dr. Ashlynn Stillwell, your expertise and passion for the water/energy nexus is a continued inspiration. Additionally, I appreciate the diverse input and education from Dr. Andrey Bernstein and Dr. Balaji Rajagopalan - the skills and understanding gained through your courses are demonstrated throughout this thesis.

I would like to thank all the graduate students who gave me support: specifically, Ash Pigott - for teaching me about home energy management, Mostafa Mohammadian - for always brightening my day, and Barra Peak - for our collaborations to make our university a better place.

I thank Dr. Carlo Brancucci and all my fellow colleagues at Encoord for showing me that the skills and perspectives gained through my dissertation play a critical role in the energy transition.

I also want to thank Dr. Katherine Schlef and everyone at my undergraduate institution for piquing my interest in academic research.

I thank my literal and spiritual families. I am grateful for my parents, brother, and extended family - their emphasis on kindness and thoughtfulness from a young age was critical to my success in graduate school. To the Graduate Christian Fellowship, Crestview Church, and New Hope Church, thank you for your prayers over the years. Last and not least, I want to thank my wife Danielle for her love, emotional support, spiritual guidance, and inspiration.

Contents

Chapter

Tables

Table

Figures

Figure

Chapter 1

Introduction

The annual cost of energy system operations in the U.S. is approximately $105 billion (U.S. dollars) and the estimated economic value of U.S. power plants is approximately $1 trillion (U.S. dollars) [Fares, 2017, Rhodes, 2017]. Globally, 25 percent of emissions come from electric power production [Hockstad and Hanel, 2018]. Even as many power systems transition to renewable generation sources, it is currently estimated that 89 percent of energy sector greenhouse gas emissions are a result of fossil fuel combustion and industrial processes [IEA, 2021] with a similar percentage of total power coming from such sources. In the U.S., an estimated 48 percent of fresh surface water withdrawals (water that is diverted from a source) can be attributed to thermoelectric power plant electricity generation [Dieter et al., 2018]. Although the water consumed (water that is evaporated) is far less, proposed technological solutions to reduce emissions, such as carbon capture systems, have been shown to increase water consumption [Zhai and Rubin, 2010].

The impacts of climatological grid stressors expose how power plants are at the intersection of a functioning economy, healthy waterways, reliable energy systems, and a clean atmosphere. Droughts and heatwaves increase the temperature of cooling water and electricity demands - thus impacting energy reliability, increasing water withdrawal and consumption, creating negative impacts on riverine ecology from elevated-temperature discharge water, increasing operational costs, and shifting system operations to higher-emitting fuel sources [Lubega and Stillwell, 2018b, Harto et al., 2012, Poumadère et al., 2005, Harto et al., 2012, Freedman, 2012, Galbraith, 2011, Reuters Staff, 2011, Eaton, 2012, Luo, 2017]. Impacts on grid reliability during heatwaves are particularly

concerning as such coupled stress events increase mortality and morbidity risk [Stone et al., 2023]. In many regions, climate change increases the severity and frequency of these coupled stress events [Auffhammer et al., 2017].

Generally, power systems operations have the objective of minimizing operational costs while satisfying operational constraints on grid reliability, thermoelectric discharge temperature regulations, and emissions regulations. However, current operational policies fail to explicitly avoid these negative impacts on cost, reliability, water use, and emissions. In practice, system operators often choose between enforcing existing policies that limit the temperature of discharged water or granting thermal variances that allow discharge beyond legal limits [Harto et al., 2012, Poumadère et al., 2005, Lubega and Stillwell, 2018a]. Thermal variances are almost always granted [Micha, 2014], often due to concerns of impacting grid reliability. However, even grid reliability is not always achieved during particularly stressful climatological events. Therefore, cost, reliability, emissions reductions, and avoidance of thermal discharge violations are, in reality, *ideals* that compete with one another. Thus, it is more honest to model these quantities as *objectives* rather than hard constraints.

Previous studies have demonstrated that modeling power system emissions, water use, and reliability as extra constraints or objectives modify operations. However, previous frameworks have studied such quantities in a two-at-a-time fashion - for example, cost-emissions [Abido, 2003a], reliability-water [Lubega and Stillwell, 2018a, van Vliet et al., 2016], cost-reliability [Billinton and Allan, 1984], and cost-water [Fooladivanda and Taylor, 2015, Sanders et al., 2014] (Figure 1.1). Water use and emissions have been effectively incorporated as objectives and constraints or multiple objectives in *long-term* power system planning problems [Jornada and Leon, 2016, Mu et al., 2020, Liu et al., 2019, Wang et al., 2018]. However, there is a need to holistically create new cost-water-emissions-reliability-informed operations. These measures promote system coordination rather than manual intervention by system operators, as well as offer a rapid way for system operators to respond to current drought events, especially if long-term solutions are infeasible due to a lack of time to implement [Pacsi et al., 2013].

Timescale	Example Paper	Cost	Water	Emissions	Reliability
Short-Term Operations (minutes to days)	This Work	✓	✓	✓	✓
	[Lubega and Stillwell, 2018]		✓		✓
	[Sanders et al., 2014]	✓	✓		
	[Abido, 2003]	✓		✓	
	[Billinton and Allan, 1984]	✓			✓
	Status Quo	✓			✓
Long-Term Planning (years to decades)	[Jornada and Leon, 2016]	✓	✓		✓
	[Wang et al., 2018]	✓	✓	✓	
	Status Quo	✓			✓

Table 1.1: Literature Context of Thesis. Multi-objective considerations of cost, water, emission, and reliability have been previously conducted for long-term system planning. However, such quantities are typically considered in a two-at-a-time fashion when considering operational timescales.

This thesis develops a multi-objective framework to create holistic power system operational policies that balance cost, water, emissions, and reliability. To achieve this, we will link single- and multi-objective optimization concepts with coupled existing and novel models of power and water systems. Through several representative case studies, we demonstrate how our proposed frameworks not only allow nuanced insights into water/energy/emissions interplay but also show that our proposed policies mitigate the impacts of various operational and climatological grid stressors.

1.1 Overview of Chapters

1.1.1 Chapter 2: Background

Chapter 2 provides a review of the technical concepts used throughout this thesis. First, this chapter provides the context on the different types of generator water use as well as how they create emissions. Generally, each of these quantities is a function of how much active power is produced by

a generator. Next, we summarize single- and multi-objective optimization theory - tools that will allow us to efficiently balance the competing interests of water/energy/emissions systems. Finally, we provide context on how this thesis simulates "grid operations" via optimal power flow (OPF) - a problem that selects the optimal power dispatch (power output) of generators in a system.

1.1.2 Chapter 3: Quantifying Water, Emissions, and Cost Tradeoffs

The first step in creating a cost/water/emissions energy policy is understanding how such quantities impact one another. For a given system, it is essential to know if low-cost operations do so at the unintended expense of increased emissions but decreased water use. Thus, Chapter 3 analyzes how cost, water use, and emissions tradeoff with one another by incorporating these quantities as multiple objectives in an OPF formulation. Each "solution" to this formulation is a unique generator power dispatch. These solutions are then used in a tradeoff analysis to understand how these solutions uniquely compromise among the objectives (See lower-left diagram in Figure 1.1).

We apply this formulation to a modified test system we call the Water-Extended IEEE 30 Bus Test System and show how energy system operations can differ drastically when emissions and water use are considered in addition to the cost of system operation. Additionally, statistical metrics quantify the degree to which these various objectives tradeoff or are consistent with one another. To focus on these fundamental tradeoffs, the chapter models a "snapshot" of grid operations and thus does not explicitly consider the various water/energy processes that change over time such as a changing load and climate. This work has been published in [Kravits et al., 2022a].

1.1.3 Chapter 4: The Impact of Water Policy on Power Systems Operations

Once the general interplay among water/emissions/cost has been established, Chapter 4 introduces a "water policy." Here, a water policy comprises operational penalties that can incentivize different degrees of water-efficient power systems operations (i.e., penalties on excessive water use). These operational water penalties are a monetary value assigned to the different types of generator

water use. These water penalties allow water use to be considered as an additional cost term in the OPF formulation. Thus, we call this formulation a water-weighted OPF formulation.

Chapter 4 also introduces the concept of exogenous grid stressors. This chapter focuses on climatologic stressors that impact thermoelectric water use (e.g., drought) as well as load stressors (e.g., heatwaves). What makes each of these stressors *exogenous* is that system operators do not have direct control of these processes, and thus, must use the previously described policies to mitigate negative impacts.

Selecting a value for these operational water penalties is nontrivial, mainly because it requires specifying a monetary value for water use which is fundamentally linked to system climatology as well as moral values on the importance of healthy water systems. Therefore, Chapter 4 quantifies the *impact* of these operational water penalties under varying degrees of exogenous grid stressors. To achieve such insights, this framework utilizes a sensitivity analysis of many "snapshots" of our proposed water-weighted OPF formulation to qualitatively and quantitatively understand how operational penalty policies can mitigate the adverse effects of exogenous stressors (See lower-middle boxes of Figure 1.1).

We create an extension of a synthetic power system test case called the Water-Extended Illinois 200 Bus System to demonstrate the utility of our framework. This test system provides a synthetic, yet realistic, model of a transmission system in the midwest U.S. - an area that has historically faced problems with respect to its thermoelectric water use [Lydersen, 2016, Tomich, 2021]. We use historical load and water use data to inform the region over which sensitivity is assessed. Through this case study we show how our framework offers generator-level and line-level insights into how exogenous stressors impact power systems. This work has been published in [Kravits et al., 2022b].

With frameworks proposed to (1) understand the cost/emissions/water tradeoffs and (2) create operational penalties to help mitigate the impacts of exogenous stressors, the next chapter seeks to create and analyze *optimal* operational penalty policies.

1.1.4 Chapter 5: Considering Cost, Water, Emissions, and Reliability When Creating Optimal Power System Policies

Chapter 5 extends the scope of a policy from the previous chapter to include emissions in addition to water use. Thus, the optimal power flow formulation of the previous chapter is also extended to include an operational penalty on emissions in addition to water use. We use the same multi-objective optimization methods of Chapter 3 to achieve optimality of these penalties with respect to several competing objectives (See lower-right Figure 1.1).

Once we have established optimal policies, we test how they mitigate the impact of exogenous system stressors, just as in the previous chapter. However, this chapter tests optimal policies' performance against operational stressors (e.g., line outage, generator outage) in addition to the previously mentioned climatological stressors.

The framework in this chapter additionally extends the previous chapters' framework by considering a higher fidelity cosimulation model to analyze interactions between power system cost, water use, reliability, and emissions. The fidelity of the water use simulations is increased to directly analyze the impact of various natural processes such as streamflow, stream temperature, and ambient air on generator water use. Additionally, the timescale of the simulation is increased to better represent the temporal processes of power systems (e.g., diurnal changes to load, generator ramping constraints, etc.).

This framework is demonstrated on the previously-introduced Water-Extended Illinois 200 Bus System using historical exogenous stressor events to gain realistic insights into the impacts of optimal policies. This framework shows that the consideration of many criteria (cost, water, emissions, and reliability) is necessary for creating an effective water-energy-emissions policy. The findings of this chapter are in preparation to be published in Environmental Research Letters.

1.1.5 Chapter 6: Concluding Remarks

The final chapter makes concluding remarks summarizing the contributions of this thesis to fields of water/energy nexus analyses and power systems policy. Additionally, current limitations, possible next steps, and calls to action are presented.

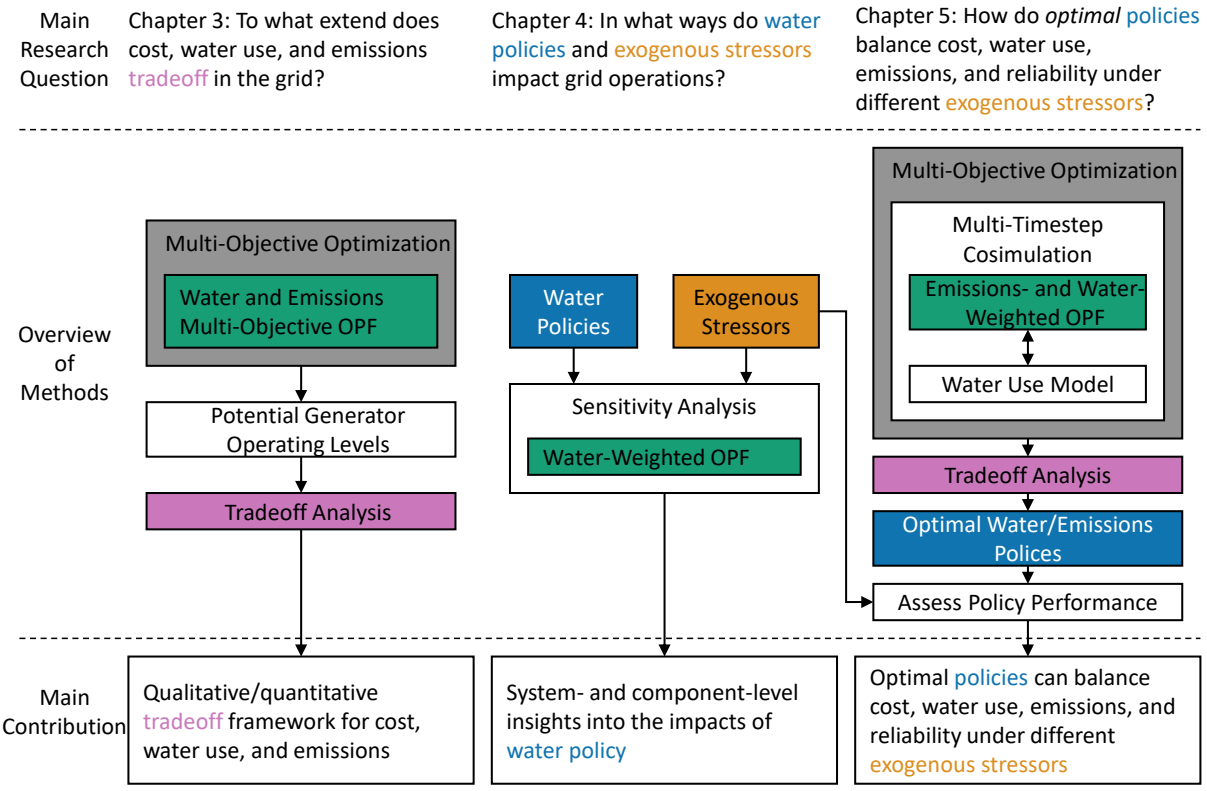

Figure 1.1: Overview of Chapter Question, Methods, and Contribution. The colors of the boxes highlight methodological commonalities across chapters. Abbreviations: optimal power flow (OPF)

Chapter 2

Background

This thesis is a *systems engineering* exercise that unites several fields: water resources engineering, power systems engineering, data science, and optimization are the most prevalent. Thus, there are many concepts, or rules of the game, required to fully understand this thesis:

> The only way to learn the rules of this Game of games is to take the usual prescribed course, which requires many years; and none of the initiates could ever possibly have any interest in making these rules easier to learn. These rules, the sign language and grammar of the Game, constitute a kind of highly developed secret language drawing upon several sciences and arts, but especially mathematics.
>
> [Hesse et al., 1969]

I, unlike the players of the Game, *do* have an interest in making this work accessible to a wide audience. Thus, this chapter provides a high-level background on the concepts that will be used throughout this thesis. Suggested references are provided throughout for additional details or context.

2.1 Thermoelectric Power Plants

Thermoelectric power generators, by definition, turn heat energy into electrical energy. The specific source of the heat varies widely. For example, natural gas generators use the combustion of natural gas, whereas modern nuclear generators use nuclear fission reactions. For many generators, these sources heat a working fluid, that eventually turns a turbine to create alternating current electrical power. There are many ongoing research efforts and descriptions of these thermodynamic

and mechanical processes Horlock [2013]. However, the specifics of these processes are beyond the scope of this thesis - we will mainly consider this process as a black box that takes as input some fuel which produces a thermal load that requires additional cooling and electrical energy.

2.1.1 Water Use

Water is often used as the working fluid in both cooling and generation technologies. This fact means that significant volumes of water are required to effectively run many types of thermoelectric generators. However, there is an important distinction in *how* the water is used during this process. Water "withdrawal" is defined as the volume of water diverted from a source. Water "consumption" is the subset of that water that evaporates during usage - and thus is not able to be returned to a body of water. We will use the term "water use" when we wish to describe both water withdrawal and consumption. We use a black box model to define water withdrawal and consumption rates which are the ratio of the volume of water withdrawn or consumed to the amount of energy produced (e.g., Gallons/MWh). These rates will be used extensively throughout this thesis. These principles can be applied to both riverine-cooling and ocean-cooled power plants. However, this thesis focuses on riverine-cooled plants.

In the U.S., an estimated 48 percent of fresh surface water withdrawals can be attributed to thermoelectric power plant electricity generation [Dieter et al., 2018]. The volumes of water withdrawn during normal operations are generally not a problem - water is often returned to its source at a slightly higher temperature but is diluted by the vast volumes of riverine water [Langford, 1990]. The problem arises during coupled droughts/heatwave events when the temperature of the intake water may be elevated and river streamflow may be reduced. In such cases, plants would have to discharge water at higher temperatures to water sources that are less capable of diluting this water (due to reduced volumes and increased temperatures), thus threatening local ecology Logan and Stillwell [2018], Logan et al. [2021]. Legally, in the U.S., the Clean Water Act regulates an upper limit on the temperature of this discharged water, which would require thermoelectric power plants to alter their operations to avoid these violations. However such limits are rarely

enforced due to concerns about the propagating impacts of modified operations on the electric grid [Micha, 2014, Lubega et al., 2014].

Roughly 2.5 percent of that water withdrawn is consumed [Horlock, 2013]. Although the magnitude of consumed water is far less than its withdrawal counterpart, the implications of water consumption are still an important operation consideration - mainly because water that is consumed is not directly returned to its source (i.e., considered water waste). Therefore, it is not available to downstream users which could include other power plants, hydropower plants, drinking water utilities, recreationists, or the myriad of other water users in modern riverine networks. Additionally, heatwaves can increase the temperature of ambient air used for providing cooling, thus increasing consumption rates [Meng and Sanders, 2019].

The extent to which water is withdrawn or consumed is largely defined by the type of cooling technology [Durmayaz and Sogut, 2006, Peer et al., 2016]. The two general categories of cooling systems are once-through cooling systems and recirculating cooling systems [Gerdes and Nichols, 2009]. The major difference between once-through and recirculating systems is that once-through cooling systems rely on the direct heating of withdrawn cooling water to provide cooling capacity. However, recirculating systems mainly use ambient air with a heat exchanger to provide cooling - thus allowing cooling water to be cooled/recycled or evaporated. Generally, once-through systems are the largest withdrawers of water whereas recirculating systems are the largest consumers of water [Peer et al., 2016].

In summary, the water that is consumed and withdrawn by thermoelectric power plants is used in large quantities, critical for power plant operations, linked to cooling technologies, impacted by external climatological/hydrological stressors, and capable of impacting local riverine ecology. These principles will be considered throughout this thesis.

2.1.2 Emissions

Most fossil-fuel-burning thermoelectric plants produce emissions during the combustion process. These emissions are generally released into the air where they can contribute to the devastating

impacts of global climate change. This thesis will incorporate analyses of several types of pollutants - sulfur-based, nitrogen-based, and carbon-based. However, the details of the chemical reactions responsible for creating these pollutants are beyond the scope of this text. As with water use, we will take a black box approach to thermoelectric power plants in that they have some fuel source as inputs and generate emissions and electrical energy. This allows us to define an analogous emissions rate of the amount of emissions per energy produced (e.g., lbs CO_2/MWh).

Globally, 25 percent of carbon emissions come from electric power production [Hockstad and Hanel, 2018]. Even as many power systems transition to renewable generation sources, it is currently estimated that 89 percent of energy sector greenhouse gas emissions are a result of fossil fuel combustion and industrial processes [IEA, 2021] with a similar percentage of total power coming from such sources.

Recently, the U.S. federal government proposed the first regulations that would greatly restrict emissions from the power sector. If passed, these measures would require coal and gas-fired power plants to eliminate nearly all of their carbon dioxide emissions by 2040 [Davenport and Friedman, 2023]. One promising solution to reducing thermoelectric power plant emissions is to capture the pollutants as they are emitted. One prevalent example of such a technology is carbon capture sequestration which compresses carbon dioxide particles from the air into solid forms that can easily be stored. However, such technologies often require additional water for cooling components. In fact, installing carbon capture sequestration technologies have been proven to significantly increase water consumption for generators with certain cooling types [Zhai and Rubin, 2010].

Nuclear generation is another energy technology with interesting links to emissions and water use. Nuclear generation is generally considered to be a low- or zero-emitting thermoelectric technology. However, due to the scale of these plants and the required thermal load that must be cooled, these plants can be both inefficient with respect to their water withdrawal and water consumption when compared with other higher-emitting generator/cooling systems combinations [Macknick et al., 2012]. In the context of system-wide operations (i.e., many plants with various generator and cooling technologies) there can arise cases where shifting system dispatch away from

nuclear reduces emissions while increasing the total water usage and emissions. Such a case will be explored in Chapter 5.

In summary, the emissions that are produced by thermoelectric generators are both significant and technologically linked to the various types of water usage.

2.2 Hydroelectric Energy Generation

Another coupling between energy systems and riverine systems is hydroelectric generation. Hydroelectric generation currently constitutes six percent of the annual energy generation and thirty percent of the renewable annual energy generation in the U.S. [Office of Energy Efficiency and Renewable Energy, 2022]. Although it is a crucial component of the water/energy nexus, hydroelectric generation will not be the focus of this thesis. However, there are relevant connections from this thesis work to hydroelectric generation.

Hydroelectric energy generation can generally be categorized into two types: run-of-river and impounded. Run-of-river hydroelectric generation works by converting the kinetic energy of running water into electrical energy via the river currents turning a turbine. Impounded electric generation works by converting the gravitational potential energy of water impounded behind a dam into electrical energy by releasing water through a turbine.

Both types of hydroelectric generation typically use dams to regulate the natural flow of the river and guide water to turbines for energy production. Much like power plant water use, there are several environmental impacts of hydroelectric energy generation [Union of Concerned Scientists, 2013]. One impact that is shared by power plants and hydroelectric energy generation is the impact on water consumption. Just as power plants cause water to be consumed (evaporated), the impounding of water increases the surface area, thus also increasing the consumption rates [Torcellini et al., 2003]. Thus, the findings discussed throughout this thesis have broader connections to other coupling points in water and energy systems.

2.2.1 Dam Hazard

Another result of hydroelectric generation is the hazard of potential dam failure. There are 16,000 high-hazard potential dams in the U.S. [Federal Emergency Management Agency and Department of Homeland Security, 2017]. A high-hazard potential dam is one in which it is probable that failure would cause loss of human life. Although this definition is codified at the federal level, the actual methodologies by which dams are classified are defined on a state level, with state dam officials evaluating dam hazard potential on a case-by-case basis, ultimately relying on human judgment [Federal Emergency Management Agency, 1998]. Such a system is prone to hazard potential classification inconsistencies which could lead to negative regulatory and human-safety implications.

Classifying dam hazard potential needs to be done consistently, continually, and across large spatial extents [Mamerow, 2018, Schoolmeesters, 2020]. Geospatial models [Aboelata et al., 2002, Aboelata and Bowles, 2008], dam-break flood routing numerical simulation models [Luo et al., 2009], risk-based models [Larruari and Lall, 2020] offer valuable insight into the engineering and economic consequences of dam failures but could be difficult to automate due to input feature requirements. Other works have proposed empirical relationships for estimating dam loss-of-life based on datasets of historic dam breaks [Feinberg et al., 2016]. However, these methods fail to consider the complex locational aspects of dam failure. Preliminary work done for this thesis overcomes the existing feature requirements by using a parameterized geospatial and tree-based model that has been trained using existing geospatial datasets and publicly available dam hazard datasets. We will discuss the optimization of this model in Section 2.3.3.

The results of this optimization are published in Kravits et al. [2021b]. Such an analysis laid the groundwork for understanding the propagating impacts of energy infrastructure on other systems. Specifically, this work shows how the impacts of competing systems be quantified by different objectives - and that these objectives can be balanced through multi-objective perspectives. Such a theme will be further developed throughout this thesis.

2.3 Single- and Multi-Objective Optimization Theory

Both power and water systems operations are transitioning from general operational rules to system optimization. Large-scale water systems (e.g., reservoir systems) have a long history of these rules of operations dating back to ancient Romans Lund et al. [2006]. Similarly, in the first half of the 20th century, generator power output was determined manually based on general "rules of thumb" and specialized slide rulers [Cain et al., 2012]. Following this, early attempts to formulate grid operations as an *optimization* problem were formulated, but difficult to implement due to their inability to be solved in real-time [Carpentier, 1962]. However, with the increase in computational power, optimization problems became an essential part of modern water and power system operations [Burges, 1979, Cain et al., 2012].

The shift toward optimization required the need to explicitly select "constraints" and a single "objective" for system operation. Philosophically, constraints were selected to be a physical process that must be obeyed by a system (e.g., the conservation of water moving through a reservoir system) or an extremely undesirable operational outcome (e.g., moving more than the designed power through a transmission line). An objective, on the other hand, was some operational *ideal* with the most common objective being to minimize cost.

Both the water and power systems fields have seen a shift from a single objective perspective towards a *multi-objective* perspective. One of the main drivers of this shift has been the immense difficulty in agreement on the relative importance of the previously mentioned "extremely undesirable" constraints and objectives.

The following sections explore different methods of implementing single- and multi-objective perspectives in optimization problems. We will use a generic optimization problem where the decisions of the problem can be collected into a vector $\mathbf{x}$ of length d (for this thesis, bold-face variables indicate multi-dimensional or nonscalar values). Assume that there are g objectives of interest that are a function of our decisions $\mathbf{x}$. Additionally, assume that all the constraints can be distilled into a function of the decisions $h(\mathbf{x})$. The function h may not be a closed-form equation,

in fact, it could be a complex black-box simulation of many physical systems. Such details will become important when solving these optimization problems (these details will be addressed as we proceed throughout the thesis).

2.3.1 Single Objective

Assume that it is possible to choose the design of a system to solely maximize or minimize a single given objective (f_1). In such cases, we can formulate our problem as a traditional single-objective problem:

$$\min_{\mathbf{x}} \quad f_1(\mathbf{x}) \tag{2.1}$$

$$\text{s.t.} \quad h(\mathbf{x}) = 0 \tag{2.2}$$

Given requirements on the mathematical form of the objective and constraint, it is often possible to find a single optimal objective value $f_1(\mathbf{x}^*)$ and corresponding decision vector $\mathbf{x}^*$. This fact is a general advantage of this formulation in addition to the general efficiency with which they can be solved (assuming simple cases of h).

2.3.2 Weighted Objective

Let's now assume we can normalize all remaining objectives $[f_2, f_3, ..., f_p]$ to the units and/or magnitude of the first objective f_1 by introducing weights on the remaining objectives $[w_2, w_3, ..., w_p]$ which can be collected into a vector $\mathbf{w}$ of length W. This weighting scheme allows us to turn multi-objective problems into weighted-objective problems. Thus, we can define our optimization problem as such:

$$\min_{\mathbf{x}} \quad f_1(\mathbf{x}) + w_2 f_2(\mathbf{x}) + ... + w_p f_p(\mathbf{x}) \tag{2.3}$$

$$\text{s.t.} \quad h(\mathbf{x}) = 0 \tag{2.4}$$

Just as in the previous formulation, this formulation benefits from efficiency and a single optimal objective value (with the corresponding decision(s)). Additionally, introducing weights can have some physical meaning for a system (e.g., they may reflect a price or preference). However, deciding on a weighting scheme $\mathbf{w}$ can be difficult - particularly in cases with many decision makers with competing interests [Smith et al., 2017] or when it is unknown how processes within h may impact the relationship between different objectives.

Sensitivity Analysis

One way to unpack the relationships between these various quantities would be to conduct a sensitivity analysis. Sensitivity analysis seeks to find the influence of uncertain input parameters on the distribution of output parameters. To explore this, sampling is (randomly or systematically) used. For example, through a Sobol sensitivity analysis, one could quantify how changes in the weighting schemes $\mathbf{w}$ or h impact optimal solutions $\mathbf{x}^*$ or objective behavior f [Sobol, 1990]. It is important to note that the point of the sensitivity analysis itself is not to produce optimal solutions, but rather to understand the general behavior of the model.

2.3.3 Multi-Objective

A multi-objective formulation is often desirable when analysts are concerned with how each objective impacts the other, in other words, an objective tradeoff. Often, this is particularly useful when it is unknown how objectives tradeoff with one another.

To demonstrate a multi-objective optimization problem, we review a case study published in Kravits et al. [2021b] with additional details/insights in Appendix B. In this problem, you make a model for dam hazard classification - recall, a high-hazard potential dam is one in which it is probable that failure would cause loss of human life. You must decide the input data for this model and values for various model parameters. The goal is to ensure that your decision results in the best-performing classification model. To achieve this, you propose objectives to quantify what "best-performing" decisions actually are.

Table 2.1 shows how dams can be correctly and incorrectly classified. On the diagonal, we

have our correctly classified dams (true positive and negative). These cases are ideal in that they mean that our model agrees with the current classification. However, consider the incorrectly classified off-diagonal (false negative and positive) cases - wrongly classifying a high-hazard dam may lead to downstream populations being put at an increased risk whereas wrongly classifying a non-high-hazard dam may lead to overinvestment.

	Predict Not High	Predict High
Actual Not High	True Positive	False Negative
Actual High	False Positive	True Negative

Table 2.1: Confusion Matrix for High and Not High Dam Hazard Classification.

Given these types of classifications, there are several objectives that exist. An accuracy objective reflects how well a model captures the "greatest good" by considering the diagonal cases. The different types of off-diagonal cases are quantified by a false positive rate (FPR) and true positive rate (TPR) - with each objective quantifying the degree to which the model increases risk or causes overinvestment. Accuracy, TPR, and FPR are hard to compare because you are forced to morally compare correctly classified threats to human life, potentially unclassified threats to human life, and wasted capital.

Multi-objective optimization allows you to understand how each of these objectives (accuracy, FPR, and TPR) tradeoff with one another. Once these tradeoffs are understood you can make an informed decision based on the observed performance. For example, based on the objective tradeoffs, you can pick a decision that balances accuracy, FPR, and TPR.

The multi-objective perspective flips the "weighting of objectives" described in Section 2.3.2. Instead of trying to get a single solution that captures a single set of weights $\mathbf{w}$, a multi-objective perspective seeks *many solutions* with each solution capturing a unique set of relative objective importance. To achieve this, we need to rethink how we can compare two sets of decisions in a multi-objective context.

We introduce the domination operator $\prec$ to allow us to compare decision solution vectors in a multi-objective context. Consider two sets of decisions to our problem $\mathbf{x}_1$ and $\mathbf{x}_2$ and the corresponding vector of objective values $\mathbf{F}_1(\mathbf{x}_1) = [f_1(\mathbf{x}_1), f_2(\mathbf{x}_1), ..., f_p(\mathbf{x}_1)]$ and $\mathbf{F}_2(\mathbf{x}_2) = [f_1(\mathbf{x}_2), f_2(\mathbf{x}_2), ..., f_p(\mathbf{x}_2)]$ both of length g. $\mathbf{F}_1 \prec \mathbf{F}_2$ if and only if $\forall i \in \{1, 2, ..., g\}, f_i(\mathbf{x}_1) \leq f_i(\mathbf{x}_2)$, and $\exists j \in \{1, 2, ..., g\}, f_j(\mathbf{x}_1) < f_j(\mathbf{x}_2)$. In other words, for a solution to dominate another solution, it must completely "beat out" the other solution. Nondomination is the converse of domination such that a nondominated solution's performance is not exceeded with respect to all objectives by another solution.

The formulation of the multi-objective problem is an extension of the single-objective problem that relies on the nondomination operator to compare decision vectors

$$\underset{\mathbf{x}}{\text{minimize}} \quad [f_1(\mathbf{x}), f_2(\mathbf{x}), ..., f_p(\mathbf{x})] \tag{2.5}$$

$$\text{s.t.} \quad h(\mathbf{x}) = 0 \tag{2.6}$$

which produces *many* nondominated decisions. The set of all the nondominated solutions to a problem is called the Pareto-optimal set of decisions to the problem. Producing a nondominated set is a major advantage and disadvantage of a multi-objective formulation. It is advantageous because it allows for tradeoff analysis as well as the selection of a nondominated solution *after the optimization has occurred* which is particularly helpful in cases when objective tradeoffs are not known in advance. However, finding a pareto-approximate set of nondominated solutions often means longer optimization times and extensive post-processing of results with human interpretation which can be problematic for operational cases where a fast solution may be required. Additionally, ensuring convergence of a search often requires post-processing and the use of metaheuristics [Zatarain Salazar et al., 2016].

2.3.4 Nested Multi-Objective Optimization Using a Single-Objective Solver and Weights

Let's assume that our problem:

- has many relevant objectives
- weights on these objectives have an important physical meaning
- the exact values of weights are difficult to determine in advance
- your problem has a sub-component to it that is traditionally solved with a single objective optimization

In this case, we nest the weighted objective formulation proposed in Section 2.3.2 in the multi-objective formulation proposed in Section 2.3.3 - thus creating an "outer" multi-objective problem with an "inner" weighted objective problem:

$$\underset{\mathbf{w}}{\text{minimize}} \quad [f_1(\mathbf{x}^*), f_2(\mathbf{x}^*), ..., f_p(\mathbf{x}^*)] \tag{2.7}$$

$$\text{s.t.} \quad \mathbf{x}^* = \{\underset{\mathbf{x}}{\text{argmin}}(f_1(\mathbf{x}) + w_2 f_2(\mathbf{x}) + ... + w_p f_p(\mathbf{x}))|h(\mathbf{x}) = 0\} \tag{2.8}$$

$$\underline{w}_i \leq w_i \leq \overline{w}_i \forall i \in \{1, 2, ..., W\} \tag{2.9}$$

where the "decisions" of the outer problem (Line 2.7) are the weights $\mathbf{w}$ which are passed into the inner optimization problem (Line 2.8) that optimizes true decisions $\mathbf{x}$ of the inner optimization. Therefore, this formulation produces a set of nondominated solutions - with each solution having a corresponding set of weights, decisions, and objectives. The inner/outer behavior of this formulation is analogous to bilevel multi-objective formulations [Deb and Sinha, 2010] or Stackelberg games [von Stackelberg, 2011]. Additionally, we constrain these weights to some upper $\overline{w}$ and lower $\underline{w}$ bounds.

Having sets of weights, decisions, and objectives has several advantages that overcome the previously mentioned challenges. Not only does this formulation facilitate the previously mentioned

tradeoff analysis between decisions and objectives but it can also facilitate a tradeoff analysis between *weights* and objectives. In cases where the weights have important physical meaning, the impacts of these weights on objective performance may be most relevant.

Another advantage of this formulation is that every feasible solution (dominated and non-dominated) to the multi-objective produces an optimal set of internal decisions. This is because the outer multi-objective problem produces weights that are then used to optimize the decisions of the inner single-objective problem. Therefore, although the convergence of the outer multi-objective problem often requires metaheuristics, the optimality of the solution to the inner weighted problem can be confirmed (e.g., if h is convex, optimality can typically be confirmed using standard proofs [Kuhn and Tucker, 1951]). This has many practical implications because a nondominated set of weights from a multi-objective optimization of h can be applied to similar h'. Although the transferred weights may be dominated under h', the resulting decisions for the inner weighted-single-objective problem are still optimal.

2.4 Optimal Power Flow

As previously discussed, with the increase in computational power, operational single-objective optimization problems have become an essential part of modern grid operations. For example, OPF is one such optimization problem that generally ensures that all the generators in a system output power in a consistent, economical, safe, and efficient manner and is typically solved by independent system operators. Modern energy systems use several OPF formulations. This thesis will use the DC OPF simplification of the full AC OPF formulation because of its ubiquity in modern power systems.

2.4.1 AC Optimal Power Flow

Given a set of power sources, loads, and other various systems topological/operational parameters, OPF seeks the active power dispatch at each generator $\mathbf{p_g}$, the reactive power at each generator $\mathbf{q}$, and the voltage at each bus $\mathbf{v}$ such that only the economic costs are minimized. The

formal AC OPF formulation is as follows:

$$\min_{\mathbf{v},\mathbf{p_g},\mathbf{q}} \quad C_0(\mathbf{v}) + \sum_{\forall j \in \mathcal{G}} C_j(p_j, q_j) \tag{2.10}$$

$$\text{s.t.} \quad (\mathbf{p_g} - \mathbf{p_L}) + j(\mathbf{q} - \mathbf{q_L}) = diag(\mathbf{v})\,\mathbf{Y}^*\mathbf{v}^* \tag{2.11}$$

$$v^{min} \leq |v_i| \leq v^{max},\ i = 1, \ldots, B \tag{2.12}$$

$$(p_{g,j}, q_j) \in \mathcal{Y}_j \tag{2.13}$$

$$v_1 = v_{ref} \tag{2.14}$$

where C_i are the various economic costs associated with a power system's voltage, active power, and reactive power. $\mathbf{p_L}$ and $\mathbf{q_L}$ are the active and reactive loads that change throughout time $\mathbf{Y}$ is the line admittance matrix that captures the network topology and potential for losses. B is the number of buses in the system. The minimum/maximum voltages at each bus are determined by v^{min} and v^{max}. $\mathcal{Y}_i$ is the set of feasible values for active and reactive power. $\mathcal{G}$ is the set of generators in the system. v_{ref} is the reference voltage for the system. Conceptually, equation 2.11 models the power balance on the lines throughout the system by solving for the system voltages while the remaining constraints are conceptually straightforward.

2.4.2 The DC Optimal Power Flow Simplification

Equation 2.11 introduces significant complexities due to the non-convex nature of the right-hand side. Because the OPF problem needs to be solved for real-time operation on the order of minutes or hours, the DC OPF simplification was introduced to reduce the computational burden. Specifically, the DC OPF assumes constant voltages for all nodes, lossless lines, and small angle approximation Taylor [2015, chap 3]. Just as AC OPF, the DC OPF approximation also seeks to find the power output $\mathbf{p_g}$ such that solely economic costs are minimized. The resulting single-objective DC OPF formulation is:

$$\min_{\{\theta_i\}\forall i\in\mathcal{N},\{p_{g,i}\}\forall j\in\mathcal{G}} \quad \sum_{\forall j\in\mathcal{G}} C_j\left(p_{g,j}\right) \tag{2.15}$$

$$\text{s.t.} \quad p_{g,i} - p_{L,i} = \sum_{n=1}^{N} B_{in}\left(\theta_i - \theta_n\right), \forall i \in \mathcal{N} \tag{2.16}$$

$$p_{g,j}^{min} \leq p_{g,j} \leq p_{g,j}^{max}, \forall j \in \mathcal{G} \tag{2.17}$$

$$-\Lambda_{max,im} \leq B_{im}\theta_{im} \leq \Lambda_{max,im}, \quad \forall im \in \mathcal{L} \tag{2.18}$$

with B_{im} as the (i, m) entry of the susceptance matrix $\mathbf{B}$. The difference in the voltage phase angles between neighboring buses i and m is denoted as θ_{im}. Although the angle at each bus is formally a decision variable, this thesis will mainly consider it as an internal parameter calculated in order to satisfy the constraints of the DC OPF formulation. The product of B_{im} and θ_{im} approximates the electricity flowing through line im in the set of all lines $\mathcal{L}$. Equation 2.16 constrains the line flows using the previously defined simplifications, and Equation 2.17 constrains the active power output, and Equation 2.18 constrains the power flowing through the lines (Λ_{max}).

2.5 Applications of Background Concepts Throughout Thesis

Throughout this thesis, we apply various optimization formulations to water/energy/emissions systems. Generally, the decisions ($\mathbf{x}$) are power dispatch of a power system's generators, h is a DC OPF simulation of power system operations, and the various objectives (f) each capture an aspect of a system's cost, emissions, and water use.

In Chapter 3, we use a multi-objective formulation to study the tradeoffs of cost, water use, and emissions objectives f. Our simulation (h) is a single timestep of DC OPF. Then, in Chapter 4, we shift our formulation to be more policy-focused by introducing weights ($\mathbf{w}$) to reflect an operational cost penalty assigned to each of these objectives, not unlike a water or emissions "price". We conduct a sensitivity analysis to show how those operational policies as well as different stressors on the system (captured by different h) impact the system cost and water use objectives (f). Finally, in Chapter 5, we use a nested multi-objective optimization using

a single-objective solver and weights to *optimize* these operational policies to a multi-timestep water/energy/emissions/reliability simulation (h). We show how such policies optimized to a single scenario (h) can still perform well over several different scenarios (h').

Chapter 3

Quantifying Water, Emissions, and Cost Tradeoffs

In this chapter, we demonstrate how to analyze the tradeoffs of water use, emissions, and cost in thermoelectric-dominated power systems. To achieve this, we introduce four objectives to capture the cost, water withdrawal, water consumption, and emissions in the system. We combine these objectives into a novel multi-objective water/emissions-informed DC OPF formulation. This formulation is applied to a synthetic case system where we analyze the system components responsible for these tradeoffs as well as quantify the degree to which each objective is redundant (or not redundant) with one another. The findings of this chapter have been adapted from their publication in Kravits et al. [2022a].

3.1 Introduction

The interactions of water, cost, and emissions of thermoelectric-dominated power systems have been quantified over long timescales and across large spatial extents [Meng et al., 2020, Peer et al., 2016]. However, less work has been done to incorporate such processes into the sub-hourly operations of the grid. The work that has been done typically focuses on two objectives at a time. For example, emissions and cost have been previously incorporated into operational problems such as optimal power flow [Abido, 2003b, Wu et al., 2010]. Similar work has incorporated water used by thermoelectric plants into the constraints of the OPF problem [Fooladivanda and Taylor, 2015] or as objectives in the economic dispatching problem [Sanders et al., 2014]. However, few studies have incorporated all three objectives (cost, emissions, and water use) into a multi-objective formulation.

Therefore, this chapter provides a multi-objective OPF formulation that considers cost, emissions, and types of thermoelectric water use as separate objectives.

Previous efforts to convey objective tradeoffs among solutions to multi-objective OPF mainly relied on interpreting plots of solution objective performance [Abido, 2003b, Kravits et al., 2021a]. These visual-interpretation methods are intuitive for visualizing objective tradeoffs among a few dimensions. However, comparing tradeoffs among many dimensions (as is the case in our formulation) or across different problems becomes especially difficult due to human subjectivity; thus, metrics exist to quantify tradeoffs in many objective systems [Wu et al., 2021, Chen et al., 2020, Tang et al., 2019]. In this chapter, we propose methods for quantifying objective tradeoffs, within a pre-specified objective tolerance, for our multi-objective OPF formulation. We also provide examples of how to intuitively visualize these tradeoff metrics to allow for within-system objective tradeoff comparisons.

3.2 Methodology

First, we introduce the decisions of this optimization problem. Then, we propose several objectives to quantify the performance of a power system with respect to its cost, water use, and emissions. Finally, we incorporate these objectives and decisions into a multi-objective extension of the traditional DC OPF problem previously outlined in Section 2.4.2.

3.2.1 Decisions

The decisions of this problem are the same as the traditional DC OPF formulation introduced in Section 2.4.2. Recall, these decisions are the active power dispatch of a set of generators ($\mathbf{p_g}$) over a single timestep. This chapter *extends* the traditional DC OPF formulation by considering multiple objectives.

3.2.2 Objectives

The first objective is the traditional OPF objective of fuel costs associated with active power output [Frank and Rebennack, 2016, Taylor, 2015]. These fuel costs are a quadratic function of the active power output at each generator and are summed across the entire system. The total fuel costs in the system (f_{gen}) are expressed as:

$$f_{gen}(\mathbf{p_g}) = \sum_{j \in \mathcal{G}} a_j + b_j p_{g,j} + c_j p_{g,j}^2 \tag{3.1}$$

where $\mathbf{p_g}$ is a vector of all the active power outputs and a_j, b_j, and c_j are the cost coefficients of the active power output of generator j. The units on a_j, b_j, and c_j are such that the final units of f_{gen} is \$ / hr. The set of all the generators is $\mathcal{G}$.

The second objective captures the total atmospheric pollutants of sulfur oxides (SOx) and nitrogen oxides (NOx) emitted by the system [Abido, 2003b]. The total emissions in the system (F_{emit}) are expressed as:

$$f_{emit}(\mathbf{p_g}) = \sum_{j \in G} 10^{-2} \left(\alpha_j + \beta_{emit,j} p_{g,j} + \gamma_j p_{g,j}^2\right) + \xi_j e^{\lambda_j p_{g,j}} \tag{3.2}$$

where α_j, β_j, γ_j, ξ_j, and λ_j are the emission coefficients of active power output of generator j (power in per-unit). The quadratic form reflects the SOx pollutants while exponential terms reflect the NOx pollutants Ghasemi et al. [2015]. The final units of f_{emit} are total emissions in U.S. ton / hr.

The third and fourth objectives capture the thermoelectric water use of the generators. These objectives capture the water withdrawn and water consumed. The total water consumed by the system (f_{con}) and withdrawn by the system (f_{with}) are expressed as:

$$f_{with}(\mathbf{p_g}) = \sum_{j \in \mathcal{G}} \beta_{with,j} p_{g,j} \tag{3.3}$$

$$f_{con}(\mathbf{p_g}) = \sum_{j \in \mathcal{G}} \beta_{con,j} p_{g,j} \tag{3.4}$$

where $\beta_{with,j}$ and $\beta_{con,j}$ are the withdrawal and consumption rates of generator j. Such rates are defined as the amount of water required to produce some unit of electricity and have the units of gal / MWh. These rates are dependent on fuel type, cooling system type, as well as external climatic/hydrologic factors Macknick et al. [2012], Miara et al. [2018]. The product of these rates and the power output yields the final units of f_{with} and f_{con} of gal/hr.

3.2.3 Water/Emissions-Informed DC OPF Formulation

These objectives are incorporated into a multi-objective DC OPF formulation, which finds the decisions (active power dispatch $\mathbf{p_g}$) that minimize the vector of the four objectives $[f_{gen}(\mathbf{p_g}), f_{emit}(\mathbf{p_g}), f_{with}(\mathbf{p_g}), f_{con}(\mathbf{p_g})]$:

$$\underset{\mathbf{p_g}}{\text{minimize}} \quad [f_{gen}(\mathbf{p_g}), f_{emit}(\mathbf{p_g}), f_{with}(\mathbf{p_g}), f_{con}(\mathbf{p_g})] \tag{3.5}$$

$$\text{s.t.} \quad p_{l,i} - \sum_{k \in \mathcal{G}_i} p_{g,k} = \sum_{m \in \mathcal{N}} B_{im}\theta_{im}, \quad \forall i \in \mathcal{N} \tag{3.6}$$

$$-\Lambda_{max,im} \leq B_{im}\theta_{im} \leq \Lambda_{max,im}, \quad \forall im \in \mathcal{L} \tag{3.7}$$

$$\underline{p}_{g,j} \leq p_{g,j} \leq \bar{p}_{g,j}, \quad \forall j \in \mathcal{G} \tag{3.8}$$

This DC OPF formulation uses the same notation introduced in Section 2.4.2. Additionally, see Section 2.3.3 for further details on multi-objective formulations.

3.3 Case Study: Water-Extended IEEE 30 Bus Test System

We demonstrate this formulation and the insights gained through it with the IEEE 30-bus test system using default line and generator parameters Thurner et al. [2018]. However, the coefficients needed to compute the objectives required by this formulation are not supplied by default but rather are inferred to ensure a system that has both realistic generators and cooling systems as well as realistic objective performance. Fuel costs and emission coefficients were based on previously published coefficients Abido [2003b], Wu et al. [2010]. Based on these coefficients, we assumed

representative fuel and cooling system types for each generator and estimated withdrawal and consumption rates based on national estimates Macknick et al. [2012]. We assume bus zero is the slack bus that is connected to an active power generator. This modified test system we call the Water-Extended IEEE 30 Bus test system.

Figure 3.1 presents the overview of how we get the set of nondominated solutions. Initially, the power output bounds of every generator are known, and infer the slack bus based on system topology. Then, we define a uniform grid of 10 steps over every generator except the slack bus. The DC power flow equations are then solved for all 100,000 entries in the grid using a Newton-Raphson solver Thurner et al. [2018]. Infeasible grid entries are dropped and the objectives are computed for the remaining entries.

We implement an epsilon nondomination filter to find our solutions to the multi-objective problem Woodruff and Herman [2013]. Practically, *epsilon* nondomination allows us to give a user-defined precision on each objective function. Epsilon nondomination is an extension of the nondomination definition presented in Section B.3 where a tolerance is specified, which must be exceeded for domination to occur [Laumanns et al., 2002].

For this problem, f_{gen}, f_{emit}, f_{with}, and f_{con} are assigned the epsilons of 10.0, 0.01, 100000.0, and 10000.0, respectively. These choices are based on the precision of the objective quantities made in the literature Abido [2003b], Wu et al. [2010], Macknick et al. [2012]. The number of steps in the grid was chosen by iteratively increasing the step number until no additional epsilon-nondominated solutions were found by increasing further.

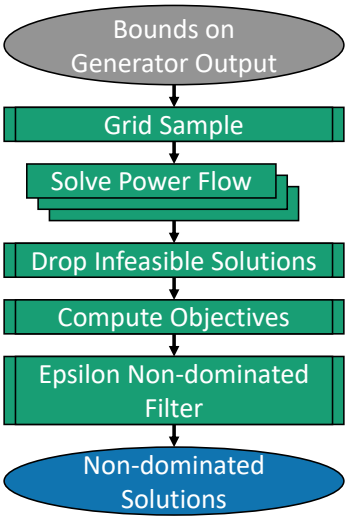

Figure 3.1: Overview of Solving Multi-objective OPF

We ran this search on the RMACC Summit supercomputer across one node with two CPUs (Intel Xeon E5-2680 v3, 2.50 GHz, 24 cores/node) with 4.84 GB RAM per core. This optimization took a wall time of roughly 10 minutes.

3.4 Results and Discussion

3.4.1 Qualatitive Tradeoff Analysis

The objective performance of the nondominated set of solutions (power dispatches) for our multi-objective OPF formulation applied to the Water-Extended IEEE 30 Bus system is presented in Figure 3.2. Each line on this plot is a unique nondominated solution to the multi-objective OPF just as the plot discussed in 2.3.3. Objectives have been oriented such that desired solutions intersect towards the bottom of this figure. Additionally, to aid in visualization, solutions have been colored to reflect their cost.

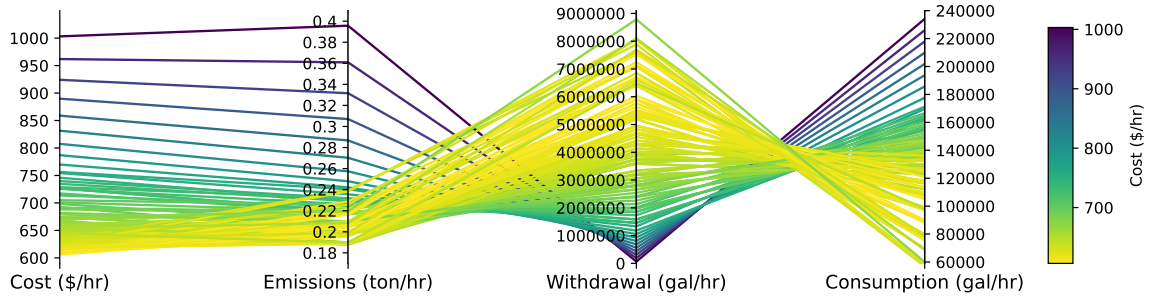

Figure 3.2: Performance of Nondominated Solutions. Visualization created using [Kravits, 2022].

Figure 3.3 depicts the actual solution values ($\mathbf{p_g}$) associated with Figure 3.2. To aid in visualization, the same coloring scheme (generator cost) is implemented in both figures. Unlike Figure 3.2, Figure 3.3 expresses no preference in the direction as each axis is simply reflecting active power dispatch.

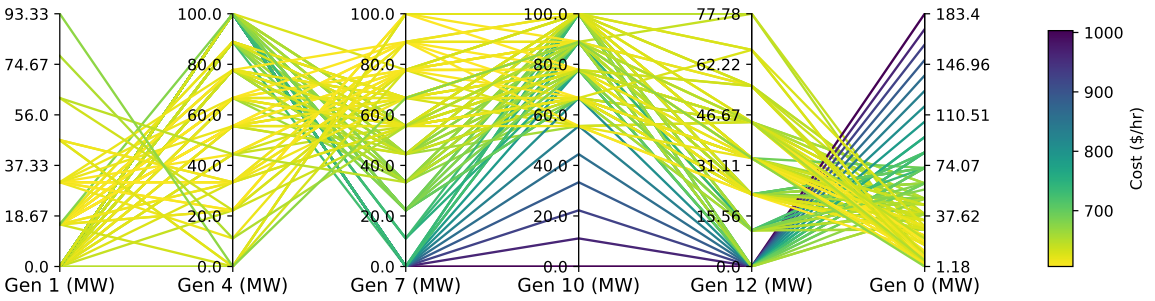

Figure 3.3: Power Output of Nondominated Solutions

From Figures 3.2 and 3.3, we gain insights into system-level performance. For example, withdrawal and consumption generally present tradeoffs consistent with broader findings in the literature Tidwell et al. [2012]. There is also a small tradeoff between cost and emissions, as evident by the few solutions crossing at the bottom of the emissions axis, which is consistent with previous findings Abido [2003b], Ah King and Rughooputh [2003].

Of notable interest are the many solutions that emerge that have low withdrawal (depicted as purple). These solutions have poor performance with respect to cost, emissions, and water

consumption (depicted as high intersections). From Figure 3.3, we see that these solutions generally do not use the once-through cooled generators (7, 10, and 12) and do use the natural gas generators with cooling towers (0 and 4). Conversely, we see many of the solutions that have low emissions (depicted as yellow) have high water withdrawal and average water consumption performance. Such solutions highlight how incorporating external objectives into traditional OPF formulations can drastically change the behavior of the system. Furthermore, such solutions highlight the potential tradeoffs among cost, water, and emissions in water-energy systems.

3.4.2 Quantitative Tradeoff Analysis

We can quantify the tradeoffs that exist in this system by visualizing the objective correlation of the nondominated sets as is done in Figure 3.4. Specifically, this figure depicts the correlation of every axis (objective) pair in Figure 3.2. To aid in visualization, the color of each cell represents the correlation value. Objectives that have a high positive correlation are generally harmonious while objective pairs with high negative correlations present tradeoffs (i.e., performance increases in one objective degrade performance in the other objective).

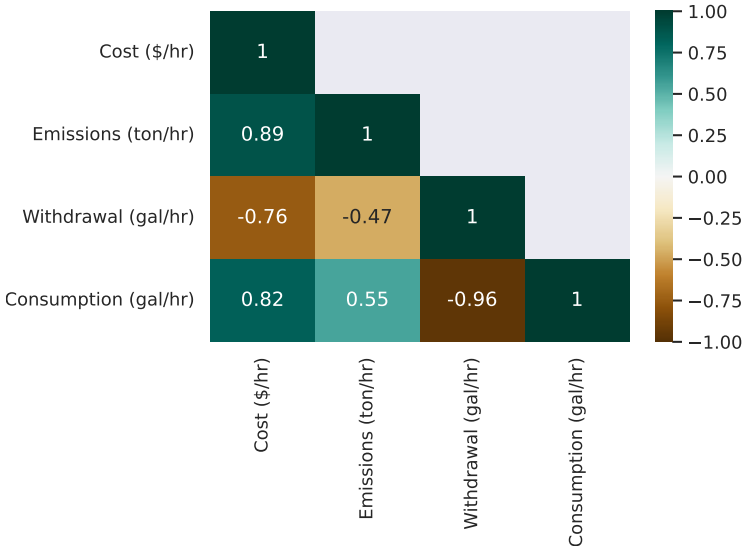

Figure 3.4: Correlation of Objectives in Nondominated Set

Figure 3.4 allows analysts to quickly summarize trends in the nondominated set. For example, the large negative correlation values of water withdrawal with consumption and cost, confirm the behavior previously discussed in Figure 3.2. Conversely, emissions are semi-harmonious with cost. This figure also allows analysts to quickly compare the degree to which tradeoffs occur. For example, Figure 3.4 allows analysts to quickly see the tradeoff between water withdrawal and consumption is stronger than the tradeoff between water withdrawal and cost. Such a trend may not be as obvious when simply looking at the nondominated performance (e.g., Figure 3.2).

Viewing Figures 3.2 - 3.4 allows analysts to quickly gain insights into system-level behavior by identifying how objectives interact with one another as well as what system components are responsible for changes in system performance. Such insights could be useful for comparing system behavior across multiple systems. For example, the methods presented in this paper would be useful if analysts were interested in comparing the tradeoffs among cost, water use, and emissions across several power systems. First, the analyst could find the nondominated set of solutions to our multi-objective OPF formulation for each system. Then, by visualizing the objective correlation plots for each system (such as Figure 3.4), the analysts could quickly compare the severity of tradeoffs among individual objective pairs. Identifying such tradeoffs would help analysts to compare potential objective performance vulnerabilities across energy systems. Such insights could be used to inform energy policy for ensuring that resources are allocated to systems with the most potential vulnerabilities.

3.5 Conclusion

In this chapter, we first demonstrated how cost, emissions, water withdrawal, and water consumption can be incorporated into a multi-objective OPF formulation that does not rely on specifically weighting each objective. We then applied this formulation to an example power system to show the system-level insights that such a formulation facilitates. Specifically, we showed how visualizing the correlations among each objective pair allows analysts to summarize system performance as well as compare performance across systems.

An additional insight gained from this work was the vast number of nondominated solutions that emerged from DC OPF operations when more than just economic costs were considered. For example, not only can solutions emerge that solely emphasize other objectives, but *numerous* solutions that compromise among all the objectives emerge from a multi-objective perspective. This idea of solutions that emerge to the multi-objective DC OPF problem will be expanded in Chapter 5.

Applying these methods to larger systems also poses a problem for real-time operation. For example, there exists a computational challenge for finding the epsilon nondominated solutions as increasing the number of generators would increase the size of the decision space. Using multi-objective evolutionary algorithms reduces the computational burden by more intelligently searching the decision space and will be applied in Chapter 5. However, decision-makers would still be required to select a nondominated solution from a set, which may be infeasible for real-time operations. The next chapter (Chapter 4) addresses this downside through a policy-focused reformulation of the multi-objective DC OPF formulation where objectives are weighted. The ability to quickly and consistently compare the tradeoffs in these systems as demonstrated in this chapter will be crucial to apply policy insights from one system to another.

Another extension of this work would be to apply the presented methods to more realistic power systems over several timesteps. Although care was taken to ensure the power system in this work had realistic behavior, the tradeoffs identified in this work do not necessarily reflect broader trends in energy systems. To gain insights into the behavior of actual power systems, our methods would need to be implemented by analysts with access to true power system models. One possible challenge for applying these methods to real systems would be modeling water use and emissions of external grids; although representative emissions and water use coefficients could be assumed. Another option for more broadly-applicable insights would be to use synthetic models of true power systems Birchfield et al. [2017] as will be demonstrated in Chapter 5.

Chapter 4

The Impact of Water Policy on Power Systems Operations

The previous chapter established a framework to analyze the tradeoffs of water/energy systems whereas this chapter introduces a policy framework to incorporate the water used by power systems as an additional *incentive* for power system operations. In other words, the previous chapter focused on analyzing existing system performance where as this chapter introduces a mechanism to influence this behavior via a policy decision. Specifically, this policy decision is the specification of an "operational water penalty" that assigns a monetary value to the different types of generator water use. We then analyze how such decisions impact the various facets of power system operations. These findings have been adapted from their original publication in [Kravits et al., 2022b].

4.1 Introduction

Modern power grids respond to stressors that are out of the control of system operators (i.e., exogenous stressors). For example, electric loads on the grid change over time. On shorter operational timescales, electric loads vary throughout the day based on user types within an electric system [Merrick, 2016, EIA, 2020a]. These demands also vary on longer timescales such as seasonal changes [EIA, 2020a, Archibald et al., 1982] as well as the additions of new loads (e.g., electric vehicle charging or new development) being added to the grid [Hatziargyriou et al., 2013, Jacob, 2021]. Thermoelectric water withdrawal and consumption rates (defined in Section 2.1.1) change over time as they are impacted by extreme climatic events such as droughts, heatwaves, or upstream

water users [Scanlon et al., 2013b, Lydersen, 2016, Meng and Sanders, 2019].

The temporal variability of electric loads, thermoelectric withdrawal rates, and thermoelectric consumption rates are particularly important during extreme natural events. These events can be broadly categorized into events that impact electric loads, events that impact thermoelectric water use rates, and events that impact both. For example, a drought event may impact the thermoelectric water use rates while a heatwave may impact the electric loading [Scanlon et al., 2013b, Harto et al., 2012]. Such system-stressing events can also occur simultaneously, further stressing energy systems [Galbraith, 2011, Freedman, 2012]. In these extreme operational scenarios, system operators often manually intervene in traditional operations (e.g., shutting down specific generators or granting thermal variances) [Harto et al., 2012, Poumadère et al., 2005, Lubega and Stillwell, 2018a].

The previous chapter demonstrated the value of incorporating thermoelectric water use into system operations using the example of a water-informed OPF formulation. Such water-informed operations are important as they (1) promote system coordination rather than manual intervention by system operators, as well as (2) offer a rapid way for system operators to respond to current drought events, especially if long-term solutions are infeasible due to a lack of time to implement [Pacsi et al., 2013]. This chapter refines the previous water-informed OPF formulation to specify an operational weight for the water consumed and withdrawn - thus eliminating the need to choose a nondominated generator dispatch in real-time.

Solving a single case of a water-informed OPF, such as was done in the previous chapter, only allows for insights into a single snapshot of system performance. For example, in the demonstration of their formulation, Fooladivanda and Taylor [2015] assume a single price of water consumed ($\$1/m^3$), load demand case, withdrawal rates, and consumption rates. However, Lubega and Stillwell [2019] found that a thermoelectric cooling water price is a function of many dynamic economic factors. Furthermore, a $\$1/m^3$ cost is a high price for cooling water when compared to traditional market prices [Lubega and Stillwell, 2019, Brewer et al., 2007]. Similarly, loads, withdrawal rates, and consumption rates are all impacted by extreme demand and climate events as previously stated. Many studies have modeled loads as a stochastic process to attempt to capture the uncertainty of

the temporal variability of loads in the grid [Taiyou Yong and Lasseter, 2000, Hu et al., 2010]. Such studies have found that by including this variability, solutions to the OPF problem are drastically different from their deterministic counterparts. Therefore, to allow insights into longer-term system performance, our operational scenario analysis framework considers the water optimization weights, generator water consumption rates, generator water withdrawal rates, and system loadings as "exogenous parameters" that are outside of the control of the system operator, and therefore could be different every time the OPF is solved, due to system conditions. Such a novel consideration allows us to isolate the impacts of various inputs on the water-energy system.

The operational scenario analysis framework proposed in this chapter also extends the previous literature by conducting several sensitivity analyses to quantify the individual significance and effects of each exogenous parameter. We show that such a novel framework allows analysts both system-wide insights into the operations of a power system as well as identifying the most critical generators that impact various aspects of system performance. This framework allows the most important generators of a power system to emerge from the underlying mathematics of short-term power systems operations, rather than assuming generator importance a priori. We first define our operational scenario analysis framework consisting of our water-informed OPF formulation, an embedding of the water-informed OPF into a larger multi-objective water/power systems cosimulation, and two sensitivity analyses of the cosimulation model. We then demonstrate the insights possible through the operational scenario analysis framework on a synthetic case study located in the Midwestern United States.

4.2 Methodology

An overview of the cost/water power system cosimulation is presented in Figure 4.1. First, we define all the exogenous parameter inputs to the cosimulation. Then, the water-weighted OPF formulation finds the optimal power output at each generator. Finally, multiple objectives are a function of the optimal power outputs and the exogenous parameters.

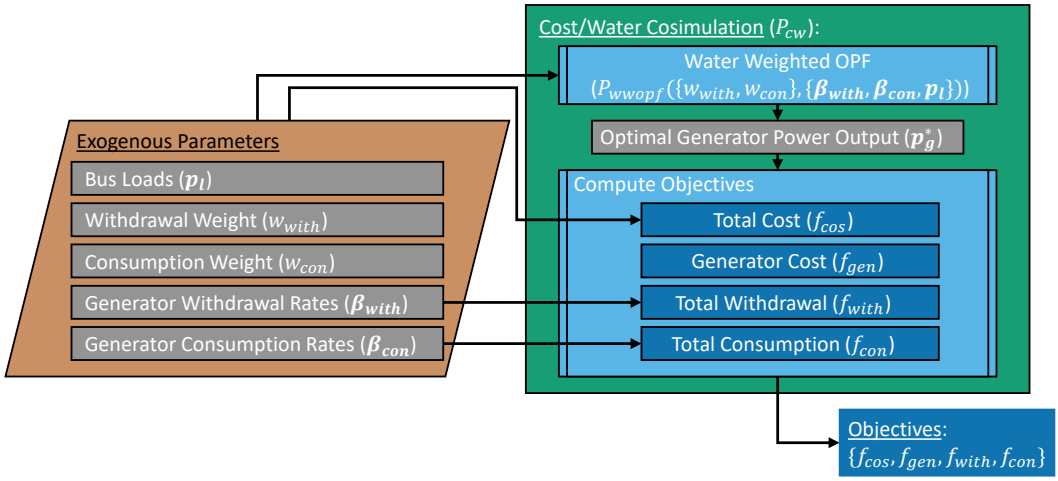

Figure 4.1: Overview Cost/Water Power System Cosimulation. Exogenous parameters, parameters out of the control of system operators, are inputs to the cosimulation. These parameters are used in the water-weighted OPF formulation to find the optimal generator output. These parameters are also used to compute objectives as indicated. Every feasible set of exogenous parameters corresponds to a set of objective values.

4.2.1 Water-Weighted OPF Formulation

Just as the multi-objective water-emission-informed OPF formulation from the previous chapter, the water-weighted OPF formulation (P_{wwopf}) finds the set of generator power dispatch $\mathbf{p_g}$ that minimizes an objective function while also satisfying the DC simplification of the power flow equations. The major difference between the formulation in this chapter is the objective function is a weighted sum of water and economic costs (See 2.3.2 for more reference on weighted formulations).

The inputs of (P_{wwopf}) are exogenous parameters. As previously mentioned, exogenous parameters are outside of the control of the system operator, and therefore could be different every time the OPF is solved, due to system conditions. In this formulation, these exogenous parameters include the water withdrawal and consumption rates at each generator, the loads at each bus, as well as the weights of water withdrawn and consumed.

The withdrawal rate and consumption rate at each generator represent a generator's "water

efficiency", the amount of water used to produce a given amount of electricity. The withdrawal rate at generator j is denoted as $\beta_{with,j}$. Similarly, the consumption rate at generator j is denoted as $\beta_{con,j}$. These terms are collected into vectors $\boldsymbol{\beta_{with}}$ and $\boldsymbol{\beta_{con}}$ of length G, the number of generators in the system.

Value ranges of withdrawal and consumption rates can be estimated based on historic datasets of electricity production, water withdrawal, and water consumption. Additionally, general ranges of withdrawal and consumption rates have been estimated based on fuel and cooling system types [Macknick et al., 2012]. Physically, withdrawal and consumption rates can be interpreted such that water-efficient generators would have lower rates than water-inefficient generators (i.e., it takes water-efficient generators less water to produce a unit amount of electricity).

Other exogenous parameters include the loads $p_{l,i}$ at each bus i. These terms can also be collected into a vector $\mathbf{p_l}$. The set of buses in the system $\mathcal{N}$ has the length B. Therefore, $\mathbf{p_l}$ also has the length B (buses with no load have a zero as its corresponding entry in $\mathbf{p_l}$).

The two remaining parameters in this formulation are the operational weight associated with the water withdrawn w_{with} and the operational weight associated with water consumed w_{con}. Each of these terms specifies a water penalty assigned to generators that withdraw or consume water. The units of these weights are a monetary cost per volume of water used. For example, a policy that assigns a low value of the withdrawal weight w_{with} and a high value of the consumption weight w_{con} gives preference to generators that do not consume water. Therefore, generators that consume a lot of water would have a low power output while generators that consume less water will have a higher output. Through varying values of w_{with} and w_{con}, we create operational policies based on differing levels of withdrawal and consumption preference. These preferences could be correlated with constraints in the water system. In real-world systems, these weight values could be in the form of a monetary tax on water use, for example.

Our water weighted OPF formulation (P_{wwopf}) is defined as follows:

$$\min_{\mathbf{p_g}} \quad \sum_{j\in\mathcal{G}} a_j + b_j p_{g,j} + c_j p_{g,j}^2 + w_{with} \sum_{j\in\mathcal{G}} \beta_{with,j} p_{g,j} t + w_{con} \sum_{j\in\mathcal{G}} \beta_{con,j} p_{g,j} t \tag{4.1}$$

$$\text{s.t.} \quad p_{l,i} - \sum_{k\in\mathcal{G}_i} p_{g,k} = \sum_{m\in\mathcal{N}} B_{im}\theta_{im}, \quad \forall i \in \mathcal{N} \tag{4.2}$$

$$-\Lambda_{max,im} \leq B_{im}\theta_{im} \leq \Lambda_{max,im}, \quad \forall im \in \mathcal{L} \tag{4.3}$$

$$\underline{p}_{g,j} \leq p_{g,j} \leq \bar{p}_{g,j}, \quad \forall j \in \mathcal{G} \tag{4.4}$$

This formulation uses the same notation introduced in Section 2.4.2.

The objective function is a weighted sum of generator costs, water withdrawal, and water consumption. The coefficients of a_j, b_j, and c_j reflect the monetary cost as a function of active power output for each generator j. $\beta_{with,j}$ and $\beta_{con,j}$ reflect the water withdrawn and consumed as a function of active power output for each generator j. t represents the timestep conversion factor of the optimization problem, which converts the power output of generators to an energy output such that the water withdrawal and consumption rates can be applied. As previously discussed, w_{with} and w_{con} capture the monetary cost of the water withdrawn and consumed, respectively.

4.2.2 Objective Outputs

The cost and water cosimulation relies on the water-weighted OPF but produces several objective outputs that each capture unique and analyst-relevant aspects of a system's performance. One such measure of the system performance is the objective function from the water-informed OPF. This objective captures the "total effects" of the system (i.e., it captures the generator costs, costs from withdrawal, and costs from consumption). The total cost objective is defined as

$$f_{cos} = \sum_{j\in\mathcal{G}} a_j + b_j p_{g,j} + c_j p_{g,j}^2 + w_{with} \sum_{j\in\mathcal{G}} \beta_{with,j} p_{g,j} t + w_{con} \sum_{j\in\mathcal{G}} \beta_{con,j} p_{g,j} t \tag{4.5}$$

The total cost objective F_{cos} is critical as it captures both the direct monetary costs of operations as well as the costs associated with the generator water usage. As was visually depicted in Figure 4.1, it is the only objective that directly uses all the exogenous parameters.

Another measure of system performance is the summation of all the direct generator operational costs defined as

$$f_{gen} = \sum_{j \in \mathcal{G}} a_j + b_j p_{g,j} + c_j p_{g,j}^2 \tag{4.6}$$

This "traditional" OPF objective of generator costs serves as a reference for analysts familiar with system performance under traditional OPF formulations. As is visualized in Figure 4.1, this objective is the only objective that is *solely* a function of generator power outputs, such that it also serves as a proxy for measuring total system generator outputs and will not be directly impacted by varying exogenous parameters. It will only be impacted by exogenous parameter values that change the generator power output values ($\mathbf{p_g}$).

The final two objectives capture the total amount of water withdrawn and consumed in the system and are defined as

$$f_{with} = \sum_{j \in \mathcal{G}} \beta_{with,j} p_{g,j} t \tag{4.7}$$

$$f_{con} = \sum_{j \in \mathcal{G}} \beta_{con,j} p_{g,j} t \tag{4.8}$$

Recall that t is a conversion factor to convert the power output to an energy output over a timestep. These objectives serve as a ground truth of the volume of water that would be used in the system over the optimization timestep (and does not consider the withdrawal weight w_{with} or consumption weight w_{con}). Such information is important for operations during climatic extremes where the total amount of water usage can have detrimental ecological effects as well as operational impacts.

4.2.3 Sensitivity Analysis of Uniform Variability

Our operational framework focuses on two ways that exogenous parameters can vary: uniformly and non-uniformly. We define uniform variability as changes that impact parameters in all parts of the system in the same way. For example, during an extreme loading event, a system

may experience increased loading across all buses. However, non-uniform variability impacts each exogenous parameter differently. For example, the water use of an upstream utility may only impact generator withdrawal rates at a single downstream plant. We introduce different coefficients on each exogenous parameter to mathematically model the different types of variability. Our operational scenario analysis framework utilizes two different types of sensitivity analyses of these introduced coefficients to gain insights into both the uniform and non-uniform variability of our multi-objective water-informed OPF model.

The demands at each bus ($\mathbf{p}_L$) are assumed to vary uniformly throughout system operation (i.e., all the loads increase at once). Mathematically, we present this uniform variability as a uniform loading coefficient (c_{load}) multiplied by $\mathbf{p_L}$. A uniform loading coefficient (c_{load}) greater than one means that the system is experiencing increased loading relative to its baseline loading case. Such uniform increases would generally be the result of higher system-wide temperatures being linked to higher system-wide loading [PJM, 2019].

The generator withdrawal rates ($\boldsymbol{\beta}_{with}$) and generator consumption rates ($\boldsymbol{\beta}_{con}$) also vary uniformly. Similar to the loading uniform variability, the uniform water exogenous parameter variability is mathematically represented as a uniform water coefficient c_{water} multiplied by $\boldsymbol{\beta_{with}}$ and $\boldsymbol{\beta_{con}}$. A uniform water coefficient (c_{water}) less than one means that the generators are becoming more water efficient (using less water to produce the same unit of electricity) while a coefficient of greater than one means the generators are becoming less water efficient (using more water to produce the same unit of electricity). Such variability has been categorized across cooling technology, fuel technology, space, and time [Macknick et al., 2012, Peer and Sanders, 2016, Huston, 1975]. We focus on sources of variability in time, based on assuming a system with non-changing cooling technologies and generators. Uniform variability, i.e., processes that would impact all generators in a given system, include seasonal, climatic, and hydrologic/hydraulic variability [Lee et al., 2020, Clement et al., 2017, Dziegielewski et al., 2002].

In the uniform sensitivity analysis, we test the sensitivity of the operational water penalties w_{with} and w_{con}, as well as the exogenous uniform loading coefficient (c_{load}) and uniform water coef-

ficient (c_{water}). These four parameters of our sensitivity analysis are referred to as "input factors" to avoid confusion with the entire set of operational water penalties and exogenous parameters [Pianosi et al., 2016]. The goal of this analysis is to (1) identify how the water and load uniform variability interact with one another to gain insights into what general mechanisms impact system performance, as well as (2) determine which regions of the input factor space cause extreme objective performance for each of the objectives in our water-weighted OPF model.

We use a qualitative global mapping sensitivity analysis to analyze the uniform variability [Pianosi et al., 2016, Singh et al., 2014, Harper et al., 2011]. First, we conduct a sampling of the input factor space as depicted in Figure 4.2. This sampling creates a set of input factor scenarios and each scenario's corresponding four objective values. The underlying assumptions of this sampling are dependent on the analysts' access to data as well as system configurations. After the sampling, we create several plots to visualize the impacts of the input factors on both system performance as well as the behavior of individual system components. In Section 4.4.1, we demonstrate how to find the bounds of these input factors, one possible way to conduct sampling of the input factor space, as well as how to interpret the resulting visualizations.

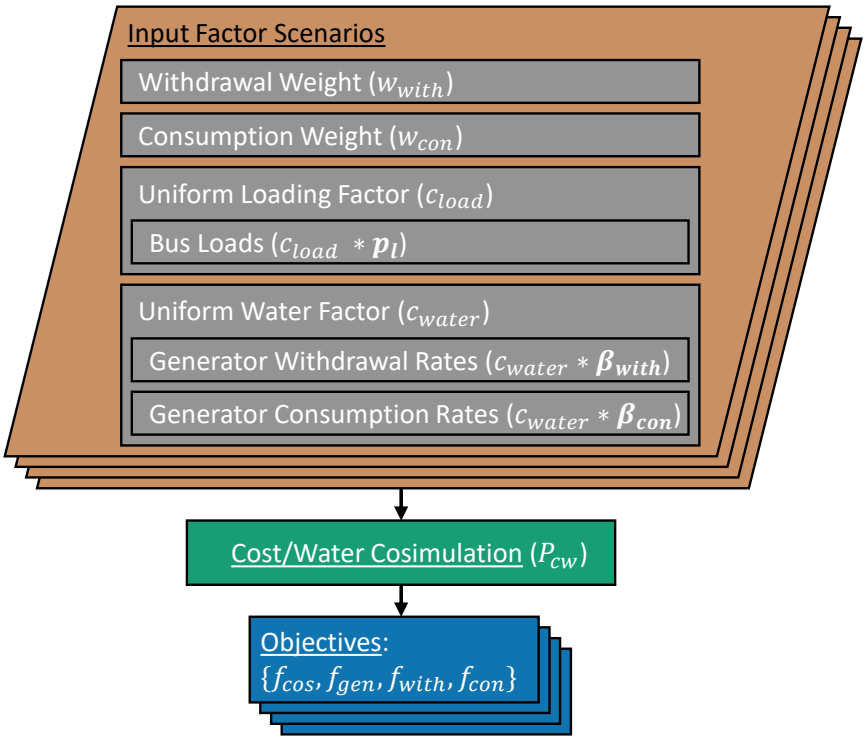

Figure 4.2: Sampling for Sensitivity Analysis of Uniform Variability

4.2.4 Sensitivity Analysis of Non-Uniform Variability

As previously discussed, the non-uniform variability of generator withdrawal rates ($\boldsymbol{\beta}_{with}$) and generator consumption rates ($\boldsymbol{\beta}_{con}$) can be attributed to plant-to-plant discharging interactions, a change in cooling system operational policies, or other water discharges in the system [Tidwell et al., 2019, Miara et al., 2018, Yang and Dziegielewski, 2007, Fooladivanda and Taylor, 2015]. Physically, these processes all impact different fuel/cooling type combinations differently and pose a key operational challenge. The non-uniform sensitivity analysis allows us insights into how these non-uniform processes impact system-wide performance under several exogenous operational and policy scenarios. These exogenous operational and policy scenarios are defined by the input factors already examined in the uniform sensitivity analysis: the withdrawal weight w_{with}, the consumption weight w_{con}, and the uniform loading coefficient c_{load}.

Unlike the uniform sensitivity analysis where a single uniform water coefficient (c_{water}) im-

pacted generator water use *at all plants*, in the non-uniform case, we introduce unique non-uniform water coefficients for each plant g denoted as $c_{water,g}$. Assuming there are G unique plants in a system, there will be G non-uniform water coefficients. This formulation assumes that generators in the same plant have the same fuel and cooling types such that no processes impact single generators differently within a plant. If a single plant location consists of multiple generator/cooling system types, a unique non-uniform water coefficient is assigned to each set of unique generators/cooling system types. This condition is demonstrated in the case study in Section 4.4.2.

The G non-uniform water coefficients constitute the input factors of the non-uniform sensitivity analysis. Just as in the uniform sensitivity analysis, the input factor space must be sampled for each exogenous operational and policy scenario. The sampling of the non-uniform input factor space is visualized in Figure 4.3. Starting with the outermost layer, we see the exogenous operational and policy scenario defines the values for the withdrawal weight w_{with}, the consumption weight w_{con}, and the uniform loading coefficient c_{load}. Then, the input factors whose sensitivity is tested are the non-uniform water coefficient of each plant in the system from g to G. Again, just as is in the uniform case, each set of input factor scenarios produces a set of objective function values. This entire sampling is repeated for each exogenous operational and policy scenario.

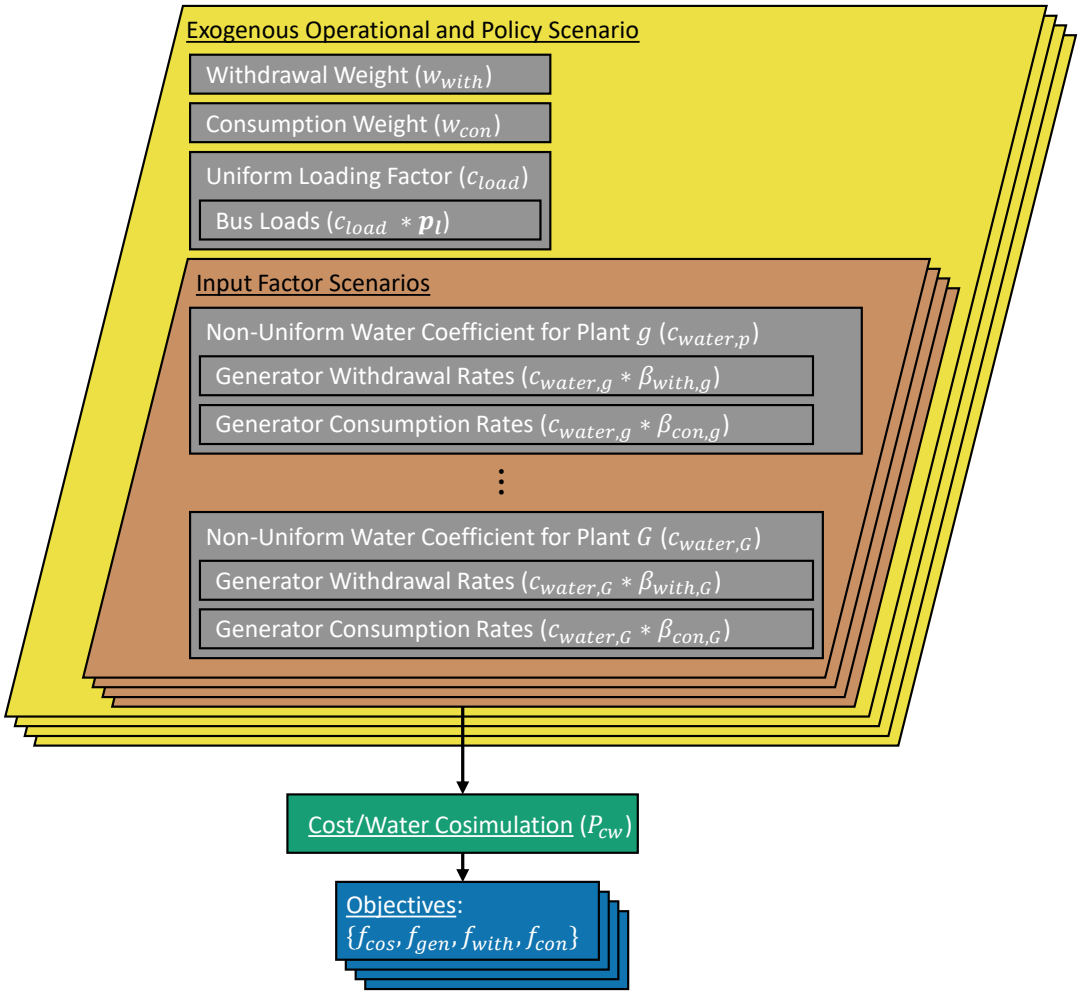

Figure 4.3: Sampling for Sensitivity Analysis of Non-Uniform Variability. This approach samples each plant's water coefficient from g to G in a system.

A variance-based sensitivity analysis is implemented for the non-uniform variability analysis because it allows us to rank and quantify the significance of input factor relationships. Variance methods assume that the input factors are stochastic variables that produce distributions of each objective value. Therefore, they assume that the variance of the output distribution is a suitable proxy for uncertainty and that the contribution of an input factor to the output variance is a measure of its uncertainty [Pianosi et al., 2016]. Several indices have been proposed to quantify this process, with the Sobol index being widely accepted. The first order Sobol index ($S_{i,j}^{First}$) for objective j captures the "main effect" of an input factor x_i and is defined as

$$S_{i,j}^{First} = \frac{V_{x_i}\left[E_{x_{\sim i}}\left(y_j \mid x_i\right)\right]}{V(y_j)} \tag{4.9}$$

where y is the objective value for objective j, V is variance, E is the expected value, and $x_{\sim i}$ is all the input factors except the i^{th} value. Conceptually, $S_{i,j}^{First}$ is the expected reduction in output variance that can be obtained when fixing x_i [Pianosi et al., 2016, Sobol, 1990]. Physically, $S_{i,j}^{First}$ quantifies how important input factor x_i is to objective j. For example, $S_{c_{water,1},f_{cos}}^{First}$ quantifies how important the water use at plant 1 is to the total cost of the system.

In Section 4.4.2, we demonstrate a nonparametric method for both sampling the non-uniform input factor space as well as estimating the first order Sobol index. However, many methods for estimating Sobol indices could be implemented for a non-uniform sensitivity analysis as long as all assumptions are satisfied.

4.3 Case Study: Water-Extended Illinois 200 Bus System

The following section describes the synthetic yet realistic case study chosen to demonstrate our operational scenario analysis framework we call the Water-Extended Illinois 200 Bus System. We show how we use EIA-reported thermoelectric water use information to ensure realistic water use for our synthetic test system. This water-use-assigned test case is then used to demonstrate the insights possible from both the uniform and non-uniform sensitivity analyses. An overview of the case study is provided in Figure 4.4.

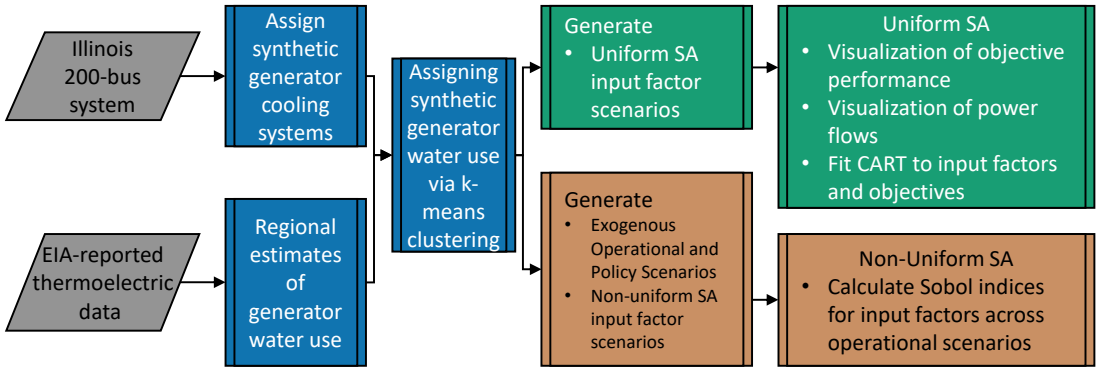

Figure 4.4: Case Study Preparation Overview. Case study applies the proposed uniform sensitivity analysis (SA) as well as the non-uniform SA. Dark blue boxes correspond to sections 4.3.2 - 4.3.4. Green boxes correspond to the sections 4.4.1 and brown corresponds to 4.4.2

4.3.1 Synthetic Grid

Due to national security concerns, models of the actual electricity grid contain sensitive data, so many frameworks have been developed to generate synthetic grids that retain many valuable properties of the true grid while not revealing sensitive data [Birchfield et al., 2017]. The framework generally consists of two phases: substation placement and transmission topology specification. The substation placement phase specifies the locations and specifications of loads and generators. This phase is based on a weighted distance clustering algorithm of loads in each postal code and known generator locations. One constraint in the algorithm is that hydroelectric, nuclear, or renewable energy resources cannot be grouped with nonrenewable energy sources. The final results of this phase are synthetic but realistic substation locations containing loads and generators. The second phase then connects these substations based on an iterative algorithm with several criteria based on line property constraints as well as line topology constraints. Finally, a variety of other devices are inserted in the network to regulate reactive power and voltage, such as shunt capacitor banks, transformer taps, and synchronous condensers.

We use the Illinois 200-bus synthetic grid currently hosted in the Electric Grid Test Case Repository [Birchfield et al., 2017]. As the name implies, this synthetic grid is based on a part

of the transmission system in Illinois - a region that has historically been prone to thermoelectric temperature discharge violations. This 180-line transmission system has a 2800 MW capacity with half of its capacity coming from coal and the remaining capacity being equally split between natural gas, wind, and nuclear.

Instead of simulating economic dispatch, we manually dispatch all generators in the system. However, the simulation of other operational processes is discussed in Section 4.4. Recall, that these generators *do not* explicitly correspond to true generators but are rather synthetic generators based on aggregation. Fortunately, these synthetic generators *do* have coordinates on a coordinate reference system specified by the distance weighting algorithm and are available in the PowerWorld formats of the synthetic case. Figure 4.5 shows these locations. The locations of the generators reported to the U.S. Energy Information Agency (EIA) are also depicted. These generators are called "EIA generators" for the remainder of this analysis.

The Illinois 200-bus synthetic grid does not initially include withdrawal rates (β_{with}) or consumption rates (β_{con}) for the synthetic power generators. Therefore, we infer realistic withdrawal rates (β_{with}) and consumption rates (β_{con}) in a two stage process. As explained below, we infer the synthetic generator cooling system type based on location and characteristics. Then, we determine withdrawal rates (β_{with}) and consumption rates (β_{con}) from regional aggregations of publicly available power systems data [EIA, 2020b].

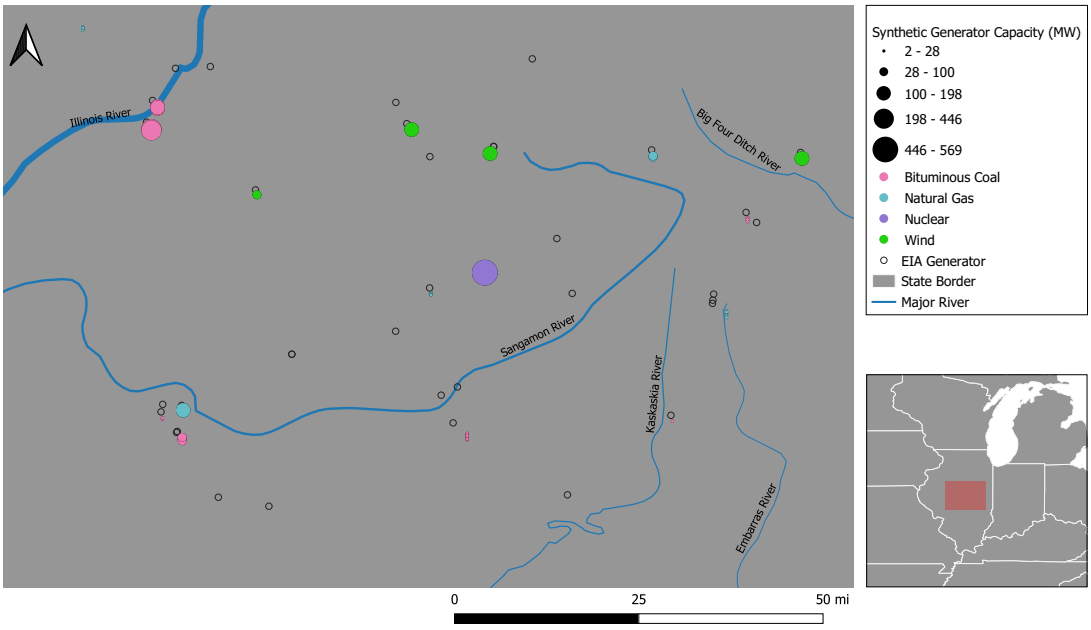

Figure 4.5: Location and Breakdown of Generators from Illinois 200-Bus System. The color of the synthetic generator marker reflects the fuel type. The size of the synthetic generator marker reflects the maximum power output of the generator (splits based on Jenks classification). The size of the river line reflects the relative annual flows for 2019.

4.3.2 Assigning Synthetic Generator Cooling Systems

We first assigned each synthetic generator a cooling system. We manually matched the synthetic generators to EIA generators who reported data on Forms 860 and 923. Figure 4.5 shows both synthetic and EIA generators. From inspection of this figure, we assign cooling systems to the synthetic generators. For each synthetic generator, we assign a cooling system based on an EIA generator that is spatially close, has a matching fuel type, and has a similar capacity to the synthetic generator. This process ensures that the synthetic generators are assigned representative and realistic cooling systems.

4.3.3 Regional Estimates of Generator Water Use

We gathered regional estimates of withdrawal rates (β_{with}) and consumption rates (β_{con}) for the fuel type/cooling system combinations present in our case study. Specifically, we use data from EIA-reported generators in the state of Illinois, as this approach ensures that water use data come from generators that have the same political regulations and climatic conditions as the synthetic generators. Because the EIA generator dataset is generated from human-reported data, this dataset is notoriously noisy and often requires preprocessing [Tidwell et al., 2019, Meng and Sanders, 2019, Grubert and Sanders, 2018, Harris and Diehl, 2017, Peer and Sanders, 2016, Scanlon et al., 2013a, Averyt et al., 2013]. We build upon the frameworks presented in these studies and implement the following filtering criteria for the regional EIA dataset:

- Generators must be located in Illinois.
- Only consider generator fuel type/cooling system combinations present in synthetic generators
- Only keep observations that reported finite withdrawal and consumption rates (i.e., remove zeros or division by zero errors)
- Only keep generators that reported water use at least half of the months between the period of observation (2014-2019)
- Remove outlier withdrawal and consumption values based on the Modified Z-Score test [Iglewicz and Hoaglin, 1993] for each generator, which was previously used to filter the EIA dataset in Peer and Sanders [2016].

The distributions of the resulting regional EIA-reported estimates of withdrawal rates (β_{with}) and consumption rates (β_{con}) are presented in Figure 4.6. This plot is consistent with the findings from Peer and Sanders [2016], where we see that once-through cooling systems have a more pronounced impact on withdrawal rate than fuel type.

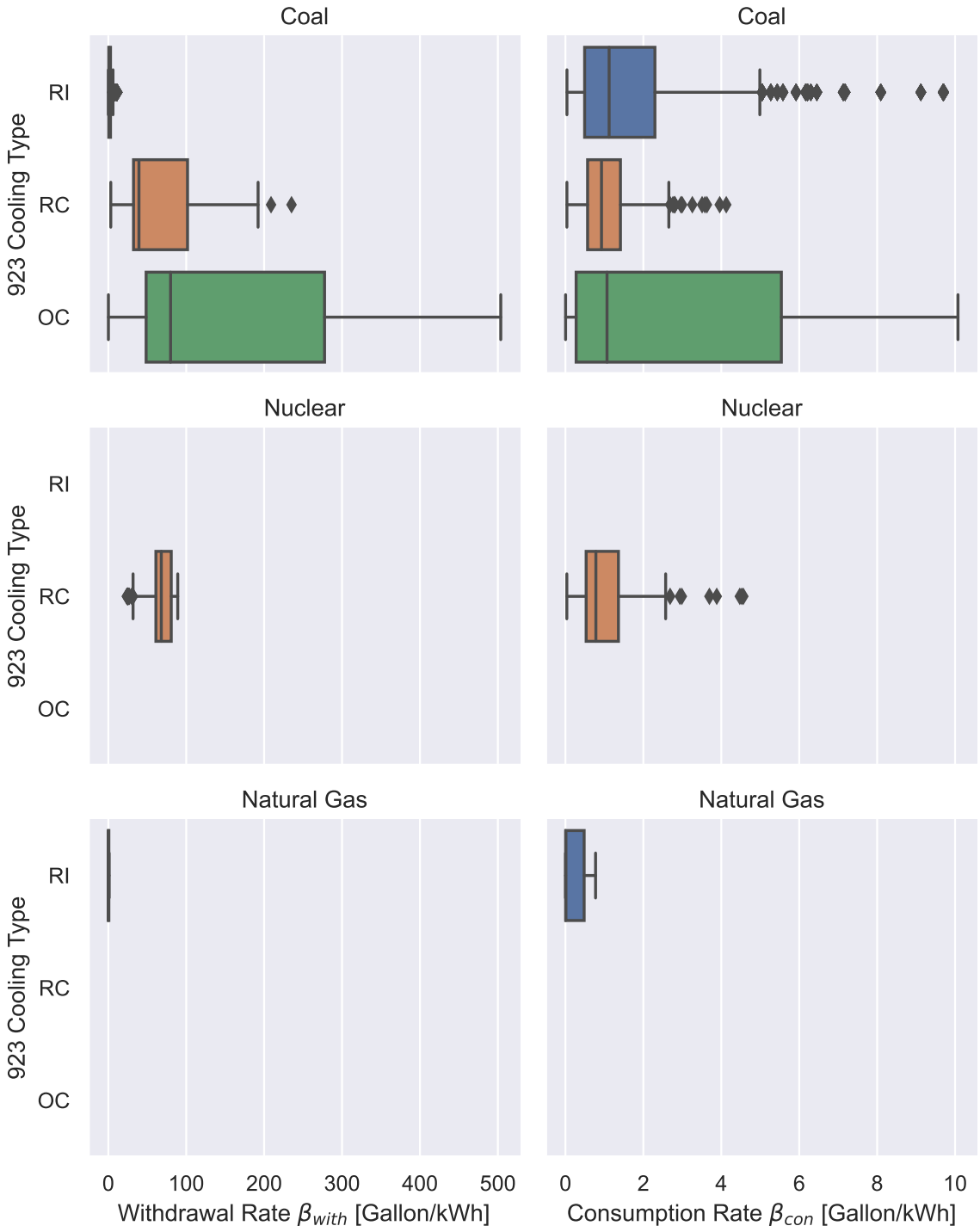

Figure 4.6: Regional EIA-Reported Dataset of Water Usage. Abbreviations: Recirculating with Induced Draft Cooling Tower (RI), Recirculating with Cooling Ponds (RC), Once-through with Cooling Ponds (OC)

With regional estimates of withdrawal rates (β_{with}) and consumption rates (β_{con}) for the generator fuel type/cooling system combinations in our synthetic grid, we find representative values of water use for each synthetic generator.

4.3.4 Assigning Synthetic Generator Water Use Via K-Means Clustering

We use the regional estimates of withdrawal rates (β_{with}) and consumption rates (β_{con}) to assign the withdrawal rates and consumption rates for each synthetic generator. For the nuclear and natural gas regional generators, the median value is justified due to the symmetry of the distributions and lack of variation. However, the coal generators exhibit a notable spread in withdrawal and consumption rates, as shown in Figure 4.6. The variation of coal generator withdrawal rates (β_{with}) and consumption rates (β_{con}) can be attributed to the variation of coal generator capacities for this region. This trend emerges by plotting the withdrawal rates (β_{with}) and consumption rates (β_{con}) against the capacities of the coal plants. Several clusters emerge for each cooling type based on the capacities of the generators. The median value of each corresponding cluster informs the synthetic generator water use.

This regional-estimate-with-clustering methodology is not used for wind and solar generators, which do not require cooling systems, and have zero values for their exogenous water parameters. Similarly, small-capacity natural gas combustion turbines are also assumed to use negligible amounts of water, so zero values are assumed for their exogenous water parameters [Stillwell et al., 2011].

4.4 Results and Discussion

The following section demonstrates our operational scenario analysis previously outlined in Section 4.2 for the case study. We perform a global sensitivity analysis of the uniform and non-uniform variability of our multi-objective water-informed OPF model. This section provides an example of both uniform and non-uniform sensitivity analyses based on publicly available data. However, applying these sensitivity analyses to different datasets or system configurations may

require modification of the specific implementation demonstrated in this analysis.

4.4.1 Impacts of Uniform Variability on System Performance

We apply the uniform sensitivity analysis outlined in Section 4.2.3 to our case study to first demonstrate the efficacy of the water-informed OPF formulation as well as examine how system-wide sources of variability impact system performance. Table 4.1 outlines the bounds of the four input factors for our case study. Starting with the loading in the synthetic grid, the algorithm in Birchfield et al. [2017] creates realistic load profiles based on population densities. Additionally, we assume that the default loading supplied by this test case is generally reflective of normal loading conditions (i.e., $c_{load} = 1.0$). We tested feasible uniform loading coefficients c_{load} by increasing values until the traditional DC OPF became infeasible due to thermal line limits or lack of generation capacity. This simulated increase resulted in a maximum feasible c_{load} value of 1.6. To ensure that this bound is reasonable given actual conditions, we also examined historic loads. The synthetic grid for this case study would be located in the Midcontinent Independent System Operator (MISO). MISO only provides load data for its entire system and not for individual hubs. The distribution of historic load data as well as the uniform loading coefficients for the years 2018 to 2019 were analyzed yielding that 1.6 is just out of the historic range of load coefficients so we set the max uniform load coefficient value to be 1.5 to ensure a value that is both feasible and has occurred in the historic record. To ensure that this value is realistic, we observe that a value of 1.5 is roughly the 99th percentile of historic loading. Studies have shown that the frequency of the historic 99th percentile loading occurring is expected to increase up to 1500 percent depending on the region and climatic predictions utilized [Auffhammer et al., 2017]. Therefore, we set 1.5 as the upper bound of the uniform loading coefficient as it is both a historically realistic value, feasible for our system, as well as a potential planning metric for analyzing a power system's preparedness for uncertain future conditions.

A similar process was followed to assign the ranges of the uniform water coefficient c_{water}. First, well-behaved ranges were found to be between 0.5 and 1.5 (i.e., beyond these values the

water-informed OPF becomes ill-conditioned and fails to converge). The distribution of historical c_{water} values suggested that our variable is in the range of historical bounds. Additionally, we use empirical estimates from standard thermoelectric water use models to show that such changes can result from reasonable changes to inlet cooling temperature water [Rutberg et al., 2011].

The water withdrawal and consumption optimization weights (w_{with} and w_{con}) ranges are selected to prevent against the previously mentioned ill-conditions for convergence.

Table 4.1: Sampling Space of Input Factors for Uniform Sensitivity Analysis

Input Factor	Min	Max	Number of Steps
w_{with}	0.0	0.1	10
w_{con}	0.0	1.0	10
c_{load}	1.0	1.5	10
c_{water}	0.5	1.5	10

To grid sample the input factor space, each of the four input factors is divided into an equal number of steps between its bounds as outlined in Table 4.1. This approach produces a uniform sampling of the input factor space yielding 10,000 combinations of the input factors (w_{with}, w_{con}, c_{water}, and c_{load}), and the multi-objective water-informed OPF model was run for each combination producing four objective values ($f_{cos}, f_{gen}, f_{with}, f_{con}$). The sampling was run on the RMACC Summit supercomputer across one node with two CPUs (Intel Xeon E5-2680 v3, 2.50 GHz, 24 cores/node) with 4.84 GB RAM per core, taking a wall time of roughly 12 minutes.

A subset of this sampling is depicted in Figure 4.7. This figure shows both how our water-informed OPF reduces system-wide water withdrawals as well as how a water-informed system is able to take on additional loads with marginal increases to overall water use. This subset is chosen to demonstrate extreme values for the withdrawal and consumption coefficients. The horizontal

axis of Figure 4.7 represents increasing electricity demand. The vertical axis depicts the total water withdrawal objective F_{with}, which was defined in Equation 10. The color of the lines reflects the uniform water coefficient (c_{water}). Darker lines correspond to more severe system-wide water constraints (e.g., drought). Finally, the marker styles reflect a subset of the minimum and maximum withdrawal weight (w_{with}).

Comparing system withdrawals between the same water constraint/increased electricity demand scenarios but different withdrawal weights in Figure 4.7, we gain insights into the efficacy of the water-informed OPF. Visually, the two lightest lines (uniform water coefficient equal to 0.61) correspond to the highest water efficiency. As the system experiences increases in electricity demand (i.e., moves to the right along the horizontal axis), the withdrawal weight has an increasing effect on reducing overall system withdrawals. In fact, for loading coefficients less than 1.2, by considering a withdrawal weight, the system adapts to rely on plants that either have low or zero withdrawal weights to cover added loads. This outcome results in the system having only marginal increases to water withdrawal as the system experiences larger loads. Across varying system-wide water efficiencies (line color in Figure 4.7), we see that the effect of the withdrawal weight increases as the system gets more water inefficient. To demonstrate the largest system-wide water inefficiencies (e.g., drought; uniform water coefficient equal to 1.5), we see that by assigning a withdrawal weight (e.g., implementing a policy focused on withdrawal), we reduce system withdrawal to a level expected at a better system-wide water efficiency (uniform water coefficient of 1.06).

Another trend from Figure 4.7 is that linear increases in electricity demands do not cause linear increases to water use. This result might be expected given that water withdrawal is modeled as a linear coefficient on generator power output. The reasons for this nonlinearity arise from other power flow considerations in the water-informed OPF that cause individual generators to generate electricity with nonlinear increases even under linear increases to total system loadings.

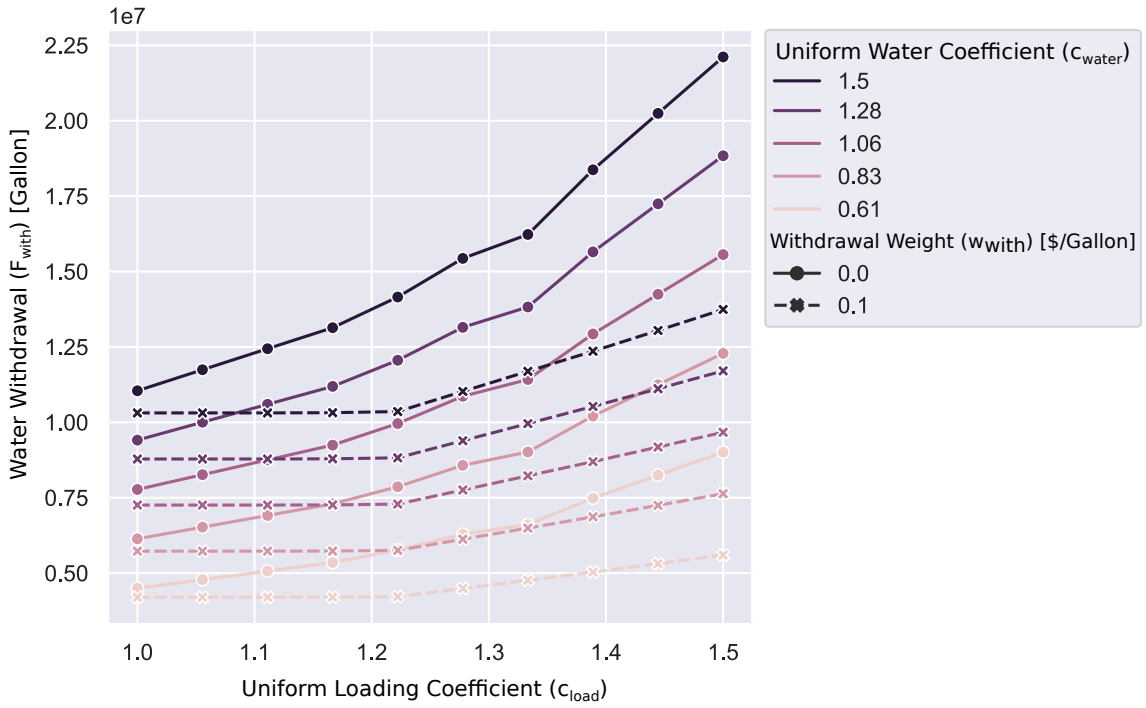

Figure 4.7: Effect of Withdrawal Weight on Total System Withdrawal. This figure shows both how our water-informed OPF reduces system-wide water withdrawals as well as how a water-informed system is able to take on additional loads with marginal increases to overall water use. This figure subsets the data such that the consumption coefficient $w_{con} = 0$.

To gain insights into what is happening on the plant level, we depict plant output capacity factors in Figure 4.8, with each plant shown as a different line color and type. Generator output capacity factors are defined as the ratio of the current power output to its total power output capacity, shown on the vertical axis of Figure 4.8. As in Figure 4.7, the electricity demand (uniform loading coefficient) is plotted on the horizontal axis. Each panel moving from left to right reflects a different group of plants with the same fuel/cooling system type (with unique legends for each row on the bottom). Each row of the figure reflects a different subsetting of the data as denoted by the labels on the right.

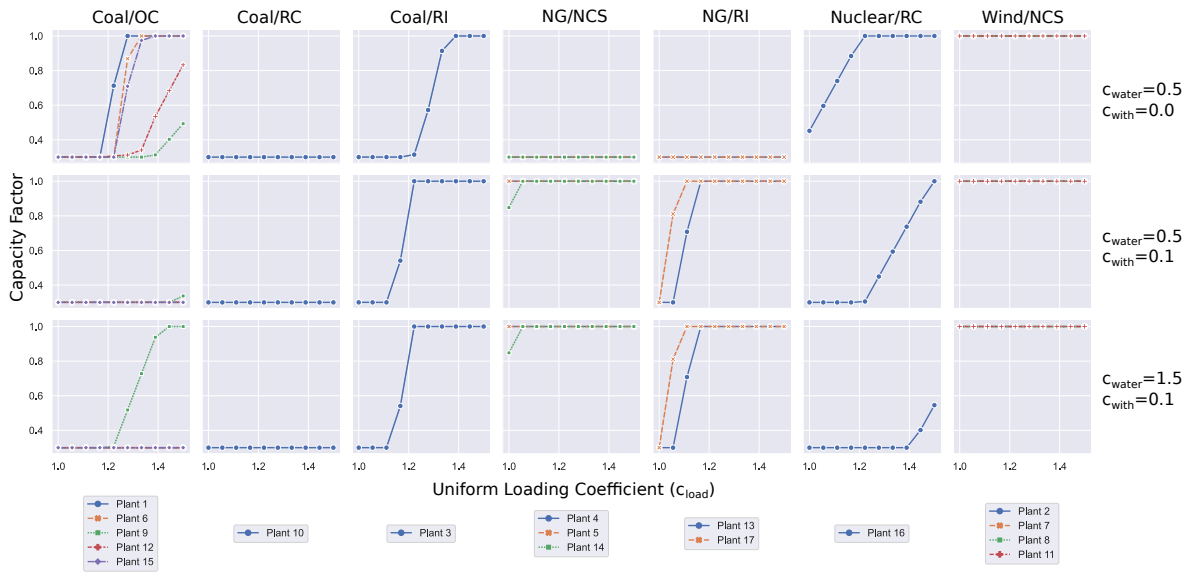

Figure 4.8: Effect of Withdrawal Weight and Uniform Water Coefficient on Plant Output. Samples subset such that consumption weight (w_{con}) equals 0.0. Subsets of the uniform water coefficient (c_{water}) and the withdrawal weight (w_{with}) are depicted to right. Abbreviations: Recirculating with Induced Draft Cooling Tower (RI), Recirculating with Cooling Ponds (RC), Once-through with Cooling Ponds (OC), No cooling system (NCS), Natural Gas (NG)

From Figure 4.8, we see the general trend that as loading increases (moves along the horizontal axis), plants either output the same or more power (vertical axis). For example, there is no case when system loading increases but an individual generator outputs less. This behavior is expected given the nature of power systems and their governing equations. However, a more interesting insight from Figure 4.8 is *which* plants output more power under linear increases to system load. Looking at the top row of Figure 4.8 (lowest water constraint with traditional OPF), we see that the increased electricity demand is generally supplied by the coal and nuclear plants. We see initial electricity demand increases are first supplied by the nuclear generator, which quickly reaches maximum generation as uniform loading coefficients increase beyond 1.2. Continued electricity demand increases are then supplied by the coal plants with once-through and recirculating induced draft cooling systems. Within the coal/once-through plants, the cheaper plants reach maximum

capacity quickly (such as plants 9 and 12), whereas the more expensive plants reach capacity much slower (plant 6). Certain plants, like 1 and 6, never reach maximum generation, even at the highest uniform loading case. This finding suggests that something else about this network, like a line constraint, is leading to the infeasibility of solutions beyond uniform loading coefficients of 1.6 as there is extra generation capacity.

Comparing across rows in Figure 4.8, we see the impact that the withdrawal weight has on individual plant power output. Recall that by putting a high weight on the withdrawn water, the system operates to minimize the power output of plants with high withdrawal rates. This condition is clear when comparing the coal/once-through plant output. In the top row (traditional OPF), the system relies on coal/once-through plants to cover the initial increases in electricity demand. However, when these water-inefficient plants are penalized, they do not output power until the most severe loading conditions (first column, second row of Figure 4.8). In fact, the system is able to rely on plants with lower withdrawal rates (coal/recirculating induced) or plants with zero withdrawal rates (natural gas/no cooling system) to cover the initial load increases. Beyond loading coefficients of 1.2 the nuclear plant is selected, which causes the increase in water withdrawal. Specifically, this result is why system withdrawals did not increase until a loading coefficient of 1.2 as was observed in Figure 4.7.

We can further subset the sampling data to observe the effect that applying a withdrawal weight has on the actual flows through the system. We choose two solutions that both have a consumption weight of 0.0, a uniform loading coefficient value of 1.5, and a uniform water coefficient of 0.5. The only difference between the two solutions is that one is a traditional OPF formulation with no withdrawal weight and the other is a water OPF formulation with a withdrawal weight of 0.1. Each solution produces a value of line loading for each line that we can express as a percentage of each line's limit. We visualize the *difference* in line loading between the traditional and water OPF as is done in Figure 4.9. The convention for this figure is *relative to the traditional OPF*, such that negative changes mean that under the water OPF flows went *down* in that particular line. Busses are depicted as blue circles and transformers are depicted as black circles.

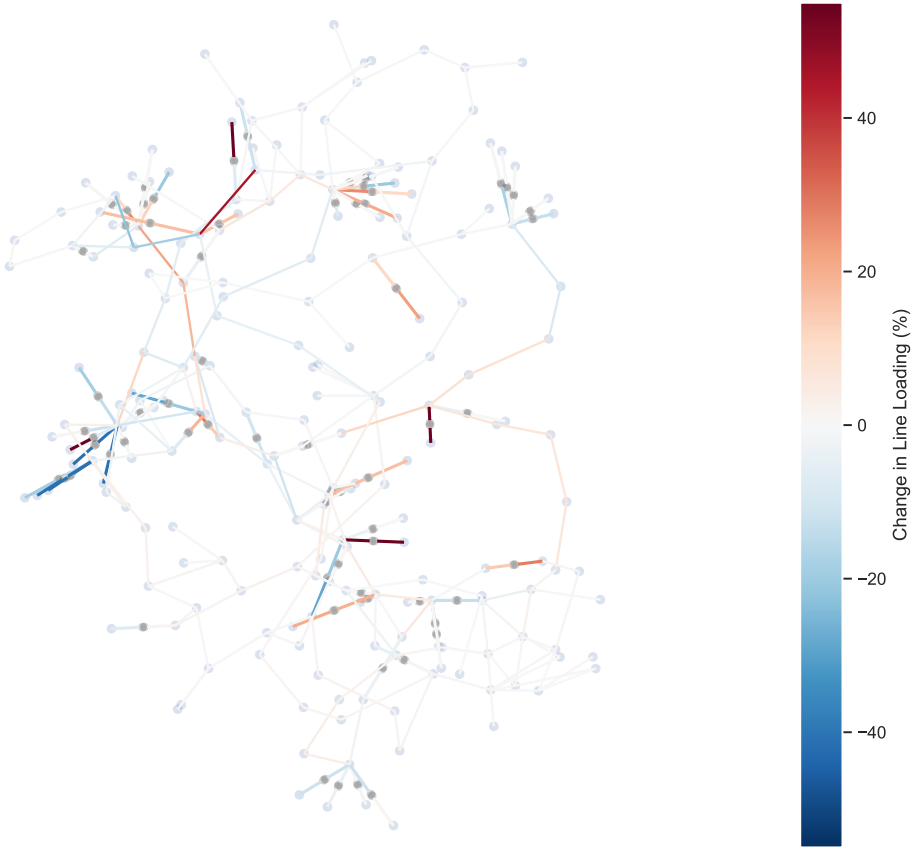

Figure 4.9: Effect of Withdrawal Weight on Line Flows. Samples subset such that consumption weight (w_{con}) equals 0.0, uniform loading coefficient (c_{load}) equals 1.5, and the uniform water coefficient (c_{water}) equals 0.5. Traditional OPF defined by withdrawal weight (w_{with}) equal 0.0 and the water OPF defined by withdrawal weight (w_{with}) equal 0.1. Lines are colored based on the percent change relative to the traditional OPF case. Bus locations in the plot are not representative of actual geospatial locations.

From Figure 4.9, we see that by incorporating water into the OPF formulation, flows throughout the network change. We see that there are certain sections of the area that experience an increase in line loading (depicted as dark red), while other areas experience significant decreases in loading.

Through the uniform sensitivity analysis, we show that our water-informed OPF formulation can effectively mitigate impacts on water consumption and withdrawal from changes in system

water inefficiencies or increased loading. These water-informed operational policies are especially useful if systems are experiencing sudden water constraints as these operational policies would be much quicker to deploy than more long-term solutions like a water pipeline or upgrades to plant components [Pacsi et al., 2013], and could avoid ecosystem damage from widespread granting of thermal variances [Lubega and Stillwell, 2018a, Micha, 2014, Logan et al., 2021]. The proposed water-informed power system operations complement the efforts to include water in long-term planning operations [Jornada and Leon, 2016]. These efforts are also analogous to the efforts to incorporate air pollutants into both long-term grid planning and short-term grid operations [Kumar et al., 2020, Flores and Brouwer, 2018, Ren et al., 2010] both of which generally fall under the need to create a grid that meets environmental targets [Ipakchi and Albuyeh, 2009].

Our framework is also helpful for determining what *actions* system operators or policymakers could implement by showing which individual plants/generators are impacted by various external stressors. For example, targeted maintenance or generator-level operational policies could be put in place so that critical generators are ready to operate when needed. Similarly, through analysis of line flows, analysts can identify areas of the transmission system that would be most impacted by water-informed operational policies. Because increasing line loading closer to capacity can result in increased losses, such parts of the transmission system could be preemptively upgraded. Such insights address broader issues of creating policy that integrates day-to-day component-level operations to long-term system planning and behavior [Battey et al., 2014].

Comparing the second and last rows of Figure 4.8 we see the impact that generator water efficiency has on a system governed by our water-informed OPF. We see that the main differences come from plant 9 and plant 16. Under more severe water inefficiencies, the coal/once-through plant 9 reaches capacity before the recirculating/nuclear plant 16. However, what happens if local processes impact the water withdrawal rates of these plants? The non-uniform sensitivity analysis allows us to quantify the sensitivities of each individual plant's water use on the various aspects of system performance.

4.4.2 Impacts of Non-Uniform Variability on System Performance

In the previous section, we assumed that water changed uniformly (i.e., all generators experience the same increase/decrease) in the system. In this section, we investigate how allowing individual plant water usage to vary impacts system performance under a variety of exogenous operational and policy scenarios. We apply the non-uniform sensitivity analysis outlined in Section 4.2.4 to several scenarios. The scenarios as well as their mathematical representations are presented in Table 4.2. We see that these scenarios capture different loading cases and policy cases. For loading cases, there are normal loading conditions ($c_{load} = 1.0$) as well as increased scenarios ($c_{load} = 1.5$). For policy cases, we consider the traditional OPF (which does not incorporate water use). We also consider the decreased withdrawal case, which puts a high optimization weight on the water withdrawn and a low weight on consumption (e.g., policy focus on reducing withdrawal). The converse is true of the decreased consumption case. Recall that the choice of these values was based on both feasibility and historical validity as discussed in Section 4.4.1.

Table 4.2: Exogenous Operational and Policy Scenarios for Non-Uniform SA

Exogenous Operational and Policy Scenario	w_{with}	w_{con}	c_{load}
Normal loading with traditional OPF	0.0	0.0	1.0
Increased loading with traditional OPF	0.0	0.0	1.5
Increased loading with decreased withdrawal	0.1	0.0	1.5
Increased loading with decreased consumption	0.0	1.0	1.5

Within each exogenous operational and policy scenario, we test the sensitivity of the water use coefficient corresponding to each plant for this system. Our synthetic grid contains multiple generators of different fuel/cooling types located in the same plant. As previously discussed in Section 4.2.4, such groups of generators are given separate plant designations. Therefore, there are a total of 17 unique plants. However, only 10 of those plants have cooling systems. We assign non-uniform

water coefficients to each of these ten plants $C_{water,plant9}$, $C_{water,plant6}$, $C_{water,plant12}$, $C_{water,plant15}$, $C_{water,plant1}$, $C_{water,plant10}$, $C_{water,plant3}$, $C_{water,plant17}$, $C_{water,plant13}$, and $C_{water,plant16}$. These coefficients are the input factors of the non-uniform sensitivity analysis.

Recall from Section 4.2.4, the non-uniform sensitivity analysis uses Sobol indices to quantify input factor sensitivity. However, many of the traditional methods for estimating Sobol indices are dependent on assumptions on the input factor distributions [Cousin et al., 2019, Hart and Gremaud, 2018]. However, from the analysis of the historic distributions of the 10 input factors for the regional dataset, we see that the input factors do not exhibit the behavior of common parametric distributions. Fortunately, previous works have proposed methods to estimate Sobol indices based on samples alone [Li and Mahadevan, 2016]. These sample-based methods allow us to bootstrap sample the historic input factors. The number of bootstrap samples was determined to be 22,528 based on $1024 * (2 * 10 + 2)$ with the value of ten for the number of input factors and 1024 based on literature recommendations [Herman and Usher, 2017, Saltelli, 2004]. This sampling is repeated for each of the four operational scenarios. This sampling was run on the RMACC Summit supercomputer across ten nodes with two CPUs (Intel Xeon E5-2680 v3, 2.50 GHz, 24 cores/node) with 4.84 GB RAM per core which took a wall time of approximately 30 minutes.

We compute approximate first-order sensitivity indices for each of the four objectives using the methods proposed in Li and Mahadevan [2016], for each of the ten input factors, repeated for each of the four operational and policy scenarios. We arrange them in a heatmap as is visualized in Figure 4.10. Each column in the figure represents the non-uniform water coefficient associated with the plant labeled on the bottom. Each row indicates a unique objective labeled on the left. Each panel column represents a grouping of plants based on their fuel and cooling system type as indicated on the top. Each panel row indicates an operational and policy scenario as indicated by the labels on the right. The color of each cell represents the first-order sensitivity of the input factor on the objective.

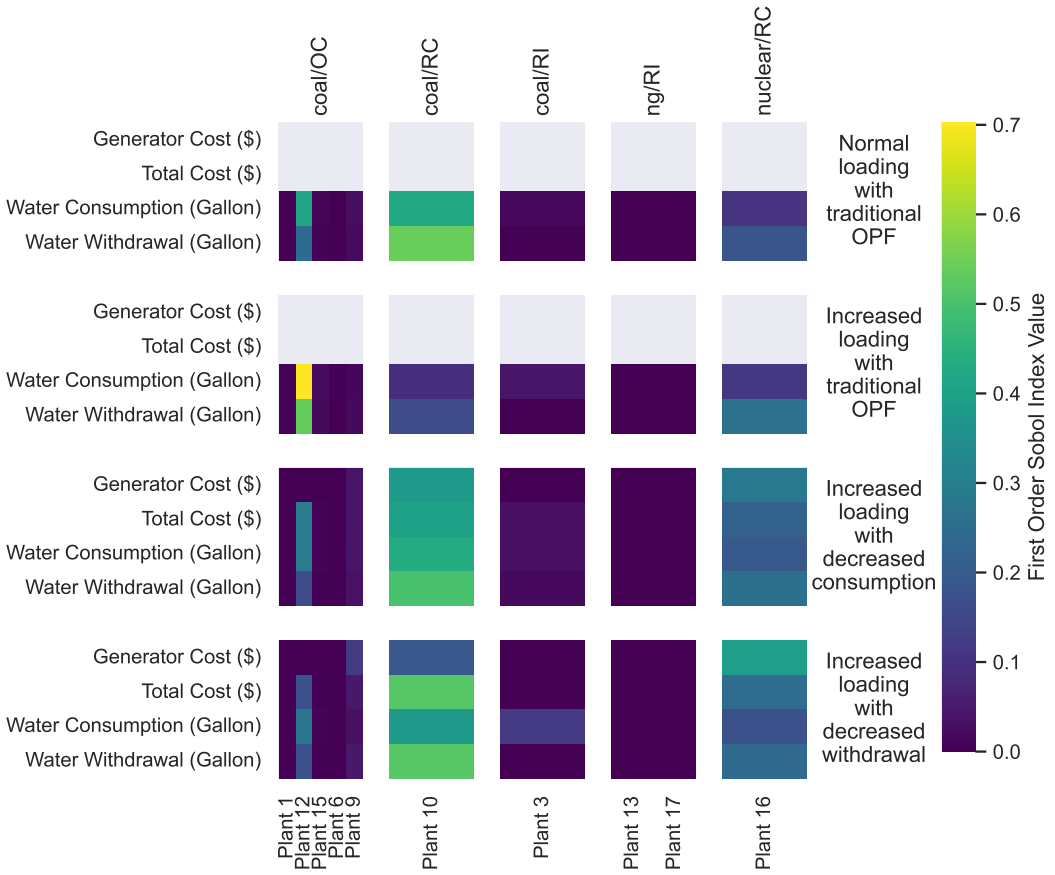

Figure 4.10: First Order Sobol Indices Non-Uniform Sensitivity Analysis. Each row is a different objective. Each column is a different input factor. Each panel column represents a grouping of plants based on their fuel and cooling system type as indicated on the top. Each panel row indicates an operational and policy scenario as indicated by the labels on the right. Under traditional OPF formulations, the generator cost and total cost objectives do not consider the input factors, and are undefined in the first-order sensitivities indices; thus, they are not colored.

From Figure 4.10, we see which objectives are most sensitive to which plant's water efficiency. For example, in the panel on the second row in the first column, we see that system-wide water consumption is sensitive to the water efficiency of plant 12 (depicted as bright yellow). Furthermore, we see that plants 10, 12, and 16 are almost always sensitive to all objectives and operational scenarios. This result makes sense given that these are the plants with the highest capacities. We also see that plant 3 becomes more important during increased loading scenarios, confirming the

insights about plant 3 found from the uniform sensitivity analysis.

Non-uniform loading allows analysts to see which plants most impact various aspects of system performance. For example, our analysis showed that plant sensitivity to generator cost, water consumption, and water withdrawal was often different. Such insights allow for the creation of policy that directly targets the most important plants, or types of plants, with respect to a policy-maker's values. For example, our framework could inform a policy that targets water consumption under increased loading, which might be different from a policy that targets water withdrawal under normal loading.

4.5 Conclusion

Examples of extreme climate events that have impacted thermoelectric operations are common throughout the early 21st century. Perhaps the largest and most catastrophic event was the 2003 heatwave in France that forced a shutdown of 25 percent of its nuclear generators due to high cooling water inlet temperatures [Harto et al., 2012, Poumadère et al., 2005]. Less severe events include the droughts in 2006 that required the shutdown and curtailment of a number of generators in Europe [Union of Concerned Scientists, 2007], as well as in Illinois and Minnesota, U.S. [Harto et al., 2012]. The following year, a unit at Browns Ferry nuclear plant was forced to shut down and the other two units reduced capacity during a heatwave and record-setting demand [Union of Concerned Scientists, 2007]. Such reduced capacity operations cost the grid operators an estimated additional $1 million per day to purchase power from neighboring systems [Freedman, 2012]. Similarly, droughts in 2011 caused reductions in power output in Texas [Galbraith, 2011, Reuters Staff, 2011], with similar reductions occurring in the Northeastern and Midwestern United States the following year [Eaton, 2012]. Recent studies estimate generator reductions/shutdowns during the 2013-2016 droughts in India prevented 30 TWh of potential electricity generation [Luo, 2017].

One commonality among all these events is that they marked instances where system operators needed to manually intervene in the traditional power system operations to accommodate

external hydrologic, climatic, or demand factors. Instead of such reactive measures, our proposed water-weighted OPF operational scenario framework provides an opportunity to take proactive measures. We discussed how the insights gained through the operational scenario framework are useful to system analysts and policymakers.

This chapter contributes and demonstrates a novel operational scenario analysis framework to analyze power system performance under loading and water stresses. This framework is built on our water-informed formulation of the OPF problem whose solutions are a function of generator water efficiency, system loadings, and water use penalty terms. A multi-objective simulation model built on this formulation allows analysts insights into relevant aspects of system performance. Sensitivity analyses of this multi-objective model facilitated both system-level and component-level insights; such insights are relevant to both system analysts as well as policymakers.

Chapter 5

Considering Cost, Water, Emissions, and Reliability When Creating Optimal Power System Policies

The previous chapter proposed a framework where operational water penalties defined "policy" decisions. Using sensitivity analysis, that framework showed, by varying the values for the operational water penalties, the cost and water use of power systems can vary significantly. This chapter focuses on how *optimal* policies can be created that effectively compromise among emissions and reliability (concerns raised in Chapter 3) in addition to the previously analyzed cost and water use.

5.1 Introduction

This chapter unites Chapters 3 and 4. This chapter expands the policy-centric formulation from Chapter 4 and *optimizes* the policies using the same methods as was done in Chapter 3. Just as in Chapter 4, we will test the performance of the optimal policies against several exogenous stress scenarios. However, this chapter looks at operational stressors (e.g., line outages) in addition to the climatological stressors previously considered. Additionally, we will use the Water-Extended Illinois 200 Bus System just as in Chapter 4.

This chapter contributes a tradeoff analysis of the cost, water, carbon dioxide emissions, and reliability of energy systems, via proposing policies that can be rapidly and directly incorporated into existing power systems operations. We couple existing models of thermoelectric power plant water use, emissions rates, and power systems reliability with an optimal power flow for-

mulation. Through a representative case study, our generated policies mitigate the impacts of various operational and climatological stressors. The combined water-emissions policies show improved performance relative to policies solely created using water or emissions improvements, thus demonstrating how effective energy policy would benefit from a multi-perspective approach.

5.2 Methodology

We expand the simulation model introduced in Chapter 4 in two major ways - the simulation in this chapter (1) considers multiple timesteps of operation and (2) uses well-accepted empirical/physical models of water use, emissions, and reliability. Power systems cost and reliability are simulated at an hourly timestep while water use and emissions are modeled on a daily timestep. Exogenous parameters, those that are out of direct control of the system operator, such as the loads in the system, streamflow, streamflow temperature, ambient air temperature, wind speed, and various generator-specific parameters are required for simulation (Figure 5.1).

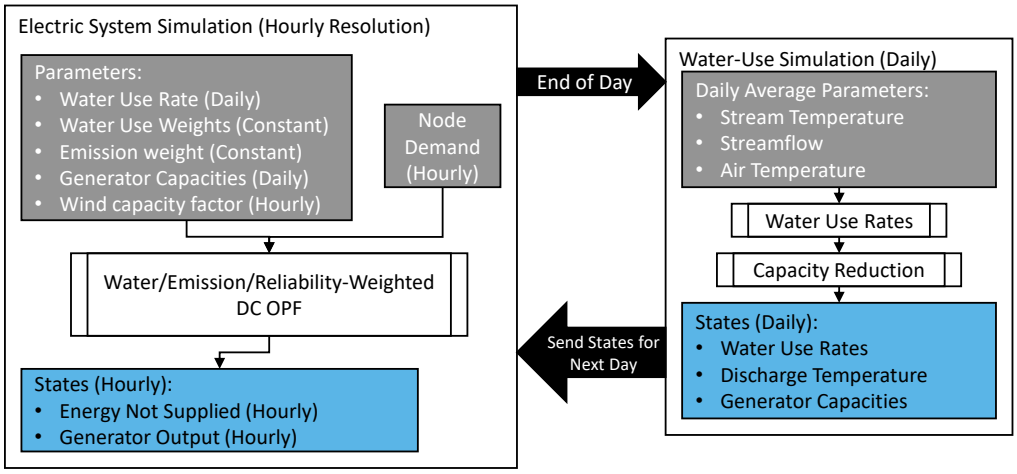

Figure 5.1: Overview of Simulation. The water use rate model is the system-level generic model (S-GEM) [Rutberg et al., 2011] and the capacity reduction model is adapted from van Vliet et al. [2016].

5.2.1 Policy Decisions

We expand the operational penalties from the previous chapter not just to include generator water withdrawal and water consumption but also generator emissions. Recall from the previous chapter that a water withdrawal penalty with the units of dollars per gallon of water allows us to define a water withdrawal cost term to be directly added to other operational costs.

A set of operational penalties constitutes a "policy". Thus, each unique policy expresses a relative preference for reducing water withdrawal, water consumption, and emissions. For example, if a policy specifies a weight on water withdrawal too low, there will be no significant reduction in system water withdrawal. However, if the value is too high, then the system drastically reduces water withdrawal at the expense of significant increases in operational costs, emissions, and water consumption. Therefore, it is crucial to make an informed policy decision that holistically considers all aspects of energy system performance.

5.2.2 Water/Energy/Emissions Cosimulation

Through creating a week-long hourly-resolution water/energy/emissions cosimulation model, we capture the system-level and generator-level performance impacts of policy decisions. The water component of the cosimulation captures the water withdrawal and consumption of the generators. The emissions component captures the carbon emissions associated with energy production. Finally, the energy component captures the underlying generator operations of the electrical power system.

5.2.2.1 Water Use Simulation

Previously in Chapter 4, we assumed the water use rates of the generators to be an exogenous factor. However, historic timeseries of these rates are not publicly available information. Therefore, in this chapter, we broaden the scope of our simulation to start with streamflow, stream temperature, and air temperature and simulate the resulting impacts on water use rates using standard models because historic streamflow, stream temperature, and air temperature are either directly available or easier to interpolate from historic data, as will be demonstrated for our case study.

To model the water withdrawal and consumption rates, we implement models from Rutberg et al. [2011] that capture the underlying thermodynamics of the thermoelectric cooling process. We have extended these models to allow for temperature discharge violations following assumptions laid out in Langford [1990], Madden et al. [2013] (Appendix Section C.1). To capture the impacts of climatology on generator capacity, we implement the models from van Vliet et al. [2016] (Appendix Section C.3). Rutberg et al. [2011] and van Vliet et al. [2016] use empirical correction factors to account for the complexities and inefficiencies of real-world generators.

5.2.2.2 Emissions Simulation

This simulation focuses on carbon emissions due to their globally increasing trends in the energy sector [Friedlingstein et al., 2022]. Fossil fuel sources have corresponding carbon emission rates (e.g., lbs of CO_2/MWh) analogous to the nitrogen oxide and sulfur oxide factors introduced in Chapter 3. Estimates of carbon emission factors are typically based on historical information and are generally well-accepted [EPA, 2021]. Therefore, our cosimulation captures total system emissions as the product of a generator's energy output and its emission rate.

5.2.2.3 Power System Simulation

The core of our simulation model is a water- and emissions-weighted DC OPF model solved on an hourly timestep. Just as the formulation from Chapter 4, the objective is still a weighted sum.

This formulation extends that of Chapter 4 in that it:

- includes an emission term and weight (w_{emit})
- includes a reliability term captured by energy not served ($f_{cost,ENS}$)
- introduces a time dimension, thus active power at hour h is given by $\mathbf{p_g}^h$

The reliability of this system is also modeled as an additional penalty term in the objective of our water- and emissions-informed DC OPF. Much like the operational penalties, the value-of-

lost-load term specifies a monetary price associated with not serving electricity demand. These monetary prices are typically expensive to avoid interruption in electricity supply [Anderson et al., 2019]. Thus, the system will only choose not to serve demand if either all generators have reached maximum capacity (so the system has no choice but not to serve demand) or, in the case of this chapter, the operational penalties on water use or emissions are priced so expensive that it is cheaper not to serve demand.

Our water/emission/reliability-weighted DC OPF formulation is as follows:

$$\min_{\mathbf{pg}^{h}\forall h} f_{gen} + f_{cost,emit} + f_{cost,water} + f_{cost,ENS} \tag{5.1}$$

$$\text{s.t.} \quad f_{gen} = \sum_{h=1}^{24} \left(\sum_{j \in \mathcal{G}} a_j + b_j p_{g,j}^h + c_j \left(p_{g,j}^h \right)^2 t \right) \tag{5.2}$$

$$f_{cost,emit} = \sum_{h=1}^{24} \left(\sum_{j \in \mathcal{G}} w_{emit} \beta_{emit,j} p_{g,j}^h t \right) \tag{5.3}$$

$$f_{cost,water} = \sum_{h=1}^{24} \left(\sum_{j \in \mathcal{G}} \left(w_{with} \beta_{with,j} + w_{con} \beta_{con,j} \right) p_{g,j}^h t \right) \tag{5.4}$$

$$f_{cost,ENS} = \sum_{h=1}^{24} \left(\sum_{j \in \mathcal{D}} p_{g,j}^h \beta_{VoLL} t \right) \tag{5.5}$$

$$p_{l,i}^h - \sum_{k \in \mathcal{G}_i} p_{g,k}^h = \sum_{m \in \mathcal{N}} B_{im} \theta_{im}^h, \quad \forall i \in \mathcal{N}, h = 1...24 \tag{5.6}$$

$$-\Lambda_{max,im} \leq B_{im} \theta_{im}^h \leq \Lambda_{max,im}, \quad \forall im \in \mathcal{L}, h = 1...24 \tag{5.7}$$

$$\underline{p}_{g,j} \leq p_{g,j}^h \leq \bar{p}_{g,j}, \quad \forall j \in \mathcal{G}, h = 1...24 \tag{5.8}$$

$$-\underline{r}_{g,j} \leq p_{g,j}^h - p_{g,j}^{h+1} \leq \bar{r}_{g,j}, \quad \forall j \in \mathcal{G}, h = 1...24 \tag{5.9}$$

which uses the same notation as the previous DC OPF notations used throughout this thesis (See Section 2.4.2. However, a few new terms have been introduced. The rate of emissions is modeled as $\beta_{emit,j}$ (e.g., lbs/MWh) and is converted to a cost using w_{emit}. The value of the lost load is β_{VoLL} and $\mathcal{D}$ is the set of all the demands in the system. Due to the time-series nature of this simulation, ramp-up and down rates ($\underline{r}_{g,j}$ and $\bar{r}_{g,j}$) are also considered. Importantly, day-to-day

ramping constraints are considered (i.e., hour 24 constraints hour 1 of the next day).

5.2.3 Objectives

Just as in Chapter 3, we compile several objectives that each appeal to a different decision-maker-relevant aspect of system performance. We assume that the simulation runs for some number of days D.

We use the traditional DC OPF objective from Equation 5.2 to quantify the total system generator costs (f_{gen}) defined as

$$f_{gen,tot} = \sum_{d=1}^{D} (f_{gen}^{d}) \tag{5.10}$$

Similarly, we capture the total withdrawal ($f_{with,tot}$) and total consumption ($f_{con,tot}$) as

$$f_{with,tot} = \sum_{d=1}^{D} \sum_{h=1}^{24} \sum_{j \in \mathcal{G}} \beta_{with,j}^{d} * p_{g,j}^{h} \tag{5.11}$$

$$f_{con,tot} = \sum_{d=1}^{D} \sum_{h=1}^{24} \sum_{j \in \mathcal{G}} \beta_{con,j}^{d} * p_{g,j}^{h} \tag{5.12}$$

We capture the total thermoelectric discharge violations across all the generators with $f_{disvi,tot}$

$$f_{disvi,tot} = \sum_{d=1}^{D} \sum_{h=1}^{24} \sum_{j \in \mathcal{G}} \left(\beta_{with,g} - \beta_{con,g}\right) p_{g,j}^{h} \Delta T_{violation,j}^{d} \tag{5.13}$$

where $\Delta T_{violation,j}^{d}$ is the discharge violation for generator j on day d. The estimated discharge is captured by tracting the withdrawal from the consumption. The final units of this objective are the volume of water times violation temperature such that both the volume of water discharge beyond regulatory limits as well as the temperature are being captured.

Emissions are modeled as a linear rate

$$f_{emit,tot} = \sum_{d=1}^{D} \sum_{h=1}^{24} \sum_{j \in \mathcal{G}} \beta_{emit,j} p_{g,j}^{h} \tag{5.14}$$

We model grid reliability with energy-not-served modeled over the set of demands $\mathcal{D}$ as

$$f_{ENS,tot} = \sum_{d=1}^{D} \sum_{h=1}^{24} \sum_{j \in D} p_{g,j}^{h} \tag{5.15}$$

where $p_{g,i}^{h}$ is the energy not supplied at to load j during hour h. Recall that energy is not served at a demand if its value exceeds the value of lost load β_{VoLL}.

To capture the fact that system operators want to impose the lowest weights on the system, we consider each of the decisions (w_{with}, w_{con}, w_{emit}) to be additional objectives that are to be minimized.

5.2.4 Nested Multi-Objective Optimization Using a Single-Objective Solver and Weights

To recap, our water/energy simulation (Figure 5.1) is a function of decisions (operational penalty weights) and exogenous parameters $\mathbf{c_{ex}}$ (processes that cannot be controlled by system operators). The simulation produces several objectives as described in the previous section. We denote our water/energy simulation (Figure 5.1) as a function P_{cewr}.

Because our simulation includes a weighted single objective optimization and we are interested multi-objective optimization of those weights, we can use the same nested multi-objective formulation proposed in Section 2.3.4. Recall that in this formulation we have an "inner" weighted-single-objective optimization and an "outer" multi-objective optimization of those weights. Therefore, our formulation is

$$\underset{w_{with},w_{con},w_{emit}}{\text{minimize}} \quad [f_{gen,tot}, f_{with,tot}, f_{con,tot}, f_{disvi,tot}, f_{emit,tot}, f_{ENS,tot}, w_{with}, w_{con}, w_{emit}] \tag{5.16}$$

$$\text{s.t.} \quad P_{cewr}(\{w_{with}, w_{con}, w_{emit}\}, \{\mathbf{c_{ex}}\}) = [f_{gen,tot}, f_{with,tot}, f_{con,tot}, f_{disvi,tot}, f_{emit,tot}, f_{ENS,tot}] \tag{5.17}$$

$$\underline{w}_{with} \leq w_{with} \leq \overline{w}_{with} \tag{5.18}$$

$$\underline{w}_{con} \leq w_{con} \leq \overline{w}_{con} \tag{5.19}$$

$$\underline{w}_{emit} \leq w_{emit} \leq \overline{w}_{emit} \tag{5.20}$$

where $\underline{w}_{with}, \underline{w}_{con}, \underline{w}_{emit}$ represents the lower bound on each decision variable and $\overline{w}_{with}, \overline{w}_{con}, \overline{w}_{emit}$ represent the upper bound on each decision variable. The result of solving this problem is a nondominated set of policies.

5.2.5 Tradeoff Analysis

Once we have our nondominated set of policies, we conduct a tradeoff analysis to first understand the general interplay between our objectives. This allows us general insights into the systemic behavior of water/energy systems. For example, we understand which objectives compete with one another and which are harmonious.

In the final phase of our framework, we select a single representative "water-emissions" policy that seeks an equal compromise with respect to *several* objectives (cost, water withdrawal, water consumption, emissions) from the nondominated set. We simulate its performance under a variety of system stressors. Through this, we understand how an optimal energy system policy can mitigate the impacts of various stressors.

5.3 Extension of Case Study from Chapter 4

This chapter extends the synthetic case study that was used in the previous chapter (Chapter 4). Therefore, the same methods are implemented for assigning cooling system types for synthetic

generators. Recall that the scope of the exogenous parameters has been broadened to allow for a time-series simulation. Therefore, this chapter does not employ the statistical methods for sourcing exogenous parameters previously outlined in Section 4.3.3 and 4.3.4. Instead, we use historical data with empirical models to generate the required exogenous parameters.

5.3.1 Sourcing Exogenous Parameters

For ambient air temperature data, we use a National Solar Radiation Data Base location near Springfield, Illinois from 2015 to 2020 [Sengupta et al., 2018]. For this system, the streamflow temperature data does not have consistent temporal coverage. To supplement this, we fit the empirical air temperature to the stream temperature model proposed in Mohseni et al. [1998], which has been applied to similar thermoelectric modeling problems [Koch and Vögele, 2009, van Vliet et al., 2016]. The fitted model appears in Appendix Figure D.1.

Due to the synthetic nature of this grid, hourly bus-level loading information must be synthetically generated based on the publicly-available historic information. We start with the hourly system-level load data for MISO, the geographic location in which our synthetic test system is located (Figure 4.5).

We need to disaggregate this system-level load to the bus level. We model bus-level loads as the product of the average bus-level loads, a system-wide capacity factor, and an hour-to-hour bus-level load variation capacity factor. The average bus-level loadings are supplied in the synthetic grid. We transform historic publicly available load data for our system by dividing it by the yearly average to get the system-wide capacity factors. Finally, we use synthetic bus-level hourly profiles to compute the hour-to-hour variation by dividing subsequent hours by one another to compute our hour-to-hour load factors [Li et al., 2021]. For more details, consult Appendix Section D.

Wind capacity factors assume that turbines cut in at 6 mph, are rated for 25 mph, and turn off beyond 50 miles per hour. Thus historic windspeed capacity factors are normalized to this range.

5.4 Results and Discussion

We apply the multi-objective policy search and tradeoff analysis previously outlined in Section 5.2 to create our "water-emissions" policy. We solve the multi-objective problem using the Borg multi-objective evolutionary algorithm [Hadka and Reed, 2013]. The Borg MOEA employs epsilon dominance, a user-defined precision on each objective function. Within the dominance calculation, a solution survives only if its performance differences are more significant than that epsilon value, limiting the number of solutions found and easing the interpretability of tradeoffs. Practically, epsilons act as a method for specifying the desired precision across the objective space. An initial population of 100 was specified with a maximum of 7,500 function evaluations for this search. Default parameter values were used for the remaining parameters which are justifiable given demonstrations of Borg's performance using its default parameterization Hadka et al. [2012]. This search was conducted on the University of Colorado's Alpine supercomputer across 128 cores (AMD Milan CPUs, 3.7 GHz, 3.75 GB/Core) for a wall time of 7.5 hours. To investigate the overall success of the search, we analyze the hypervolume of the objective front throughout the search. The hypervolume takes the volume of space covered by the objective front relative to a reference point and is commonly used as a diagnostic for multi-objective searches [Zatarain Salazar et al., 2016]. We select a single policy from the resulting nondominated set which we label "Water-Emissions Policy".

5.4.1 Generating Policies for Comparision

For comparison, we also generate four unique policies using single-objective optimization (Table 5.1). These comparison policies have been chosen such that each focuses on a single aspect of water-energy-emissions system coupling. For example, the value of the water withdrawal penalty for the "high water withdrawal penalty" policy is determined by increasing the penalty until no additional reductions to water withdrawal were observed. An analogous process is followed for the "high water consumption penalty" and the "high emissions penalty" policies. The final "status

quo" policy reflects current economic-only operations. These four policies ignore the coupling of water-energy-emissions systems as they each focus solely on a single objective at a time. Thus, they will be used as a comparison to the holistic "water-emissions" policy.

Table 5.1: Single-Objective Policies

w_{with}	w_{con}	w_{emit}	Policy
0.0	0.0	0.0	Status Quo
0.0	0.043	0.0	High Water Consumption Penalty
0.036	0.0	0.0	High Water Withdrawal Wenalty
0.0	0.0	0.0044	High Emission Penalty

5.4.2 Exogenous Scenarios

We test our simulation/optimization on several historic exogenous parameter scenarios. The *average week* scenario is simulated as a baseline reference for how the system behaves when all the generators are available under average loading. The *extreme load/climate* scenario captures the week that had the highest 7-day average air and water temperature. Such extreme weather produced heavy loads. The *nuclear outage* scenario simulates a nuclear outage either due to operational constraints or as a result of policy decisions. The *line outage* scenario simulates a planned or unplanned line outage under average loading. The *avoid temperature violation* scenario assumes that plant operators reduce capacity to avoid temperature violations.

Table 5.2: Exogenous Scenarios

Scenario Name	Description
Average Week	Week with historically average temperature and load
Extreme Load/Climate	Week with historically high temperature and load
Nuclear Outage[1,2]	Non-operation of a nuclear plant
Critical Line Outage[2]	Drastic changes in the transmission topology
Avoid Temperature Violation	Shift in existing policy enforcement where generators ensure no temperature violations occur by reducing output

[1] For example, due to either maintenance or a water-related outage Krier [2012], Freedman [2012].

[2] The load and climatological stressors are set to average levels for these scenarios (i.e., outages are the only differences, with all other factors remaining constant)

5.4.3 The Interplay of Cost, Water Withdrawal, Water Consumption, and Emissions

By comparing the *relative* performance of each policy for an average week, we gain insights into the general interplay of cost, water withdrawal, water consumption, and emissions. The performance of each policy is depicted in Figure 5.2 such that policies intersecting axes *lower* have *better* performance (i.e., down is the preferred direction). Each policy increases operational costs compared to "status quo" operations but offers benefits such as reduced water consumption. Some policies offer focused benefits with respect to only a single objective while sacrificing performance in other objectives. For example, the "high water consumption penalty" policy reduces status quo water consumption by 80 percent but increases status quo emissions by 120 percent. Policies that consider emissions ("high emissions penalty" and "water-emissions") highlight that it is possible to

reduce a system's water withdrawal, water consumption, and emissions at a marginal (five percent) increase in operational cost.

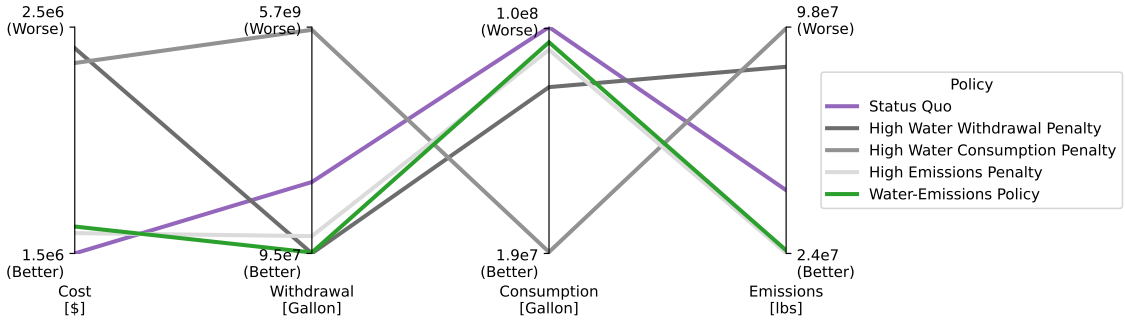

Figure 5.2: Tradeoffs in Policy Performance for an Average Week. Status quo operations de-emphasize water consumption, withdrawal, and emissions. However, through multi-objective policy optimization, we find holistic policies that effectively compromise among all objectives.

This analysis reveals a nuanced tradeoff between water use, emissions, and cost. The general tradeoff between water consumption and withdrawal has been established [McCall and Macknick, 2016], but the impacts of this tradeoff on operational costs and emissions have not been demonstrated. Generator cooling technologies that are water-consumption-efficient tend to be water-withdrawal-inefficient and vice versa. This is mainly because cooling technologies can be broken down into open-loop technologies that rely on the direct warming of diverted liquid water (increased withdrawal) and recirculating systems that warm air and recirculating water via heat exchanger (increased consumption). The two policies that attempt only water reductions ("high water withdrawal penalty" and "high water consumption penalty") have poor cost and emissions performance because they shift the power dispatch of the system toward costly water-efficient and emission-inefficient generators (e.g., natural gas combustion turbines seen in Appendix Figure E.1). However, the *way* that these policies achieve this performance is different; in our case study, each policies' relative emphasis determines the extent to which the system relies on expensive natural gas generators with recirculating cooling systems or coal generators with once-through cooling systems. Therefore, even though these two policies have similar costs, one produces the minimum

withdrawal while the other produces the maximum withdrawal of the policies tested. However, this minimum/maximum behavior was not observed for system water consumption. Instead, the policy that minimized withdrawal had the fourth highest consumption. For our system, this nuanced behavior was due to the inclusion of a nuclear generator whose cooling system was inefficient with respect to both water withdrawal and consumption. This behavior led to "status quo" operations exhibiting the highest consumption. Unfortunately, the severity of this tradeoff would be further exacerbated if generators install emission-capturing devices without considering how these devices further increase water consumption [Zhai and Rubin, 2010]. Clearly, how policies impact the interplay of cost, water withdrawal, water consumption, and emissions in energy systems, is both nuanced and critical for the future of our energy systems.

5.4.4 Comparing Climatological and Operational Stressors

Modern energy grids, and the policies associated with them, must respond to various climatological and operational stressors [Pfenninger et al., 2014, Miara et al., 2017]. The policy performance (bars) over each scenario (column) for every objective (row) is depicted in Figure 5.3. We compare our policy's performance for several scenarios with varying degrees of climatological and operational stressors (Table 5.2) to the average week performance previously discussed in Section 5.4.3.

Operational stressors not commonly associated with water/energy interactions, like a nuclear outage, can have more pronounced impacts on systems than the traditionally considered climatological stressors particularly due to their geographical correlation Bernstein et al. [2014]. The *nuclear outage* scenario leads to increases in operational costs, water withdrawals, and emissions compared to the *extreme load/climate* scenario under current operations. Physically, this result is because the system has lost an operationally inexpensive and low-emitting fuel source. This finding suggests that, for our case study, a nuclear outage is a larger stressor than historical climatological extremes.

Other uncommon water/energy operational stressors, like a line outage, can also impact policy performance. Physically, the transmission network topology constrains generator dispatch. Although the *critical line outage* scenario led to slight (roughly 10 percent) increases in operational

cost, withdrawal, and consumption, system emissions saw a greater impact. Particularly, "status quo" emissions saw a twenty percent increase. However, the largest impact was to system reliability as a result of the "high water withdrawal penalty" policy. Such behavior further highlights the importance of topological consideration in creating a holistic energy policy.

Our policies effectively mitigated impacts on system performance during our simulated scenarios. Figure 5.4 highlights the performance of the informed policies *relative* to "status quo" by depicting this policy performance as bars and the relative change of the policy performance as lollipops. Therefore, a downward-facing lollipop shows a decrease (i.e., improvement) in objective performance relative to "status quo".

The scenarios applied to our case study reveal that external stressors can have widely varying impacts on policy performance. Recall the tendency from Section 5.4.3 that the two policies that attempt only water reductions tend to strongly emphasize water-related objectives at the severe cost of all other objectives. The *extreme load/climate* scenario illustrates the severity of this tendency. By introducing a high consumption penalty, some generators discharge significant volumes of elevated-temperature water beyond legal limits posing threats to riverine ecology. Conversely, the "high withdrawal penalty policy" impacts system reliability as the cost of withdrawn water outweighs the cost of not serving demand. However, the *nuclear outage* scenario illustrates that these two policies actually *improve* emissions while not impacting reliability or discharge violations.

A policy focused only on emissions reduction has benefits for the various water-related objectives of the system across all simulated scenarios. We see the emission-focused policy ("high-emissions penalty") only marginally (less than 6 percent) increases cost across all scenarios. However, for this cost increase, it is able to unanimously improve status quo water withdrawal, water consumption, and emissions performance. It even offers some benefits to reducing thermal discharge violations in the *extreme load/climate* scenario. Importantly, we see that the reliability of the system is maintained with an emissions-only-focused policy. In our next section, we discuss how our holistic water and emissions policy is able further to improve on the emissions-only policy.

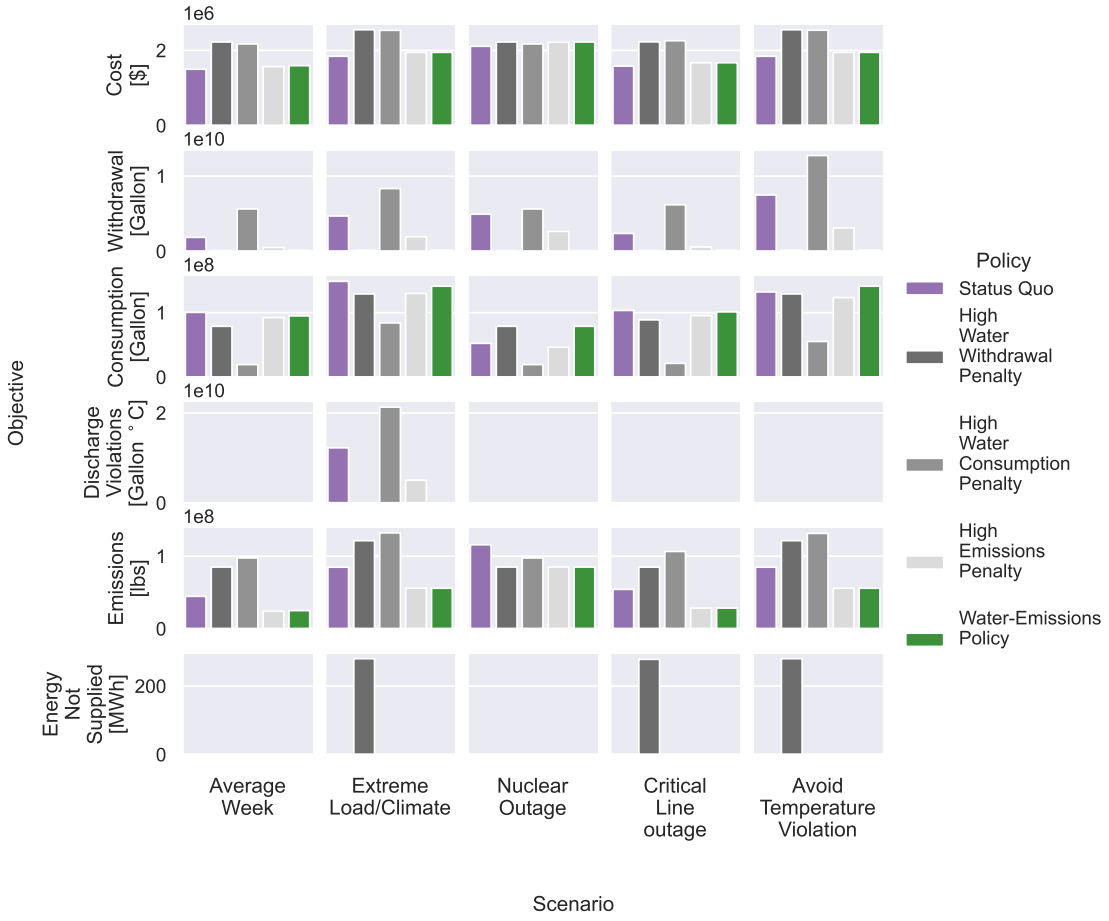

Figure 5.3: Policy Performance Over Several Scenarios. Objectives, scenarios, and policies are depicted as rows, columns, and colors, respectively. We introduce the discharge violations objective defined as the amount and temperature of water discharged beyond the legal limit as well as the energy not supplied by the system (i.e., reliability) as additional system objectives. Objective performance is impacted by the scenario regardless of the policy.

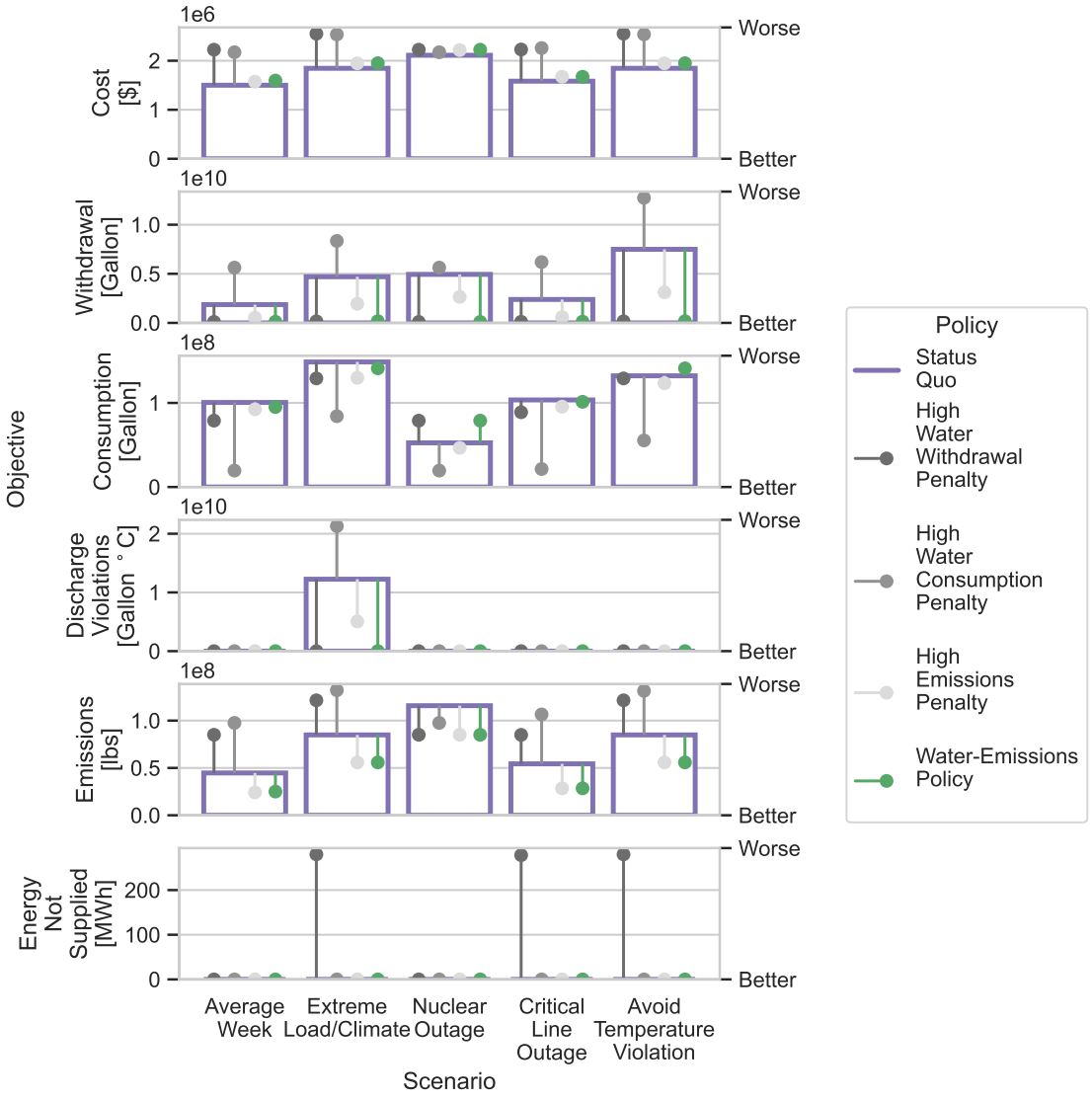

Figure 5.4: Policy Performance Relative to Status Quo Operations. "Status quo" policy is depicted as bars. Downward lollipops portray an improvement in policy performance relative to "status quo" policy. Through water- and emission-informed policy, the impacts of various climatological and operational stressors can be effectively mitigated.

5.4.5 The Benefits of Holistic Policy Considerations

Life-threatening impacts on fish populations due to thermal discharge violations from power plants [Logan et al., 2021, Barnthouse and Coutant, 2022] are avoidable through well-created and

enforced energy policies. However, the physical grid reliability can be threatened by policies that completely eliminate such violations (e.g., "high water withdrawal penalty"). Meanwhile, other policies offer only some reductions to these thermal discharge violations (e.g., "high emissions penalty").

Our holistic "water-emissions" policy capitalizes on some of the strengths of the "high emissions penalty" policy while augmenting the ability to operate the system with no discharge violations. Specifically, this holistic policy leads to no thermal discharge violations while yielding improvements in system withdrawal, consumption, and emissions without major increases in operational cost. Additionally, this policy's performance is preserved across climatological and operational stressors.

Our "water-emissions" policy also has enforcement benefits. The proposed policies are incorporated *directly* into the existing operational problem of optimal power flow without adding substantial complexity. Such direct incorporation avoids the need for enforcement that is dependent on human judgment. For example, currently, many existing laws prevent discharge temperature violations. However, such laws are rarely enforced [Micha, 2014, Liu et al., 2017]. In the *avoid temperature violation* scenario, we simulate a reality in which such laws are enforced and generators reduce capacity *instead* of allowing temperature violations. Even under such scenarios, our policy still offers benefits to reducing water withdrawal and emissions. Although our policy only slightly increases overall system costs, there does exist the "who pays?" question regarding that increase. One such method that has been implemented for emissions reduction is a cap-and-trade scheme; however, the specific methods are an area of future research.

5.5 Conclusion

In this chapter, we pose alternative water- and emissions-informed policies, comprised of weights on water use and emission, for operating energy systems such that impacts associated with extreme operational and climatological system stressors can be effectively mitigated. However, selecting the specific value of these weights is nontrivial. We create several reference policies that

capture the status quo and traditional single-objective operational approaches (i.e., policies that just focus on reducing cost, just focus on reducing emissions, etc.). Through simulation applied to a case study, we discover fundamental interactions among system operational costs, water withdrawal, water consumption, emissions, and reliability. Additionally, we show that the consideration of both operational and climatological stressors, as well as a high-fidelity power systems model, are crucial when creating energy policies. If these considerations are ignored, policies intended to have benefits with respect to certain aspects of system performance may severely degrade other areas of performance. We compare the performance of our reference policies to the performance of a holistic water/emissions policy created using a multi-objective policy search framework that allows policymakers to create holistic policies that reflect their specific preferences for system operation. We show that such holistic policies balance the impact of operational and climatological exogenous system stressors. Thus, a multi-objective perspective is necessary to create holistic energy system policies.

Chapter 6

Concluding Remarks

This dissertation proposed several novel frameworks for the multi-objective operation of power systems - specifically, focusing on the interactions among of thermoelectric water use, emissions, cost, and reliability. The first of these frameworks contributed a novel multi-objective water- and emissions-informed tradeoff framework. The second of these frameworks used a sensitivity analysis of a policy-focused water/energy model to show how policy decisions can help mitigate the adverse effects of external climatological stressors. The final framework contributes a multi-objective method to find optimal operational penalties as well as a novel cosimulation model to simulate interactions between power system cost, water use, reliability, and emissions.

Throughout this thesis, we have demonstrated the utility of these frameworks to the current and future power systems community. Currently, the insights gained through these frameworks are primarily valuable to power system planners. We gained both system and component-level insights into how various climatological stressors impact the water, emissions, cost, and reliability of the grid. Such information is critical for grid planning decisions, such as generator decommissioning or power plant cooling system retrofitting decisions. Our high-fidelity approach to modeling power systems operations as well as the rigorousness with which the multi-objective methods were applied also allowed us detailed insights into water/energy system interactions. Our demonstration of such approaches is invaluable to the current and future water/energy academic community.

The value of this work will hopefully one day translate into water- and emissions-informed real-time power systems operations. However, before such a pilot program could be attempted,

additional efforts would need to be investigated to answer the "who pays" question which was largely out of the scope of this thesis. Although the resulting cost increases throughout this thesis were often marginal, such increases can add up over time, and thus further efforts are needed to determine how these costs could be equitably split. One common solution for power systems operations would be through the creation of a market structure, however, the specific details of such a structure would require additional research efforts.

There are also several ways in which this research could be extended for power system planning purposes. One obvious extension would be to create *projected* grid stressors instead of historic events [Verdin et al., 2015, Prairie et al., 2012]. The projection of synthetic water/energy datasets is a particularly difficult task due to the natural uncertainty in natural systems as well as the compounded uncertainty in the technological advances that will impact the grid. Therefore, the future of water energy systems may be "deeply uncertain" and further efforts could take the view of ensuring *robust* policies that are designed to be effective across *many* possible states of the world [Kasprzyk et al., 2013].

Another extension of this work would be to expand the time horizon and detail of the cosimulation model. For example, a production cost power systems simulation could include both unit commitment and power flow over many years - thus allowing insight into *seasonal* water/energy/emissions/reliability impacts. Additionally, our cosimulation could include existing fishkill models to accurately capture the propagating ecological impacts of thermoelectric discharge on local fish populations [Deslauriers et al., 2017]. Similarly, such a model could be coupled with a high-fidelity river routing model to further examine the impacts of thermoelectric "interference" (i.e., the process of upstream plants impacting downstream plants) [Miara et al., 2018]. However, validating such a simulation would require extensive publicly-available thermoelectric discharge data, which unfortunately has not become ubiquitous even after recent requests [Chini et al., 2018, Meng et al., 2020]. Additionally, as further models are developed, increased efforts should be made to create user-centric software tools for water/energy cosimulations, especially if such efforts are to be repeated across many use cases.

The important choice of how to operate the energy grid leads to cascading impacts that are felt far beyond the energy sector. Neglecting such interactions during operation can have detrimental externalities. While it may be tempting to consider such externalities as a hard constraint on system operations, we have seen that when energy grids are pushed to their limits, these once-hard constraints seem like ideals. Multi-objective operational policy frameworks, such as the ones proposed in this thesis, demonstrate the ability to more honestly and consistently represent the connectedness of the modern energy system. Therefore, if we are to make effective policies for modern coupled energy systems, systems that are inherently multi-objective, we must embrace multi-objective energy policies.

Bibliography

M.A. Abido. Environmental/economic power dispatch using multiobjective evolutionary algorithms. IEEE Transactions on Power Systems, 18(4):1529–1537, 2003a. ISSN 0885-8950. doi: 10.1109/tpwrs.2003.818693. URL https://dx.doi.org/10.1109/tpwrs.2003.818693. Publisher: Institute of Electrical and Electronics Engineers (IEEE).

M.A. Abido. A novel multiobjective evolutionary algorithm for environmental/economic power dispatch. Electric Power Systems Research, 65(1):71–81, 2003b. ISSN 0378-7796. doi: 10.1016/s0378-7796(02)00221-3. URL https://dx.doi.org/10.1016/s0378-7796(02)00221-3. Publisher: Elsevier BV.

Maged Aboelata and David Bowles. LIFESim: A Tool for Estimating and Reducing Life-Loss Resulting from Dam and Levee Failures. In Proceedings of the Association of State Dam Safety Officials, Indian Wells, CA, 2008.

Maged Aboelata, David Bowles, and Duane M. McClelland. GIS Model for Estimating Dam Failure Life Loss. In Proceedings of the 10th Engineering Foundation Conference on Risk-Based Decision Making, pages 126–145, Santa Barbara, California, United States, 2002. doi: https://doi.org/10.1061/40694(2003)11.

R.T.F. Ah King and H.C.S. Rughooputh. Elitist multiobjective evolutionary algorithm for environmental/economic dispatch. In The 2003 Congress on Evolutionary Computation. IEEE, 2003. doi: 10.1109/cec.2003.1299792. URL https://dx.doi.org/10.1109/cec.2003.1299792.

Katherine H Anderson, Elizabeth L Hotchkiss, and Caitlin Murphy. Valuing Resilience in Electricity Systems. Technical Report, National Renewable Energy Lab (NREL), Golden, CO (United States), 2019.

B. Robert Archibald, David H. Finifter, and Carlisle E. Moodty. Seasonal variation in residential electricity demand: evidence from survey data. Applied Economics, 14(2):167–181, April 1982. ISSN 0003-6846. doi: 10.1080/00036848200000013. URL https://doi.org/10.1080/00036848200000013. Publisher: Routledge.

ASHRAE. ASHRAE Handbook – HVAC Systems and Equipment. Technical report, ASHRAE, Atlanta, GA, 2008.

Maximilian Auffhammer, Patrick Baylis, and Catherine H. Hausman. Climate change is projected to have severe impacts on the frequency and intensity of peak electricity demand across the United

States. Proceedings of the National Academy of Sciences, 114(8):1886–1891, 2017. ISSN 0027-8424. doi: 10.1073/pnas.1613193114. URL https://dx.doi.org/10.1073/pnas.1613193114. Publisher: Proceedings of the National Academy of Sciences.

Kristen Averyt, Jordan Macknick, J. Rogers, N. Madden, J. Fisher, James Meldrum, and Robin Newmark. Water Use for Electricity in the United States: An Analysis of Reported and Calculated Water Use Information for 2008. Environmental Research Letters, 8, 2013. doi: 10.1088/1748-9326/8/1/015001.

Lawrence W. Barnthouse and Charles C. Coutant. Modernizing thermal discharge assessments for the 21st century. Integrated Environmental Assessment and Management, 18(2):459–468, 2022. ISSN 1551-3793. doi: 10.1002/ieam.4472. URL https://onlinelibrary.wiley.com/doi/abs/10.1002/ieam.4472. _eprint: https://onlinelibrary.wiley.com/doi/pdf/10.1002/ieam.4472.

H Battey, Z Clement, F Fields, and J Li. The Water-Energy Nexus: Challenges and Opportunities. US Department of Energy, Tech. Rep, 2014.

Andrey Bernstein, Daniel Bienstock, David Hay, Meric Uzunoglu, and Gil Zussman. Power grid vulnerability to geographically correlated failures — Analysis and control implications. In IEEE INFOCOM 2014 - IEEE Conference on Computer Communications. IEEE, 2014. doi: 10.1109/infocom.2014.6848211. URL https://dx.doi.org/10.1109/infocom.2014.6848211.

R. Billinton and R.N. Allan. Power-system reliability in perspective. Electronics and Power, 30(3):231–236, March 1984. ISSN 0013-5127. doi: 10.1049/ep.1984.0118. Conference Name: Electronics and Power.

Adam B. Birchfield, Ti Xu, Kathleen M. Gegner, Komal S. Shetye, and Thomas J. Overbye. Grid Structural Characteristics as Validation Criteria for Synthetic Networks. IEEE Transactions on Power Systems, 32(4):3258–3265, 2017. ISSN 0885-8950. doi: 10.1109/tpwrs.2016.2616385. URL https://dx.doi.org/10.1109/tpwrs.2016.2616385. Publisher: Institute of Electrical and Electronics Engineers (IEEE).

Andrew P. Bradley. The use of the area under the ROC curve in the evaluation of machine learning algorithms. Pattern Recognition, 30(7):1145–1159, July 1997. ISSN 0031-3203. doi: 10.1016/S0031-3203(96)00142-2. URL http://www.sciencedirect.com/science/article/pii/S0031320396001422.

Jedidiah Brewer, Robert Glennon, Alan Ker, and Gary D Libecap. Water Markets in the West: Prices, Trading, and Contractual Forms. Working Paper 13002, National Bureau of Economic Research, March 2007. URL http://www.nber.org/papers/w13002. Series: Working Paper Series.

Stephen J Burges. Water resource systems planning in USA: 1776-1976. Journal of the Water Resources Planning and Management Division, 105(1):91–111, 1979. Publisher: American Society of Civil Engineers.

Mary Cain, Richard O'Neill, and Anya Castillo. History of Optimal Power Flow and Formulations: Optimal Power Flow Paper. Federal Energy Regulatory Commission, 1, December 2012.

Jacques Carpentier. Contribution a l'etude du dispatching economique. Bulletin de la Société Francaise des électriciens, 3(1):431–447, 1962.

Xiaoxian Chen, Yi Zheng, Bo Xu, Longfan Wang, Feng Han, and Chi Zhang. Balancing competing interests in the Mekong River Basin via the operation of cascade hydropower reservoirs in China: Insights from system modeling. Journal of Cleaner Production, 254:119967, May 2020. ISSN 09596526. doi: 10.1016/j.jclepro.2020.119967. URL https://linkinghub.elsevier.com/retrieve/pii/S0959652620300147.

Christopher M. Chini, Lucas A. Djehdian, William N. Lubega, and Ashlynn S. Stillwell. Virtual water transfers of the US electric grid. Nature Energy, 3(12):1115–1123, 2018. ISSN 2058-7546. doi: 10.1038/s41560-018-0266-1. URL https://dx.doi.org/10.1038/s41560-018-0266-1. Publisher: Springer Science and Business Media LLC.

Zachary Clement, Fletcher Fields, Diana Bauer, Vincent Tidwell, Calvin Ray Shaneyfelt, and Geoff Klise. Effects of Cooling System Operations on Withdrawal for Thermoelectric Power. In Volume 1: Boilers and Heat Recovery Steam Generator; Combustion Turbines; Energy Water Sustainability; Fuels, Combustion and Material Handling; Heat Exchangers, Condensers, Cooling Systems, and Balance-of-Plant. American Society of Mechanical Engineers, 2017. doi: 10.1115/power-icope2017-3763. URL https://dx.doi.org/10.1115/power-icope2017-3763.

A. Cousin, A. Janon, V. Maume-Deschamps, and I. Niang. On the consistency of Sobol indices with respect to stochastic ordering of model parameters. ESAIM: Probability and Statistics, 23: 387–408, 2019. ISSN 1262-3318. doi: 10.1051/ps/2018001. URL https://www.esaim-ps.org/10.1051/ps/2018001.

Coral Davenport and Lisa Friedman. E.P.A. to Propose First Controls on Greenhouse Gases From Power Plants. The New York Times, April 2023. ISSN 0362-4331. URL https://www.nytimes.com/2023/04/22/climate/epa-power-plants-pollution.html.

Kalyanmoy Deb and Ankur Sinha. An Efficient and Accurate Solution Methodology for Bilevel Multi-Objective Programming Problems Using a Hybrid Evolutionary-Local-Search Algorithm. Evolutionary Computation, 18(3):403–449, September 2010. ISSN 1063-6560. doi: 10.1162/EVCO-a-00015. Conference Name: Evolutionary Computation.

David Deslauriers, Steven R. Chipps, James E. Breck, James A. Rice, and Charles P. Madenjian. Fish Bioenergetics 4.0: An R-Based Modeling Application. Fisheries, 42 (11):586–596, 2017. ISSN 1548-8446. doi: 10.1080/03632415.2017.1377558. URL https://onlinelibrary.wiley.com/doi/abs/10.1080/03632415.2017.1377558. _eprint: https://onlinelibrary.wiley.com/doi/pdf/10.1080/03632415.2017.1377558.

Timothy H. Diehl, Melissa Harris, Jennifer C. Murphy, Susan S. Hutson, and David E. Ladd. Methods for estimating water consumption for thermoelectric power plants in the United States. USGS Numbered Series 2013-5188, U.S. Geological Survey, Reston, VA, 2013. URL http://pubs.er.usgs.gov/publication/sir20135188. Code Number: 2013-5188 Code: Methods for estimating water consumption for thermoelectric power plants in the United States Publication Title: Methods for estimating water consumption for thermoelectric power plants in the United States Reporter: Methods for estimating water consumption for thermoelectric power plants in the United States Series: Scientific Investigations Report IP-045152.

Cheryl A. Dieter, Molly A. Maupin, Rodney R. Caldwell, Melissa A. Harris, Tamara I. Ivahnenko, John K. Lovelace, Nancy L. Barber, and Kristin S. Linsey. Estimated use of water in the

United States in 2015. Report 1441, United States Geological Society, Reston, VA, 2018. URL http://pubs.er.usgs.gov/publication/cir1441.

Ahmet Durmayaz and Oguz Salim Sogut. Influence of cooling water temperature on the efficiency of a pressurized-water reactor nuclear-power plant. International Journal of Energy Research, 30(10):799–810, 2006. ISSN 0363-907X. doi: 10.1002/er.1186. URL https://dx.doi.org/10.1002/er.1186. Publisher: Wiley.

Ben Dziegielewski, Subhash C Sharma, Tom Bik, Heru Margono, and Xiaoying Yang. Analysis of water use trends in the United States: 1950-1995. Special Report, 28, 2002.

Joe Eaton. Record Heat, Drought Pose Problems for U.S. Electric Power, August 2012. URL https://www.nationalgeographic.com/science/article/120817-record-heat-drought-pose-problems-for-electric-power-grid.

EIA. Hourly electricity consumption varies throughout the day and across seasons, February 2020a. URL https://www.eia.gov/todayinenergy/detail.php?id=42915.

EIA. Thermoelectric cooling water data, October 2020b. URL https://www.eia.gov/electricity/data/water/.

EPA. Recommended Procedures for Development of Emissions Factors and Use of the WebFIRE Database. Environmental Protection Agency, 2021.

Robert Fares. The U.S. Electric Grid's Cost in 2 Charts, April 2017. URL https://blogs.scientificamerican.com/plugged-in/the-u-s-electric-grids-cost-in-2-charts/.

Federal Emergency Management Agency. Federal Guidelines for Dam Safety: Hazard Potential Classification System for Dams. Technical report, Interagency Committee Dam Safety, Washington, D.C., 1998. URL https://www.fema.gov/media-library-data/20130726-1516-20490-7951/fema-333.pdf.

Federal Emergency Management Agency and Department of Homeland Security. Multi-hazard Loss Estimation Methodology. Technical Manual, Federal Emergency Management Agency, 2017.

Bruce Feinberg, William Engemoen, William Fiedler, and Dan Osmun. Reclamation's Empirical Method for Estimating Life Loss Due to Dam Failure. In E3S Web of Conferences, volume 7, page 06002, Lyon, France, 2016. doi: 10.1051/e3sconf/20160706002. URL http://www.e3s-conferences.org/10.1051/e3sconf/20160706002.

Robert J. Flores and Jacob Brouwer. Optimal design of a distributed energy resource system that economically reduces carbon emissions. Applied Energy, 232:119–138, December 2018. ISSN 03062619. doi: 10.1016/j.apenergy.2018.09.029. URL https://linkinghub.elsevier.com/retrieve/pii/S0306261918313369.

Dariush Fooladivanda and Joshua A. Taylor. Dispatching thermal power plants under water constraints. In 2015 53rd Annual Allerton Conference on Communication, Control, and Computing (Allerton). IEEE, 2015. doi: 10.1109/allerton.2015.7447031. URL https://dx.doi.org/10.1109/allerton.2015.7447031.

Stephen Frank and Steffen Rebennack. An introduction to optimal power flow: Theory, formulation, and examples. IIE Transactions, 48(12):1172–1197, 2016. ISSN 0740-817X. doi: 10.1080/0740817x.2016.1189626. URL https://dx.doi.org/10.1080/0740817x.2016.1189626. Publisher: Informa UK Limited.

Freedman. Heat and Drought Pose Risks for Nuclear Power Plants, July 2012. URL https://www.climatecentral.org/blogs/heat-and-drought-pose-risks-for-nuclear-power-plants.

Pierre Friedlingstein, Michael O'Sullivan, Matthew W. Jones, Robbie M. Andrew, Luke Gregor, Judith Hauck, Corinne Le Quéré, Ingrid T. Luijkx, Are Olsen, Glen P. Peters, Wouter Peters, Julia Pongratz, Clemens Schwingshackl, Stephen Sitch, Josep G. Canadell, Philippe Ciais, Robert B. Jackson, Simone R. Alin, Ramdane Alkama, Almut Arneth, Vivek K. Arora, Nicholas R. Bates, Meike Becker, Nicolas Bellouin, Henry C. Bittig, Laurent Bopp, Frédéric Chevallier, Louise P. Chini, Margot Cronin, Wiley Evans, Stefanie Falk, Richard A. Feely, Thomas Gasser, Marion Gehlen, Thanos Gkritzalis, Lucas Gloege, Giacomo Grassi, Nicolas Gruber, Ozgur Gürses, Ian Harris, Matthew Hefner, Richard A. Houghton, George C. Hurtt, Yosuke Iida, Tatiana Ilyina, Atul K. Jain, Annika Jersild, Koji Kadono, Etsushi Kato, Daniel Kennedy, Kees Klein Goldewijk, Jürgen Knauer, Jan Ivar Korsbakken, Peter Landschützer, Nathalie Lefèvre, Keith Lindsay, Junjie Liu, Zhu Liu, Gregg Marland, Nicolas Mayot, Matthew J. McGrath, Nicolas Metzl, Natalie M. Monacci, David R. Munro, Shin-Ichiro Nakaoka, Yosuke Niwa, Kevin O'Brien, Tsuneo Ono, Paul I. Palmer, Naiqing Pan, Denis Pierrot, Katie Pocock, Benjamin Poulter, Laure Resplandy, Eddy Robertson, Christian Rödenbeck, Carmen Rodriguez, Thais M. Rosan, Jörg Schwinger, Roland Séférian, Jamie D. Shutler, Ingunn Skjelvan, Tobias Steinhoff, Qing Sun, Adrienne J. Sutton, Colm Sweeney, Shintaro Takao, Toste Tanhua, Pieter P. Tans, Xiangjun Tian, Hanqin Tian, Bronte Tilbrook, Hiroyuki Tsujino, Francesco Tubiello, Guido R. van der Werf, Anthony P. Walker, Rik Wanninkhof, Chris Whitehead, Anna Willstrand Wranne, Rebecca Wright, Wenping Yuan, Chao Yue, Xu Yue, Sönke Zaehle, Jiye Zeng, and Bo Zheng. Global Carbon Budget 2022. Earth System Science Data, 14(11):4811–4900, November 2022. ISSN 1866-3508. doi: 10.5194/essd-14-4811-2022. URL https://essd.copernicus.org/articles/14/4811/2022/. Publisher: Copernicus GmbH.

Kate Galbraith. Drought Could Pose Power Plant Problems, September 2011. URL https://www.texastribune.org/2011/09/16/drought-could-post-problems-texas-power-plants/.

Kristin Gerdes and Christopher Nichols. Water requirements for existing and emerging thermoelectric plant technologies. Report from DOE/NETL, pages 5–9, 2009.

Mojtaba Ghasemi, Sahand Ghavidel, Mohsen Gitizadeh, and Ebrahim Akbari. An improved teaching–learning-based optimization algorithm using Lévy mutation strategy for non-smooth optimal power flow. International Journal of Electrical Power & Energy Systems, 65:375–384, February 2015. ISSN 01420615. doi: 10.1016/j.ijepes.2014.10.027. URL https://linkinghub.elsevier.com/retrieve/pii/S0142061514006309.

Emily Grubert and Kelly T. Sanders. Water Use in the United States Energy System: A National Assessment and Unit Process Inventory of Water Consumption and Withdrawals. Environmental Science & Technology, 52(11):6695–6703, 2018. ISSN 0013-936X. doi: 10.1021/acs.est.8b00139. URL https://dx.doi.org/10.1021/acs.est.8b00139. Publisher: American Chemical Society (ACS).

Abdalla Habashy. Climate Change Impact on Nuclear Power Production. PhD thesis, Centrale Supélec, Gif-sur-Yvette, France, September 2020.

D. Hadka and P. Reed. Borg: An Auto-Adaptive Many-Objective Evolutionary Computing Framework. Evolutionary Computation, 21(2):231–259, May 2013. doi: 10.1162/EVCO-a-00075.

David Hadka, Patrick M. Reed, and Timothy W. Simpson. Diagnostic assessment of the borg MOEA for many-objective product family design problems. In 2012 IEEE Congress on Evolutionary Computation. IEEE, 2012. doi: 10.1109/cec.2012.6256466. URL https://dx.doi.org/10.1109/CEC.2012.6256466.

Elizabeth B. Harper, John C. Stella, and Alexander K. Fremier. Global sensitivity analysis for complex ecological models: a case study of riparian cottonwood population dynamics. Ecological Applications, 21(4):1225–1240, 2011. ISSN 1051-0761. doi: 10.1890/10-0506.1. URL https://dx.doi.org/10.1890/10-0506.1. Publisher: Wiley.

Melissa Harris and Tim Diehl. A Comparison of Three Federal Datasets for Thermoelectric Water Withdrawals in the United States for 2010. JAWRA Journal of the American Water Resources Association, 53, 2017. doi: 10.1111/1752-1688.12551.

Joseph Hart and Pierre Gremaud. Robustness of the Sobol' indices to marginal distribution uncertainty. arXiv pre-print server, December 2018. URL https://arxiv.org/abs/1812.07042.

C B Harto, Y E Yan, Y K Demissie, D Elcock, V C Tidwell, K Hallett, J Macknick, M S Wigmosta, T K [Environmental Science Division] Tesfa, (Sandia National Laboratory), (National Renewable Energy Laboratory), and (Pacific Northwest National Laboratory). Analysis of drought impacts on electricity production in the Western and Texas interconnections of the United States. Technical report, U.S. Department of Energy Office of Scientific and Technical Information, United States, February 2012. URL https://www.osti.gov/biblio/1035461.

N. Hatziargyriou, E. L. Karfopoulos, and K. Tsatsakis. The Impact of EV Charging on the System Demand. In Rodrigo Garcia-Valle and João A. Peças Lopes, editors, Electric Vehicle Integration into Modern Power Networks, pages 57–85. Springer New York, New York, NY, 2013. ISBN 978-1-4614-0134-6. URL 10.1007/978-1-4614-0134-6-3.

Jon Herman and Will Usher. SALib: An open-source Python library for Sensitivity Analysis. The Journal of Open Source Software, 2(9), January 2017. doi: 10.21105/joss.00097. URL https://doi.org/10.21105/joss.00097. Publisher: The Open Journal.

Herman Hesse, Winston Richard, and Winston Clard. Magister Ludi (The Glass Bead Game). Holt, Rinehart and Winston, Inc., 10 edition, 1969. ISBN 0-553-11916-8.

L. Hockstad and L. Hanel. Inventory of U.S. Greenhouse Gas Emissions and Sinks. Technical Report cdiac:EPA-EMISSIONS, Environmental System Science Data Infrastructure for a Virtual Ecosystem (ESS-DIVE) (United States), January 2018. URL https://www.osti.gov/dataexplorer/biblio/dataset/1464240.

J. H. Horlock. Advanced Gas Turbine Cycles: A Brief Review of Power Generation Thermodynamics. Elsevier, October 2013. ISBN 978-0-08-054556-1. Google-Books-ID: TJtQBAAAQBAJ.

Zechun Hu, Xifan Wang, and Gareth Taylor. Stochastic optimal reactive power dispatch: Formulation and solution method. International Journal of Electrical Power & Energy Systems, 32(6): 615–621, 2010. ISSN 0142-0615. doi: 10.1016/j.ijepes.2009.11.018. URL https://dx.doi.org/10.1016/j.ijepes.2009.11.018. Publisher: Elsevier BV.

R Huston. An overview of water requirements for electric power generation. Technical report, University of Texas Center for Research in Water Resources, Austin, TX, 1975.

IAEA. Efficient Water Management in Water Cooled Reactors. Number NP-T-2.6 in Nuclear Energy Series. INTERNATIONAL ATOMIC ENERGY AGENCY, Vienna, 2012. ISBN 978-92-0-132610-2. URL https://www.iaea.org/publications/8883/efficient-water-management-in-water-cooled-reactors.

IEA. Global Energy Review: CO2 Emissions in 2021. Technical report, International Energy Agency, Paris, 2021.

Boris Iglewicz and David C. Hoaglin. How to detect and handle outliers. Number v. 16 in ASQC basic references in quality control. ASQC Quality Press, Milwaukee, Wis, 1993. ISBN 978-0-87389-247-6.

Ali Ipakchi and Farrokh Albuyeh. Grid of the future. IEEE Power and Energy Magazine, 7(2): 52–62, 2009. ISSN 1540-7977. doi: 10.1109/mpe.2008.931384. URL https://dx.doi.org/10.1109/mpe.2008.931384. Publisher: Institute of Electrical and Electronics Engineers (IEEE).

Brittany Jacob. PG&E crews preparing for increase in electricity demand during heat wave, June 2021. URL https://abc30.com/10798583/. Section: weather.

Daniel Jornada and V. Jorge Leon. Robustness methodology to aid multiobjective decision making in the electricity generation capacity expansion problem to minimize cost and water withdrawal. Applied Energy, 162:1089–1108, 2016. ISSN 0306-2619. doi: 10.1016/j.apenergy.2015.10.157. URL https://dx.doi.org/10.1016/j.apenergy.2015.10.157. Publisher: Elsevier BV.

Joseph R. Kasprzyk, Shanthi Nataraj, Patrick M. Reed, and Robert J. Lempert. Many objective robust decision making for complex environmental systems undergoing change. Environmental Modelling & Software, 42:55–71, 2013. ISSN 1364-8152. doi: 10.1016/j.envsoft.2012.12.007. URL https://dx.doi.org/10.1016/j.envsoft.2012.12.007. Publisher: Elsevier BV.

J. C. Kloppers and D. G. Kröger. A critical investigation into the heat and mass transfer analysis of counterflow wet-cooling towers. International Journal of Heat and Mass Transfer, 48(3): 765–777, January 2005. ISSN 0017-9310. doi: 10.1016/j.ijheatmasstransfer.2004.09.004. URL https://www.sciencedirect.com/science/article/pii/S0017931004004041.

Hagen Koch and Stefan Vögele. Dynamic modelling of water demand, water availability and adaptation strategies for power plants to global change. Ecological Economics, 68(7):2031–2039, May 2009. ISSN 09218009. doi: 10.1016/j.ecolecon.2009.02.015. URL https://linkinghub.elsevier.com/retrieve/pii/S0921800909000639.

Jacob Kravits. Paxplot, April 2022. URL https://github.com/kravitsjacob/paxplot. original-date: 2021-12-11T20:59:15Z.

Jacob Kravits, Kyri Baker, and Joseph Kasprzyk. Multi-Objective Optimal Power Flow Considering Emissions and Voltage Violations. In 2021 IEEE Power & Energy Society General Meeting (PESGM), pages 1–5, Washington, DC, USA, July 2021a. IEEE. ISBN 978-1-66540-507-2. doi: 10.1109/PESGM46819.2021.9638044. URL https://ieeexplore.ieee.org/document/9638044/.

Jacob Kravits, Joseph Kasprzyk, Kyri Baker, and Konstantinos Andreadis. Screening Tool for Dam Hazard Potential Classification Using Machine Learning and Multiobjective Parameter Tuning. Journal of Water Resources Planning and Management, 147(10):04021064, 2021b. ISSN 0733-9496. doi: 10.1061/(asce)wr.1943-5452.0001414. URL https://dx.doi.org/10.1061/(asce)wr.1943-5452.0001414. Publisher: American Society of Civil Engineers (ASCE).

Jacob Kravits, Joseph R. Kasprzyk, Kyri Baker, and Ashlynn S Stillwell. Assessing Trade-Offs Between Water, Emissions, and Cost in Multi-Objective Optimal Power Flow. In 2022 IEEE Power & Energy Society General Meeting (PESGM), pages 1–5, Denver, CO, USA, 2022a.

Jacob Kravits, Joseph R Kasprzyk, Kyri Baker, and Ashlynn S Stillwell. Incorporating thermoelectric power plant water use into multi-objective optimal power flow. Environmental Research: Infrastructure and Sustainability, 2(1):015005, 2022b. ISSN 2634-4505. doi: 10.1088/2634-4505/ac4d18. URL https://dx.doi.org/10.1088/2634-4505/ac4d18. Publisher: IOP Publishing.

Robert Krier. Extreme Heat, Drought Show Vulnerability of Nuclear Power Plants, August 2012. URL https://insideclimatenews.org/news/15082012/nuclear-power-plants-energy-nrc-drought-weather-heat-water/.

Harold W. Kuhn and Albert W. Tucker. Nonlinear programming. In Proceedings of the Second Berkeley Symposium on Mathematical Statistics and Probability, pages 481–492, Berkeley, CA, USA, 1951. University of California Press.

Pankaj Kumar, Rangan Banerjee, and Trupti Mishra. A framework for analyzing trade-offs in cost and emissions in power sector. Energy, 195:116949, 2020. ISSN 0360-5442. doi: 10.1016/j.energy.2020.116949. URL https://dx.doi.org/10.1016/j.energy.2020.116949. Publisher: Elsevier BV.

T. Langford. Ecological Effects of Thermal Discharges. Springer Science & Business Media, November 1990. ISBN 978-1-85166-451-1. Google-Books-ID: f1M6lkRZ7MUC.

Paulina Concha Larruari and Upmanu Lall. Assessing the Exposure of Critical Infrastructure and Other Assets to the Climate Induced Failure of Aging Dams in the U.S. Technical report, Columbia Water Institute, 2020. URL https://globalriskinstitute.org/publications/assessing-exposure-critical-infrastructure-other-assets-climate-induced-failure/.

Marco Laumanns, Lothar Thiele, Kalyanmoy Deb, and Eckart Zitzler. Combining Convergence and Diversity in Evolutionary Multiobjective Optimization. Evolutionary Computation, 10(3): 263–282, September 2002. ISSN 1063-6560, 1530-9304. doi: 10.1162/106365602760234108. URL http://www.mitpressjournals.org/doi/10.1162/106365602760234108.

Uisung Lee, Joseph Chou, Hui Xu, Derrick Carlson, Aranya Venkatesh, Erik Shuster, Timothy J. Skone, and Michael Wang. Regional and seasonal water stress analysis of United States thermoelectricity. Journal of Cleaner Production, 270:122234, 2020. ISSN 0959-6526. doi:

10.1016/j.jclepro.2020.122234. URL https://dx.doi.org/10.1016/j.jclepro.2020.122234. Publisher: Elsevier BV.

Chenzhao Li and Sankaran Mahadevan. An efficient modularized sample-based method to estimate the first-order Sobol index. Reliability Engineering & System Safety, 153:110–121, September 2016. ISSN 09518320. doi: 10.1016/j.ress.2016.04.012. URL https://linkinghub.elsevier.com/retrieve/pii/S0951832016300266.

Hanyue Li, Ju Hee Yeo, Ashly L. Bornsheuer, and Thomas J. Overbye. The Creation and Validation of Load Time Series for Synthetic Electric Power Systems. IEEE Transactions on Power Systems, 36(2):961–969, March 2021. ISSN 0885-8950, 1558-0679. doi: 10.1109/TPWRS.2020.3018936. URL https://ieeexplore.ieee.org/document/9174809/.

Lu Liu, Mohamad Hejazi, Hongyi Li, Barton Forman, and Xiao Zhang. Vulnerability of US thermoelectric power generation to climate change when incorporating state-level environmental regulations. Nature Energy, 2(8):1–5, July 2017. ISSN 2058-7546. doi: 10.1038/nenergy.2017.109. URL https://www.nature.com/articles/nenergy2017109. Number: 8 Publisher: Nature Publishing Group.

Lu Liu, Mohamad Hejazi, Gokul Iyer, and Barton A. Forman. Implications of water constraints on electricity capacity expansion in the United States. Nature Sustainability, 2(3):206–213, March 2019. ISSN 2398-9629. doi: 10.1038/s41893-019-0235-0. URL https://www.nature.com/articles/s41893-019-0235-0. Number: 3 Publisher: Nature Publishing Group.

Lauren H. Logan and Ashlynn S. Stillwell. Probabilistic assessment of aquatic species risk from thermoelectric power plant effluent: Incorporating biology into the energy-water nexus. Applied Energy, 210:434–450, January 2018. ISSN 0306-2619. doi: 10.1016/j.apenergy.2017.09.027. URL https://www.sciencedirect.com/science/article/pii/S0306261917313107.

Lauren H. Logan, Rohini S. Gupta, Amy Ando, Cory Suski, and Ashlynn S. Stillwell. Quantifying tradeoffs between electricity generation and fish populations via population habitat duration curves. Ecological Modelling, 440:109373, January 2021. ISSN 03043800. doi: 10.1016/j.ecolmodel.2020.109373. URL https://linkinghub.elsevier.com/retrieve/pii/S0304380020304385.

William Lubega, Apoorva Santhosh, Amro M. Farid, and Kamal Youcef-Toumi. An Integrated Energy and Water Market for the Supply Side of the Energy-Water Nexus in the Engineered Infrastructure. In Volume 2: Simple and Combined Cycles; Advanced Energy Systems and Renewables (Wind, Solar and Geothermal); Energy Water Nexus; Thermal Hydraulics and CFD; Nuclear Plant Design, Licensing and Construction; Performance Testing and Performance Test Codes. American Society of Mechanical Engineers, 2014. doi: 10.1115/power2014-32075. URL https://dx.doi.org/10.1115/power2014-32075.

William N. Lubega and Ashlynn S. Stillwell. Analyzing the economic value of thermal power plant cooling water consumption. Water Resources and Economics, 27:100137, 2019. ISSN 2212-4284. doi: 10.1016/j.wre.2019.01.003. URL https://dx.doi.org/10.1016/j.wre.2019.01.003. Publisher: Elsevier BV.

William Naggaga Lubega and Ashlynn S. Stillwell. Maintaining electric grid reliability under hydrologic drought and heat wave conditions. Applied Energy, 210:538–549, 2018a. ISSN 0306-

2619. doi: 10.1016/j.apenergy.2017.06.091. URL https://dx.doi.org/10.1016/j.apenergy.2017.06.091. Publisher: Elsevier BV.

William Naggaga Lubega and Ashlynn S Stillwell. Managing impacts of hydrological droughts and heat waves on thermal power plants. PhD thesis, University of Illinois at Urbana-Champaign, June 2018b. URL http://hdl.handle.net/2142/101652.

Jay R. Lund, Ximing Cai, and Gregory W. Characklis. Economic Engineering of Environmental and Water Resource Systems. Journal of Water Resources Planning and Management, 132(6): 399–402, 2006. doi: 10.1061/(ASCE)0733-9496(2006)132:6(399).

J. Luo, L. Huang, Y. Sun, X. Wang, J. An, and T. Li. Life Loss Evaluation of Dam Failure Based on VOF Method. In 2009 3rd International Conference on Bioinformatics and Biomedical Engineering, pages 1–4, June 2009. doi: 10.1109/ICBBE.2009.5163014.

Tianyi Luo. Droughts and Blackouts: How Water Shortages Cost India Enough Energy to Power Sri Lanka. World Resources Institute, July 2017.

Kari Lydersen. Amid climate concerns, nuclear plants feel the heat of warming water, September 2016. URL https://energynews.us/2016/09/09/midwest/nuclear-plants-feel-the-heat-of-warming-water/.

J Macknick, R Newmark, G Heath, and K C Hallett. Operational water consumption and withdrawal factors for electricity generating technologies: a review of existing literature. Environ. Res. Lett., page 11, 2012. doi: 10.1088/1748-9326.

N Madden, A Lewis, and M Davis. Thermal effluent from the power sector: an analysis of once-through cooling system impacts on surface water temperature. Environmental Research Letters, 8 (3):035006, September 2013. ISSN 1748-9326. doi: 10.1088/1748-9326/8/3/035006. URL https://iopscience.iop.org/article/10.1088/1748-9326/8/3/035006.

Holger R. Maier and Graeme C. Dandy. Neural networks for the prediction and forecasting of water resources variables: a review of modelling issues and applications. Environmental Modelling & Software, 15(1):101–124, 2000. ISSN 1364-8152. doi: 10.1016/s1364-8152(99)00007-9. URL https://dx.doi.org/10.1016/S1364-8152(99)00007-9. Publisher: Elsevier BV.

Natalie Mamerow. Senate Appropriators Fund High Hazard Dam Rehab Program, June 2018. URL https://www.infrastructurereportcard.org/senate-appropriators-fund-high-hazard-dam-rehab-program/. Library Catalog: www.infrastructurereportcard.org Section: Dams.

James McCall and Jordan Macknick. Water-Related Power Plant Curtailments: An Overview of Incidents and Contributing Factors. Technical Report NREL/TP–6A20-67084, 1338176, U.S. Department of Energy, December 2016. URL http://www.osti.gov/servlets/purl/1338176/.

Measrainsey Meng and Kelly T. Sanders. A data-driven approach to investigate the impact of air temperature on the efficiencies of coal and natural gas generators. Applied Energy, 253:113486, 2019. ISSN 0306-2619. doi: 10.1016/j.apenergy.2019.113486. URL https://dx.doi.org/10.1016/j.apenergy.2019.113486. Publisher: Elsevier BV.

Measrainsey Meng, Emily Grubert, Rebecca A. M. Peer, and Kelly T. Sanders. Spatially allocating life cycle water use for US coal-fired electricity across producers, generators, and consumers. Energy Technology, 2020. ISSN 2194-4288. doi: 10.1002/ente.201901497. URL https://dx.doi.org/10.1002/ente.201901497. Publisher: Wiley.

James H. Merrick. On representation of temporal variability in electricity capacity planning models. Energy Economics, 59:261–274, 2016. ISSN 0140-9883. doi: 10.1016/j.eneco.2016.08.001. URL https://dx.doi.org/10.1016/j.eneco.2016.08.001. Publisher: Elsevier BV.

Ariel Miara, Jordan E. Macknick, Charles J. Vörösmarty, Vincent C. Tidwell, Robin Newmark, and Balazs Fekete. Climate and water resource change impacts and adaptation potential for US power supply. Nature Climate Change, 7(11):793–798, November 2017. ISSN 1758-6798. doi: 10.1038/nclimate3417. URL https://www.nature.com/articles/nclimate3417. Number: 11 Publisher: Nature Publishing Group.

Ariel Miara, Charles J Vörösmarty, Jordan E Macknick, Vincent C Tidwell, Balazs Fekete, Fabio Corsi, and Robin Newmark. Thermal pollution impacts on rivers and power supply in the Mississippi River watershed. Environmental Research Letters, 13(3):034033, March 2018. ISSN 1748-9326. doi: 10.1088/1748-9326/aaac85. URL https://iopscience.iop.org/article/10.1088/1748-9326/aaac85.

Philip K. Micha. In Hot Water: Clean Water Act Provisional Variances and Their Relationship to the Impact of Heat Waves and Droughts on the Supply and Demand of Electricity. Chicago-Kent Journal of Environmental and Energy Law, 4(1):1–34, 2014.

Omid Mohseni, Heinz G. Stefan, and Troy R. Erickson. A nonlinear regression model for weekly stream temperatures. Water Resources Research, 34(10):2685–2692, 1998. ISSN 1944-7973. doi: 10.1029/98WR01877. URL https://onlinelibrary.wiley.com/doi/abs/10.1029/98WR01877. _eprint: https://onlinelibrary.wiley.com/doi/pdf/10.1029/98WR01877.

Mengfei Mu, Zhenxing Zhang, Ximing Cai, and Qiuhong Tang. A water-electricity nexus model to analyze thermoelectricity supply reliability under environmental regulations and economic penalties during drought events. Environmental Modelling & Software, 123:104514, 2020. ISSN 1364-8152. doi: 10.1016/j.envsoft.2019.104514. URL https://dx.doi.org/10.1016/j.envsoft.2019.104514. Publisher: Elsevier BV.

Office of Energy Efficiency and Renewable Energy. Hydropower Basics, 2022. URL https://www.energy.gov/eere/water/hydropower-basics.

Adam P Pacsi, Nawaf S Alhajeri, Mort D Webster, Michael E Webber, and David T Allen. Changing the spatial location of electricity generation to increase water availability in areas with drought: a feasibility study and quantification of air quality impacts in Texas. Environmental Research Letters, 8(3):035029, September 2013. ISSN 1748-9326. doi: 10.1088/1748-9326/8/3/035029. URL https://iopscience.iop.org/article/10.1088/1748-9326/8/3/035029.

Rebecca Peer and Kelly Sanders. Characterizing cooling water source and usage patterns across US thermoelectric power plants: a comprehensive assessment of self-reported cooling water data. Environmental Research Letters, 11(12):124030, December 2016. ISSN 1748-9326. doi: 10.1088/1748-9326/aa51d8. URL https://iopscience.iop.org/article/10.1088/1748-9326/aa51d8.

Rebecca A. M. Peer, Jared B. Garrison, Craig P. Timms, and Kelly T. Sanders. Spatially and Temporally Resolved Analysis of Environmental Trade-Offs in Electricity Generation. Environmental Science & Technology, 50(8):4537–4545, 2016. ISSN 0013-936X. doi: 10.1021/acs.est.5b05419. URL https://dx.doi.org/10.1021/acs.est.5b05419. Publisher: American Chemical Society (ACS).

Stefan Pfenninger, Adam Hawkes, and James Keirstead. Energy systems modeling for twenty-first century energy challenges. Renewable and Sustainable Energy Reviews, 33:74–86, May 2014. ISSN 1364-0321. doi: 10.1016/j.rser.2014.02.003. URL https://www.sciencedirect.com/science/article/pii/S1364032114000872.

Francesca Pianosi, Keith Beven, Jim Freer, Jim W. Hall, Jonathan Rougier, David B. Stephenson, and Thorsten Wagener. Sensitivity analysis of environmental models: A systematic review with practical workflow. Environmental Modelling & Software, 79:214–232, May 2016. ISSN 13648152. doi: 10.1016/j.envsoft.2016.02.008. URL https://linkinghub.elsevier.com/retrieve/pii/S1364815216300287.

PJM. How Energy Use Varies with the Seasons, June 2019. URL https://learn.pjm.com/three-priorities/keeping-the-lights-on/how-energy-use-varies.

Marc Poumadère, Claire Mays, Sophie Le Mer, and Russell Blong. The 2003 Heat Wave in France: Dangerous Climate Change Here and Now. Risk Analysis, 25(6):1483–1494, 2005. ISSN 0272-4332. doi: 10.1111/j.1539-6924.2005.00694.x. URL https://dx.doi.org/10.1111/j.1539-6924.2005.00694.x. Publisher: Wiley.

James Prairie, Balaji Rajagopalan, and Terrance Fulp. Stochastic Streamflow Generation Incorporating Paleo-Reconstruction. World Environmental and Water Resources Congress, pages 1–21, April 2012. doi: 10.1061/40927(243)424. URL https://ascelibrary.org/doi/10.1061/40927%28243%29424. Publisher: American Society of Civil Engineers.

Hongbo Ren, Weisheng Zhou, Ken'ichi Nakagami, Weijun Gao, and Qiong Wu. Multi-objective optimization for the operation of distributed energy systems considering economic and environmental aspects. Applied Energy, 87(12):3642–3651, December 2010. ISSN 03062619. doi: 10.1016/j.apenergy.2010.06.013. URL https://linkinghub.elsevier.com/retrieve/pii/S0306261910002278.

Reuters Staff. Drought adds to 2012 Texas power supply worry. Reuters, October 2011. URL https://www.reuters.com/article/utilities-texas-drought-idAFN1E79H1L620111018.

Joshua Rhodes. The old, dirty, creaky US electric grid would cost $5 trillion to replace, March 2017.

Michael J. Rutberg, Anna Delgado, Howard J. Herzog, and Ahmed F. Ghoniem. A System-Level Generic Model of Water Use at Power Plants and its Application to Regional Water Use Estimation. In Volume 1: Advances in Aerospace Technology; Energy Water Nexus; Globalization of Engineering; Posters. ASMEDC, 2011. doi: 10.1115/imece2011-63786. URL https://dx.doi.org/10.1115/imece2011-63786.

Dirk Rübbelke and Stefan Vögele. Impacts of climate change on European critical infrastructures: The case of the power sector. Environmental Science & Policy, 14(1):53–63, January 2011.

ISSN 14629011. doi: 10.1016/j.envsci.2010.10.007. URL https://linkinghub.elsevier.com/retrieve/pii/S1462901110001371.

A. Saltelli, editor. Sensitivity analysis in practice: a guide to assessing scientific models. Wiley, Hoboken, NJ, 2004. ISBN 978-0-470-87093-8.

Kelly T. Sanders, Michael F. Blackhurst, Carey W. King, and Michael E. Webber. The Impact of Water Use Fees on Dispatching and Water Requirements for Water-Cooled Power Plants in Texas. Environmental Science & Technology, 48(12):7128–7134, 2014. ISSN 0013-936X. doi: 10.1021/es500469q. URL https://dx.doi.org/10.1021/es500469q. Publisher: American Chemical Society (ACS).

Bridget Scanlon, Robert Reedy, Ian Duncan, William Mullican, and Michael Young. Controls on Water Use for Thermoelectric Generation: Case Study Texas, US. Environmental science & technology, 47, August 2013a. doi: 10.1021/es4029183.

Bridget R Scanlon, Ian Duncan, and Robert C Reedy. Drought and the water–energy nexus in Texas. Environmental Research Letters, 8(4):045033, December 2013b. ISSN 1748-9326. doi: 10.1088/1748-9326/8/4/045033. URL http://stacks.iop.org/1748-9326/8/i=4/a=045033?key=crossref.e8b27993539095fa8683794f17739077.

Ryan Schoolmeesters. The hazard classification of a dam can change over time (hazard creep)., 2020. URL https://damfailures.org/lessons-learned/the-hazard-classification-of-a-dam-can-change-over-time-hazard-creep/.

Manajit Sengupta, Yu Xie, Anthony Lopez, Aron Habte, Galen Maclaurin, and James Shelby. The National Solar Radiation Data Base (NSRDB). Renewable and Sustainable Energy Reviews, 89:51–60, June 2018. ISSN 1364-0321. doi: 10.1016/j.rser.2018.03.003. URL https://www.sciencedirect.com/science/article/pii/S136403211830087X.

R. Singh, T. Wagener, R. Crane, M. E. Mann, and L. Ning. A vulnerability driven approach to identify adverse climate and land use change combinations for critical hydrologic indicator thresholds: Application to a watershed in Pennsylvania, USA. Water Resources Research, 50(4):3409–3427, 2014. ISSN 0043-1397. doi: 10.1002/2013wr014988. URL https://dx.doi.org/10.1002/2013wr014988. Publisher: American Geophysical Union (AGU).

Rebecca Smith, Joseph Kasprzyk, and Lisa Dilling. Participatory Framework for Assessment and Improvement of Tools (ParFAIT): Increasing the impact and relevance of water management decision support research. Environmental Modelling & Software, 95:432–446, 2017. ISSN 1364-8152. doi: 10.1016/j.envsoft.2017.05.004. URL https://dx.doi.org/10.1016/j.envsoft.2017.05.004. Publisher: Elsevier BV.

Ilya Meerovich Sobol. On sensitivity estimation for nonlinear mathematical models. Matematicheskoe modelirovanie, 2(1):112–118, 1990. Publisher: Russian Academy of Sciences, Branch of Mathematical Sciences.

Ashlynn S. Stillwell, Carey W. King, Michael E. Webber, Ian J. Duncan, and Amy Hardberger. The Energy-Water Nexus in Texas. Ecology and Society, 16(1), 2011. ISSN 1708-3087. URL https://www.jstor.org/stable/26268863. Publisher: Resilience Alliance Inc.

Brian Jr. Stone, Carina J. Gronlund, Evan Mallen, David Hondula, Marie S. O'Neill, Mayuri Rajput, Santiago Grijalva, Kevin Lanza, Sharon Harlan, Larissa Larsen, Godfried Augenbroe, E. Scott Krayenhoff, Ashley Broadbent, and Matei Georgescu. How Blackouts during Heat Waves Amplify Mortality and Morbidity Risk. Environmental Science & Technology, May 2023. ISSN 0013-936X. doi: 10.1021/acs.est.2c09588. URL https://doi.org/10.1021/acs.est.2c09588. Publisher: American Chemical Society.

Taiyou Yong and R.H. Lasseter. Stochastic optimal power flow: formulation and solution. In 2000 Power Engineering Society Summer Meeting (Cat. No.00CH37134). IEEE, 2000. doi: 10.1109/pess.2000.867521. URL https://dx.doi.org/10.1109/pess.2000.867521.

Rong Tang, Wei Ding, Lei Ye, Yuntao Wang, and Huicheng Zhou. Tradeoff Analysis Index for Many-Objective Reservoir Optimization. Water Resources Management, 33(13):4637–4651, 2019. ISSN 0920-4741. doi: 10.1007/s11269-019-02363-z. URL https://dx.doi.org/10.1007/s11269-019-02363-z. Publisher: Springer Science and Business Media LLC.

Joshua Adam Taylor. Convex Optimization of Power Systems. Cambridge University Press, Cambridge, 2015. ISBN 978-1-107-07687-7. doi: 10.1017/CBO9781139924672. URL https://www.cambridge.org/core/books/convex-optimization-of-power-systems/4CCA9CC35F35AE7EB222B07F2AD7FA98.

L. Thurner, A. Scheidler, F. Schäfer, J. Menke, J. Dollichon, F. Meier, S. Meinecke, and M. Braun. pandapower — An Open-Source Python Tool for Convenient Modeling, Analysis, and Optimization of Electric Power Systems. IEEE Transactions on Power Systems, 33(6):6510–6521, November 2018. ISSN 0885-8950. doi: 10.1109/TPWRS.2018.2829021.

Vincent Tidwell, Calvin Shaneyfelt, Katherine Cauthen, Geoffrey Klise, Fletcher Fields, Zachary Clement, and Diana Bauer. Implications of Power Plant Idling and Cycling on Water Use Intensity. Environmental Science & Technology, 53(8):4657–4666, 2019. ISSN 0013-936X. doi: 10.1021/acs.est.9b00627. URL https://dx.doi.org/10.1021/acs.est.9b00627. Publisher: American Chemical Society (ACS).

Vincent C. Tidwell, Peter H. Kobos, Len A. Malczynski, Geoff Klise, and Cesar R. Castillo. Exploring the Water-Thermoelectric Power Nexus. Journal of Water Resources Planning and Management, 138(5):491–501, 2012. ISSN 0733-9496. doi: 10.1061/(asce)wr.1943-5452.0000222. URL https://dx.doi.org/10.1061/(asce)wr.1943-5452.0000222. Publisher: American Society of Civil Engineers (ASCE).

Jeffrey Tomich. Midwest coal plant in crosshairs of Ill. energy bill, June 2021. URL https://www.eenews.net/stories/1063734851.

P Torcellini, N Long, and R Judkoff. Consumptive Water Use for U.S. Power Production. Technical Report NREL/TP-550-33905, 15005918, National Renewable Energy Lab (NREL), December 2003. URL http://www.osti.gov/servlets/purl/15005918/.

Union of Concerned Scientists. Rising Temperatures Undermine Nuclear Power's Promise. Technical report, Union of Concerned Scientists backgrounder, Washington, DC, August 2007. URL http://www.nirs.org/climate/background/ucsrisingtemps82307.pdf.

Union of Concerned Scientists. Environmental Impacts of Hydroelectric Power, March 2013. URL https://www.ucsusa.org/resources/environmental-impacts-hydroelectric-power.

Michelle T. H. van Vliet, David Wiberg, Sylvain Leduc, and Keywan Riahi. Power-generation system vulnerability and adaptation to changes in climate and water resources. Nature Climate Change, 6(4):375–380, April 2016. ISSN 1758-678X, 1758-6798. doi: 10.1038/nclimate2903. URL http://www.nature.com/articles/nclimate2903.

Andrew Verdin, Balaji Rajagopalan, William Kleiber, and Richard W. Katz. Coupled stochastic weather generation using spatial and generalized linear models. Stochastic Environmental Research and Risk Assessment, 29(2):347–356, February 2015. ISSN 1436-3259. doi: 10.1007/s00477-014-0911-6. URL https://doi.org/10.1007/s00477-014-0911-6.

Heinrich von Stackelberg. Market Structure and Equilibrium. Springer Berlin Heidelberg, Berlin, Heidelberg, 2011. ISBN 978-3-642-12585-0 978-3-642-12586-7. doi: 10.1007/978-3-642-12586-7. URL https://link.springer.com/10.1007/978-3-642-12586-7.

Chunyan Wang, Gustaf Olsson, and Yi Liu. Coal-fired power industry water-energy-emission nexus: A multi-objective optimization. Journal of Cleaner Production, 203:367–375, December 2018. ISSN 0959-6526. doi: 10.1016/j.jclepro.2018.08.264. URL https://www.sciencedirect.com/science/article/pii/S0959652618326155.

Matthew Woodruff and Jon Herman. pareto.py: a epsilon-nondomination sorting routine, 2013. URL https://github.com/matthewjwoodruff/pareto.py.

L.H. Wu, Y.N. Wang, X.F. Yuan, and S.W. Zhou. Environmental/economic power dispatch problem using multi-objective differential evolution algorithm. Electric Power Systems Research, 80(9):1171–1181, 2010. ISSN 0378-7796. doi: 10.1016/j.epsr.2010.03.010. URL https://dx.doi.org/10.1016/j.epsr.2010.03.010. Publisher: Elsevier BV.

Zhenhui Wu, Yadong Mei, Bei Cheng, and Tiesong Hu. Use of a Multi-Objective Correlation Index to Analyze the Power Generation, Water Supply and Ecological Flow Mutual Feedback Relationship of a Reservoir. Water Resources Management, 35(2):465–480, January 2021. ISSN 0920-4741, 1573-1650. doi: 10.1007/s11269-020-02726-x. URL http://link.springer.com/10.1007/s11269-020-02726-x.

Xiaoying Yang and Benedykt Dziegielewski. Water Use by Thermoelectric Power Plants in the United States1. JAWRA Journal of the American Water Resources Association, 43(1):160–169, 2007. ISSN 1093-474X. doi: 10.1111/j.1752-1688.2007.00013.x. URL https://dx.doi.org/10.1111/j.1752-1688.2007.00013.x. Publisher: Wiley.

Jazmin Zatarain Salazar, Patrick M. Reed, Jonathan D. Herman, Matteo Giuliani, and Andrea Castelletti. A diagnostic assessment of evolutionary algorithms for multi-objective surface water reservoir control. Advances in Water Resources, 92:172–185, June 2016. ISSN 03091708. doi: 10.1016/j.advwatres.2016.04.006. URL https://linkinghub.elsevier.com/retrieve/pii/S0309170816300896.

Haibo Zhai and Edward S. Rubin. Performance and cost of wet and dry cooling systems for pulverized coal power plants with and without carbon capture and storage. Energy Policy, 38(10):5653–5660, October 2010. ISSN 0301-4215. doi: 10.1016/j.enpol.2010.05.013. URL http://www.sciencedirect.com/science/article/pii/S0301421510003848.

Appendix A

Summary of Symbol Definitions

Symbol	Definition
$\mathbf{x}$	Illustrative decision vector
$\mathbf{x}^*$	Illustrative optimal decision vector
d	Length of illustrative decision vector
g	Number of illustrative objectives
h	Illustrative function for optimization constraints
f	Objective term
$\mathbf{F}$	Objective vector
p	Length of objective vector
w	Weight term
$\mathbf{w}$	Weight vector
W	Length of weighting vector
p_g	Generator active power
$\mathbf{p_g}$	Vector of active power generation
$\mathbf{p_g^*}$	Vector of optimal active power generation
q	Generator reactive power
$\mathbf{q}$	Vector of generator reactive power
p_L	Active load
$\mathbf{p_L}$	Vector of active load
v	Bus voltage
$\mathbf{v}$	Vector of bus voltages
B	Number of buses
$\mathcal{N}$	Set of buses
C	Generic cost objective function
$\mathbf{Y}$	Admitiance matrix
$\mathcal{Y}$	Feasible active and reactive powers

$\mathcal{B}$	Susceptance matrix
B	Entry in susceptance matrix
θ	Difference in the voltage phase angles
$\mathcal{L}$	Set of lines
Λ_{max}	Line limit
$\mathcal{G}$	Set of generators
t	Timestep conversion factor
G	Number of generators
a	Constant cost term
b	Linear cost term
c	Quadratic cost term
α	Constant emissions term
β_{emit}	Linear emissions term
γ	Quadratic emissions term
ξ	Linear emissions correction term
λ	Exponential emission term
β_{with}	Water withdrawal rate
β_{con}	Water consumption rate
β_{VoLL}	Value of lost load
w_{with}	Water withdrawal weight
w_{con}	Water consumption weight
c_{load}	Uniform loading factor
w_{emit}	Emission weight
c_{water}	Uniform water factor
$S_{i,j}^{First}$	First order Sobol index
$\underline{r}$	Generator ramp down rate
$\bar{r}$	Generator ramp up rate
P_{wwopf}	Water-weighted OPF formulation
P_{cw}	Cost and water simulation
P_{cewr}	Cost, emission, water, and reliability simulation
f_{cos}	Total cost objective
f_{gen}	Generator operational cost objective
$f_{gen,tot}$	Total (over time) generator operational cost objective
f_{emit}	Emissions objective
$f_{cost,emit}$	Cost of emissions objective
$f_{emit,tot}$	Total (over time) emission objective
f_{with}	Water withdrawal objective
$f_{cost,with}$	Cost of water withdrawal objective

$f_{with,tot}$	Total (over time) water withdrawal objective
f_{con}	Water consumption objective
$f_{cost,con}$	Cost of water consumption objective
$f_{con,tot}$	Total (over time) water consumption objective
$f_{cost,ENS}$	Cost of energy not served objective
$f_{tot,ENS}$	Total (over time) energy not served objective
$f_{disvi,tot}$	Total (over time) discharge violation objective

Table A.1: Summary of Symbol Definitions. Note, does not include symbols only used in Appendix.

Appendix B

Case Study: Dam Hazard Classification

There are 16,000 high-hazard potential dams in the U.S. [Federal Emergency Management Agency and Department of Homeland Security, 2017]. A high-hazard potential dam is one in which it is probable that failure would cause loss of human life. Although this definition is codified at the federal level, the actual methodologies by which dams are classified are defined on a state-level, with state dam officials evaluating dam hazard potential on a case-by-case basis, ultimately relying on human judgment [Federal Emergency Management Agency, 1998]. Such a system is prone to hazard potential classification inconsistencies which could lead to negative regulatory and human-safety implications.

Classifying dam hazard potential needs to be done consistently, continually, and across large spatial extents [Mamerow, 2018, Schoolmeesters, 2020]. Geospatial models [Aboelata et al., 2002, Aboelata and Bowles, 2008], dam-break flood routing numerical simulation models [Luo et al., 2009], risk-based models [Larruari and Lall, 2020] offer valuable insight into the engineering and economic consequences of dam failures but could be difficult to automate due to input feature requirements. Other works have proposed empirical relationships for estimating dam loss-of-life based on datasets of historic dam breaks [Feinberg et al., 2016]. However, these methods fail to consider the complex locational aspects of dam failure. This case study overcomes the existing feature requirements by using a parameterized geospatial and tree-based model that has been trained using existing geospatial datasets and publicly available dam hazard datasets. However, *how* we get the values for these parameters is tied to a single- or multi-objective perspective.

B.1 Decisions

The nine "decisions" in this problem are the seven hyperparameters of an ensemble tree-based algorithm and the two parameters of our novel geospatial dam-break estimation model. For this illustrative example, we will provide only high-level summaries of these parameters (consult Kravits et al. [2021b] for more detailed parameter descriptions). The six tree-based-model hyperparameters ($N_{estimators}$, $N_{maxdepth}$, $N_{maxfeatures}$, $N_{maxleafnodes}$, $N_{minsamplesplit}$, $N_{minsamplesleaf}$, and $N_{minweightfraction}$) work together to prevent the overfitting and handle imbalanced datasets. In lieu of doing a full hydraulic analysis of flow downstream of the dam, the geospatial model hypothesizes that the downstream statistics can be captured by two model parameters: N_{length}, a distance downstream of the dam itself; and N_{width}, a distance perpendicular to the downstream distance that represents a characteristic "width" of the zone. We collect our nine decisions into a vector that we define as $\mathbf{x}$.

B.2 Objectives

The "objectives" allow us to quantify the performance of a decision vector $\mathbf{x}$. In other words, an objective allows us insights into how "good" or "bad" a set of decisions is. However, for this problem, this choice of "good" and "bad" is deeply tied to moral values. Consider how dams can be correctly and incorrectly classified in Table 2.1. On the diagonal, we have our correctly classified dams (true positive and negative). These cases are ideal in that they mean that our model agrees with the current classification. However, consider the incorrectly classified off-diagonal (false negative and positive) cases - wrongly classifying a high-hazard dam may lead to downstream populations being put at an increased risk whereas wrongly classifying a non-high-hazard dam may lead to overinvestment. We are forced to morally compare correctly classified threats to human life, potentially unclassified threats to human life, and wasted capital.

We quantify the cases in Table 2.1 into several objectives - each capturing a different moral value. The accuracy (f_{acc}) objective, the ratio of true classifications to total classifications, is

a common choice for these types of water resources classification problems as it maximizes the greatest good [Maier and Dandy, 2000]. Although it is intuitive and easily interpretable, accuracy alone does not directly consider the types of model misclassifications. Taking ratios over the cells in Table 2.1 defines two common objectives of false positive rate (FPR) and true positive rate (TPR). The FPR objective (f_{FPR}) is the ratio of falsely classified high-hazard potential dams to true high-hazard potential dams. TPR (f_{TPR}) is the ratio of correctly classified not-high-hazard dams to actually not-high-hazard potential dams. Each objective expresses a different preference for misclassification type. One drawback of accuracy, TPR, and FPR is that they are all calculated at a single classification threshold (how algorithms quantitatively split positive and negative cases). However, it is often helpful to assess a model across many decision thresholds [Bradley, 1997]. To capture a more holistic model performance, we quantify performance over multiple classification thresholds using the area under receiver operator characteristic curve (AUROCC) objective (f_{AUC}).

B.3 Single- and Multi-Objective Formulations

Now that we have selected our objectives to relate our decisions $\mathbf{x}$ to some scalar performance (e.i, $f_{acc}(\mathbf{x})$), $f_{TPR}(\mathbf{x})$, $f_{FPR}(\mathbf{x})$, $f_{AUC}(\mathbf{x})$), we are ready to demonstrate the difference between single- and multi-objective optimization of our decisions.

Let's start with the single-objective case assuming that we want to select decision $\mathbf{x}$ such that accuracy is maximized. We would construct the following optimization problem:

$$\min_{\mathbf{x}} \quad -f_{acc} \tag{B.1}$$

$$\text{s.t.} \quad C(\mathbf{x}) = f_{acc} \tag{B.2}$$

$$\mathbf{x}_j \geq \mathbf{x}_{\mathbf{lower}\,j}, \forall j \in \{1, \ldots, d\} \tag{B.3}$$

$$\mathbf{x}_j \leq \mathbf{x}_{\mathbf{upper}\,j}, \forall j \in \{1, \ldots, d\} \tag{B.4}$$

where d is the number of decisions, our geospatial tree-based classification is C, and the upper and lower bounds on each decision variable is $\mathbf{x}_{\mathbf{lower}}$ and $\mathbf{x}_{\mathbf{upper}}$, respectively.

However, note that formulation only considers accuracy - we are ignoring the previously motivated misclassifications captured by the TPR, FPR, and AUROCC! We could add normalization weights to those objectives such that these weights reflect the relative preference of each objective. This case defines a new objective function $f_{weighted}(\mathbf{x}, f_{acc}, f_{FPR}, f_{TPR}, f_{AUC})$ such that all of the objectives are distilled into a scalar value. However, knowing what values to select for the preference weights is difficult to know in advance as well as tied to the previously outlined difficult moral comparisons. Furthermore, if the objectives do not conflict, no moral choice may need to be made.

This formulation seeks solutions that capture different compromises among the four objectives, defined by the set of nondominated solutions. This case study employs the Borg multi-objective evolutionary algorithm (MOEA) [Hadka and Reed, 2013] which is a population-based, metaheuristic framework that evolves a set of Pareto-approximate solutions by combining solutions using multiple recombination operators.

B.4 Insights From a Multi-Objective Perspective

We illustrate the types of insights gained through a multi-objective perspective using dams in Massachusetts, U.S. Figure B.1 presents the set of nondominated solutions as parallel axis plots. Figure B.1a depicts the performance of each objective as a vertical line. These axes have been formatted such that ideal solutions intersect the vertical objective axis lower. In other words, a preferred solution would appear as a horizontal line across the bottom of Figure B.1. Figure B.1b depicts the corresponding decision values, and thus there is no preferred direction. To further highlight patterns in the Phase 1 reference set, each solution has been colored to represent Phase 1 FPR.

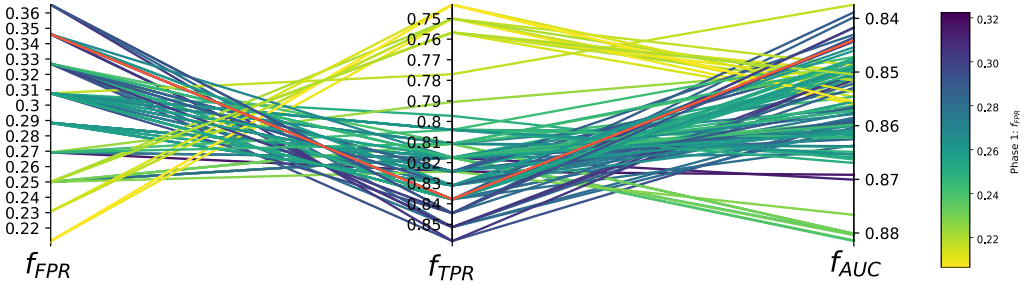

(a) Objective Performance

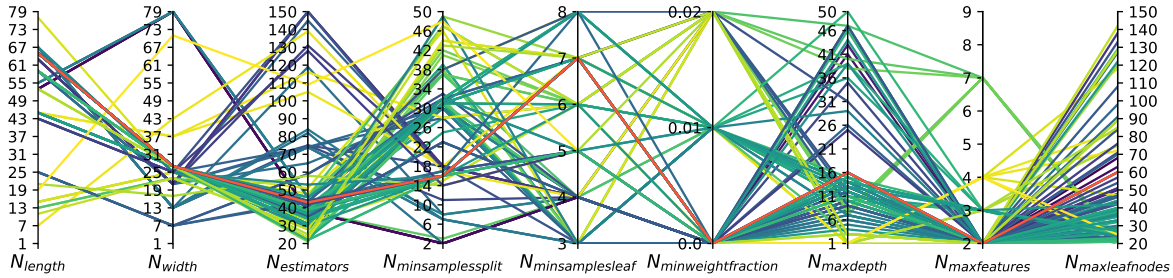

(b) Decision Values

Figure B.1: Example Nondominated Set from a Multi-Objective Problem Set. Solutions are colored according to accuracy

Figure B.1 illustrates how from a multi-objective perspective we engage in how objectives *tradeoff* with one another. For example, from Figure B.1a, there is a clear tradeoff between TPR and FPR. The result suggests that maximizing the correctly classified not high-hazard dams comes at the cost of wrongly classifying high-hazard dams. Generally, the best-performing TPR and FPR results tend to have low AUROCC. This result makes sense given that decisions that yielded extreme objective performance at a single classification threshold would have overall deteriorated performance across many classification thresholds. Additionally, AUROCC does not appear to be complementary to either FPR or TPR. This means that its inclusion in this analysis is helpful because it successfully captures holistic model behavior without emphasizing false positive or false negative classifications.

Appendix C

Water-Use Simulation Models

This section investigates the System-Level Generic Model of thermoelectric water use proposed in Rutberg et al. [2011].

C.1 Once-through Systems

Once-through systems provide cooling by directly warming colder withdrawn water by running it past a heat exchanger [Rutberg et al., 2011]. Therefore, the withdrawal and consumption of these systems are sensitive to the temperature difference between the inlet and outlet of the cooling system. We extend previous models to better capture discharge temperature violation beyond a regulatory upper limit ($s_{t,regulatory}$) in Algorithm 1. By default, plants operate such that the difference between the inlet and outlet temperature is equal to 10 degrees Celsius [Langford, 1990]. If doing so puts them beyond the regulatory discharge limits, then plants discharge directly at the regulatory limit. As inlet streamflow temperature increases, plants require higher water use rates. However, withdrawal and consumption rates have an upper limit due to the pumping, availability, or other physical characteristics of the plant. Therefore, in cases of high inlet streamflow temperatures, we fix the withdrawal and consumption rates at an operational maximum ($\beta_{withlimit,j}$, $\beta_{conlimit,j}$) for a given plant j and then solve for ΔT such that a discharge violation is occurring [Madden et al., 2013].

Algorithm 1 Overview of Once-Through Cooling Equations

$\Delta T \leftarrow 10$ ▷ From [Langford, 1990]

if $s_t + \Delta T > s_{t,regulator}$ **then** ▷ Causes violation

$\Delta T = s_{t,regulator} - s_t$ ▷ Set discharge temperature at regulatory

end if

$\beta_{with,oc} = 3600 \frac{(1-\eta_{net}-k_{os})}{\eta_{net}} \frac{1}{\rho_w c_p \Delta T} + \beta_{proc}$

$\beta_{con,oc} = 3600 \frac{(1-\eta_{net}-k_{os})}{\eta_{net}} \frac{k_{de}}{\rho_w c_p \Delta T} + \beta_{proc}$

if $(\beta_{with,oc} > \beta_{withlimit})$ or $(\beta_{con,oc} > \beta_{conlimit})$ **then** ▷ ΔT cannot be achieved

$\beta_{with,oc} \leftarrow \beta_{withlimit}$

$\beta_{con,oc} \leftarrow \beta_{conlimit}$

$\Delta T = 3600 \frac{(1-\eta_{net}-k_{os})}{\eta_{net}} \frac{1}{\rho_w c_p (\beta_{with,oc} - \beta_{proc})}$

end if

where the terms are defined:

Parameter	Description	Units
β_{with}	Withdrawal Rate	L/MWh
β_{con}	Consumption Rate	L/MWh
s_t	Inlet streamflow temperature	C
ΔT	Inlet/outlet water temperature difference	C
η_{net}	Ratio of electricity generation rate to thermal input	%
k_{os}	Thermal input lost to non-cooling system sinks	%
k_{de}	Fraction of withdrawal that evaporates downstream	%
ρ_w	Density of water	kg/L
c_p	Specific heat of water	MJ/kg-K
β_{proc}	Non-cooling rate	L/MWh

C.2 Recirculating Systems

Recirculating systems provide cooling by using cooling towers to facilitate convective heat transfer to ambient air. Therefore, the withdrawal and consumption of recirculating systems are most sensitive to the ambient air temperature [Rutberg et al., 2011, Diehl et al., 2013]. Cooling towers collect the cooled water for recirculation in the system with some water being consumed as evaporation. These processes are captured in the withdrawal and consumption equations:

$$\beta_{with,rc} = 3600 \frac{(1-\eta_{net}-k_{os})}{\eta_{net}} \frac{(1-k_{sens})}{\rho_w h_{fg}} \left(1 + \frac{1}{n_{cc}-1}\right) + \beta_{proc} \tag{C.1}$$

$$\beta_{con,rc} = 3600 \frac{(1-\eta_{net}-k_{os})}{\eta_{net}} \frac{(1-k_{sens})}{\rho_w h_{fg}} \left(1 + \frac{1-k_{bd}}{n_{cc}-1}\right) + \beta_{proc} \tag{C.2}$$

where the additional terms are defined:

Parameter	Description	Units
η_{cc}	Number of cooling cycles	#
k_{bd}	Discharge blowdown	%
k_{sens}	Heat load rejected	%
h_{fg}	Latent heat of water	MJ/kg

General estimates consider k_{sens} to be constant value [ASHRAE, 2008]. However, such methods fail to capture the impact that ambient air temperature has on water efficiency. Rutberg et al. [2011] conduct a sensitivity analysis of the cooling tower model proposed in Kloppers and Kröger [2005] and determine that k_{sens} can be estimated as:

$$k_{sens} = \frac{-0.000279t_{inlet}^3 + 0.00109t_{inlet}^2 - 0.345t_{inlet} + 26.7}{100} \tag{C.3}$$

where t_{inlet} is the dry-bulb temperature at the inlet of the cooling tower.

C.3 Capacity Reduction Model

We adapt the capacity reduciton model from van Vliet et al. [2016] to capture the impacts that thermoelectric water use limits have on generator capacity.

$$q_{OC} = KW \cdot \frac{1-\eta_{\text{total}}}{\eta_{\text{elec}}} \cdot \frac{(1-\alpha)}{\rho_w \cdot C_p \cdot max\,(\Delta T, 0)} \tag{C.4}$$

$$P_{\text{thermo,OC}} = \frac{\min((\gamma \cdot Q), q_{OC}) \cdot \rho_w \cdot C_p \cdot \max(\Delta T, 0)}{\frac{1-\eta_{\text{total}}}{\eta_{\text{elec}}} \cdot \lambda \cdot (1-\alpha)} \tag{C.5}$$

$$q_{RC} = KW \cdot \frac{1-\eta_{\text{total}}}{\eta_{\text{elec}}} \cdot \frac{(1-\alpha)\cdot(1-\beta)\cdot\omega\cdot EZ}{\rho_w \cdot C_p \cdot max\,(\Delta T, 0)} \tag{C.6}$$

$$P_{\text{thermo,RC}} = \frac{\min((\gamma \cdot Q), q_{RC}) \cdot \rho_w \cdot C_p \cdot \max(\Delta T, 0)}{\frac{1-\eta_{\text{total}}}{\eta_{\text{elec}}} \cdot \lambda \cdot (1-\alpha)\cdot(1-\beta)\cdot\omega\cdot EZ} \tag{C.7}$$

where the parameter definitions are given:

Parameter	Description	Units
$P_{thermo,OC}$	Once through useable capacity	$[MW]$
$P_{thermo,RC}$	Recirculating useable capacity	$[MW]$
KW	Capacity	$[MW]$
η_{total}	Total efficiency	
η_{elec}	Electric efficiency	
α	Share of waste heat not discharged by cooling water	
β	Share of waste heat released into the air	
ω	Correction factor accounting for effects of changes in air temperature and humidity within a year	
EZ	Densification factor accounting for replacement of water in cooling towers to avoid high salinity levels	
λ	Correction factor accounting for the effects of reductions in efficiencies when power plants are operating at low capacities	
γ	Maximum fraction of streamflow to be withdrawn for cooling of thermoelectric power	
Q	Daily streamflow	$\left[\frac{m^3}{s}\right]$

Values for $q_{with,OC}$ and $q_{with,RC}$ are passed from the previously described water use models. Total and electric efficiency values are sourced from [Koch and Vögele, 2009]. α and β are assumed to be 0.01 and 0.986, respectively [IAEA, 2012, Habashy, 2020]. ω is taken as 0.95 [Koch and Vögele, 2009]. EZ is assumed to be 3 [Koch and Vögele, 2009, Rübbelke and Vögele, 2011]. λ is 1.0 for normal operations and 0.9 if the capacity is reduced more than fifty percent [van Vliet et al., 2016]. γ is taken to be 0.02 based on the maximum withdrawal rates and median streamflow temperatures for our system.

Appendix D

Case Study Generation

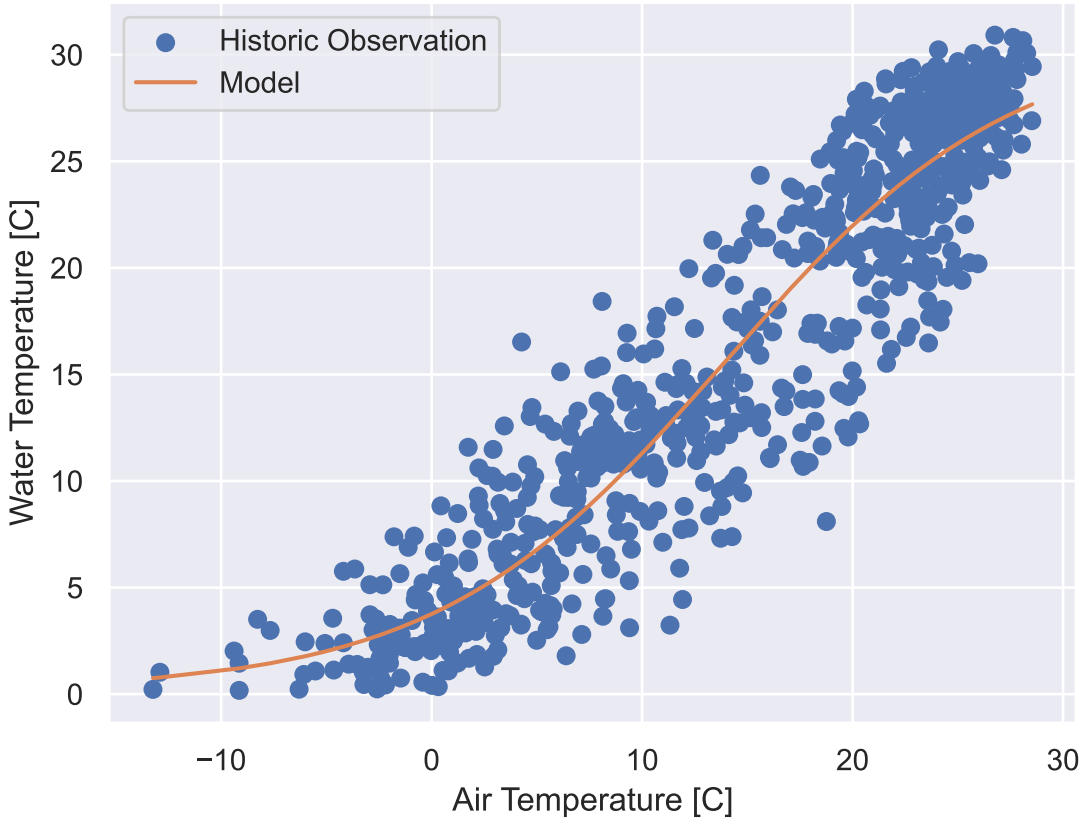

Figure D.1: Fit of Water Temperature Model From Mohseni et al. [1998] for USGS Gauge on Illinois River at Henry, IL

We need to disaggregate this system-level load to the bus level. We model bus-level loads as

$$p_{l,i}^{h} = p_{l,avg} * f_{sys}^{h} * f_{var,i}^{h} \quad \forall i \in \mathcal{N} \tag{D.1}$$

where $p_{l,i}^{h}$ is the active load at bus i during hour h. To model this the $p_{l,avg}$ captures the average difference in loading magnitudes between different buses, f_{sys}^{h} captures the hour-hour load factors among the entire system, and $f_{var,i}^{h}$ captures the relative hour-to-hour variation among loads at each bus. This process has been visualized in Figure D.2.

For our synthetic grid, the vector of bus loadings ($\mathbf{p_l}$) is supplied (Figure D.2A). We use the publicly available MISO data from and transform it into a system load factor by dividing it by the yearly average. Interpreting Figure D.2B, we see the system loadings generally vary between 90 and 140 percent of the yearly average. We use randomly assigned synthetic bus-level hourly profiles to compute the hour-to-hour variation by dividing subsequent hours by one another to compute our hour-to-hour load factors [Li et al., 2021]. The hour-to-hour variation is the most significant as visualized in Figure D.2C. Figure D.2D depicts the final loads for each bus in the system.

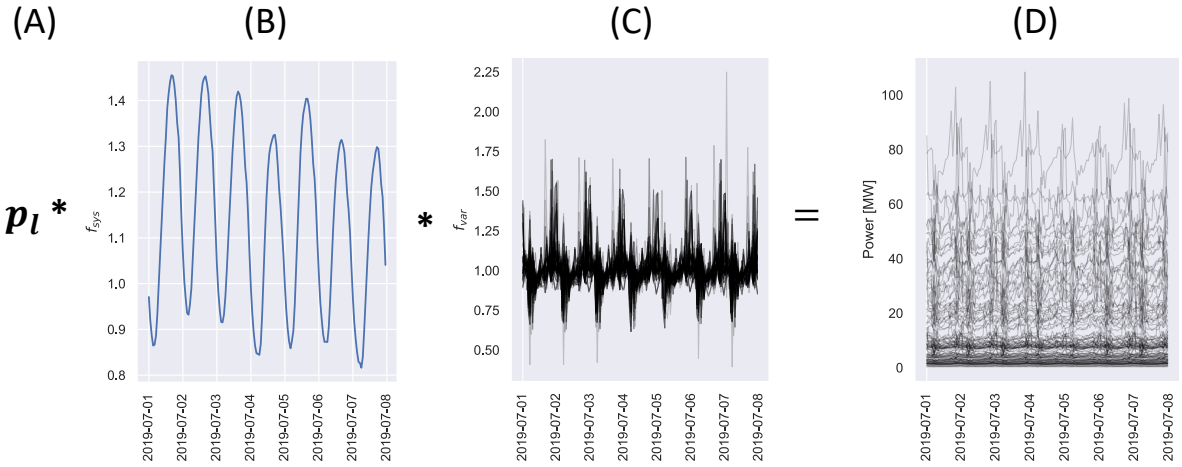

Figure D.2: Overview of Node Load Procedure. (A) $\mathbf{p_l}$ captures the average difference in bus loadings. (B) f_{sys} captures the system-wide hourly variation in loading including correlations with the exogenous parameters. (C) f_{var} captures the hour-to-hour variation in bus loading. (D) Loading profiles for each bus.

Appendix E

Extended Comparison of Policies

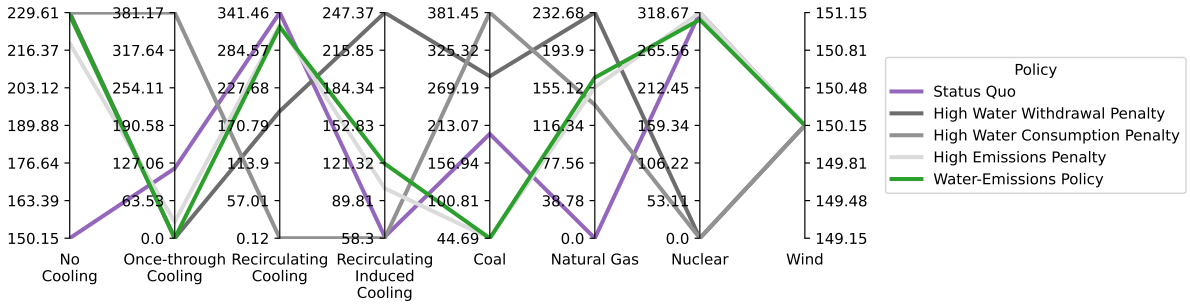

Figure E.1: Power Output by Cooling and Fuel Technology Output for an Average Week.